RATES AND EFFICIENCIES OF OXYGEN TRANSFER BY GAS PUMPING AGITATORS IN GAS-LIQUID MIXING SYSTEMS

By

Robert Peter Swiniarski

B.A.Sc. (Metallurgical Engng), University of British Columbia, 1983

A THESIS SUBMITTED IN PARTIAL FULFILLMENT OF

THE REQUIREMENTS FOR THE DEGREE OF

MASTER OF APPLIED SCIENCE

in

THE FACULTY OF GRADUATE STUDIES

METALS AND MATERIALS ENGINEERING

We accept this thesis as conforming

to the required standard

THE UNIVERSITY OF BRITISH COLUMBIA

February, 1992

In presenting this thesis in partial fulfilment of the requirements for an advanced degree at the University of British Columbia, I agree that the Library shall make it freely available for reference and study. I further agree that permission for extensive copying of this thesis for scholarly purposes may be granted by the head of my department or by his or her representatives. It is understood that copying or publication of this thesis for financial gain shall not be allowed without my written permission.

(Signature) _____

Department of METALS & MATERIALS ENGINEERING

The University of British Columbia
Vancouver, Canada

Date 1992 02 14

DE-6 (2/88)

Abstract

Research into the oxygen pressure leaching of zinc sulphide concentrates has identified that oxygen absorption is a rate-controlling process. In this study, the transfer of oxygen from air to aqueous sodium sulphite solutions by gas pumping impellers was studied as a simulation of the gas-liquid mass transfer step.

A 200 litre right-cylindrical lucite mixing vessel with near-hemispherical bottom was employed. With this tank design, interference with impeller discharge is minimized and the environment approaches the ideal case of an impeller in the ocean. Four radially mounted baffles could be inserted to induce flow conditions characteristic of industrial mixing vessels. The effects of baffles and impeller type, diameter, immersion depth, and tip speed were evaluated in terms of the oxygen transfer rate, power consumption, and power efficiency of oxygen transfer.

It was demonstrated that in the absence of baffling a critical tip speed exists, above which the impeller begins to pump gas at a rate proportional to the impeller tip speed. This critical tip speed is linked directly to the depth of immersion of the impeller on the basis of a theoretical energy balance at the impeller tip. The fit of experimental data to the theoretical was explained in terms of the geometry of the impeller and the shape of the gas vortex it produces. When baffling is introduced, the results obey the critical tip speed relation less accurately, as baffle-impeller interactions significantly alter the flow patterns and change the gas pumping mechanism to bubble capture from surface eddies.

In the unbaffled vessel, axial flow impellers pump oxygen at lower rates and energy efficiencies than radial disc impellers, unless placed at shallow immersion. Gas pumping by dual impellers offers no advantage over a single radial disc impeller operating at the

lower immersion depth.

At a given impeller speed, oxygen transfer is increased by the addition of baffles, but power consumption increases at a faster rate so that the energy efficiency is lower than without baffles. However, it was possible with impellers of smaller diameter at a shallow immersion depth to sustain a vortex in the baffled vessel, which gave the largest rates and efficiencies of oxygen transfer. This suggests it is possible to reduce the degree of baffling, and that the rate and efficiency of oxygen transfer can be optimized through judicious selection of impeller diameter and baffle size.

Table of Contents

List of Figures

List of Tables

List of Symbols

a	–	interfacial area per unit volume (gas-liquid or liquid-solid)	$L^2/L^3 = L^{-1}$
B	–	baffle width	L
c_i	–	unspecified constant	
C	–	impeller clearance from bottom of vessel	L
C	–	concentration of specie	mL^{-3}
d_b	–	bubble diameter	L
D	–	impeller diameter	L
D_d	–	impeller disc diameter	L
$\mathcal{D}_i$	–	diffusivity of component i in the liquid	L^2T^{-1}
$\mathcal{D}_w$	–	diffusivity of a substance in water	L^2T^{-1}
e	–	eccentric impeller shaft offset	L
Fl	–	Flow number for impellers Q_G/ND^3	
Fr	–	impeller Froude number N^2D/g	
g	–	gravitational constant	LT^{-2}
Ga	–	Galileo number $Re^2/Fr = D^3g/\nu^2$	
H_L	–	height of liquid from bottom of vessel	L
k_g	–	gas phase mass transfer coefficient	$mTL^{-1}M^{-1}$
k'_g	–	gas phase mass transfer coefficient	LT^{-1}
k_i	–	kinetic rate constant or proportionality constant for ith reaction or equation	
k_L	–	liquid phase mass transfer coefficient, chemical absorption	LT^{-1}
k_L^o	–	liquid phase mass transfer coefficient, physical absorption	LT^{-1}

K_G	–	mass transfer parameter	T^{-1}
K_G^{20}	–	mass transfer parameter normalized to 20°C *via* $\mathcal{D}_{O_2}^{20}$	T^{-1}
n	–	number of blades on the impeller	
N	–	impeller speed	T^{-1}
N_D	–	Discharge number for impellers Q_L/ND^3	
N_{DD}	–	critical impeller speed for drawdown of floating particles	T^{-1}
N_F	–	critical impeller speed for flooding of blades with gas	T^{-1}
N_{SA1}	–	critical impeller speed for onset of surface aeration	T^{-1}
N_V	–	critical impeller speed for onset of vortex aeration	T^{-1}
P	–	power consumption of the agitator	ML^2T^{-3}
$\mathcal{P}_i$	–	partial pressure of gas in locale i	$ML^{-1}T^{-2}$
Po	–	Power number for impellers $Pg/\rho N^3 D^5$	
Q_G	–	volumetric gas sparging rate	L^3T^{-1}
Q_L	–	volumetric discharge of liquid from impeller	L^3T^{-1}
$r(c)$	–	rate of chemical reaction	$mL^{-3}T^{-1}$
Re	–	impeller Reynolds number $ND^2\rho/\mu$	
R_i	–	rate of ith reaction	$mL^{-3}T^{-1}$
s	–	fractional rate of surface renewal	T^{-1}
S	–	spacing between impellers on agitator shaft	L
t	–	elapsed time	T
t_e	–	time of exposure of liquid surface (elements)	T
T	–	vessel diameter	L
$\mathcal{T}$	–	torque measured at impeller shaft	ML^2T^{-2}
v	–	impeller tip speed	LT^{-1}

v_C	–	critical impeller tip speed for gas pumping	LT^{-1}
v_E	–	experimentally determined critical impeller tip speed for gas pumping	LT^{-1}
v_s	–	superficial sparge gas velocity	LT^{-1}
v_t	–	terminal rise velocity of a bubble	LT^{-1}
V	–	total volume of mixing vessel contents	L^3
$\mathcal{V}$	–	molal volume of diffusing solute	L^3/m
V_B	–	unit volume of bubble	L^3
V_D	–	unit volume of dispersion or slurry at impeller tip	L^3
V_L	–	volume of liquid in mixing vessel	L^3
W	–	width of impeller blades	L
We	–	Weber number $N^2D^3\rho_L/\sigma$	
x_b	–	thickness of impeller blade	L
z^+, z^-	–	charge on an ion or complex	
Z	–	immersion depth of impeller as measured from static gas-liquid interface	L
Z_a	–	height of vortex above the static gas-liquid interface	L
Z_b	–	height of vortex below the static gas-liquid interface	L
Z_v	–	height of the vortex	L
Z'	–	total height of the combined vortex	L

Greek letters:

α	–	blade angle of pitch-bladed (axial) impeller	
δ	–	gas or liquid film thickness	L
ϵ_G	–	gas hold-up (volume fraction of gas in vessel contents)	

ϵ_L	–	volume fraction of liquid in vessel contents	
ϵ_T	–	volumetric power dissipation	$ML^{-1}T^{-3}$
λ	–	distance of reaction plane from gas-liquid interface	L
μ	–	absolute viscosity	$ML^{-1}T^{-1}$
ν	–	kinematic viscosity	L^2T^{-1}
$\phi(t)$	–	distribution function of ages of surface elements	
Φ	–	over-all power number	
ρ_D	–	density of dispersion	ML^{-3}
ρ_G	–	density of gas phase	ML^{-3}
ρ_L	–	density of liquid phase	ML^{-3}
σ	–	(interfacial) surface tension	MT^{-2}
θ	–	polar angle in the xy plane	

subscripts:

a	–	atmospheric
aq	–	aqueous phase
g	–	gassed impeller condition
u	–	ungassed impeller condition
v	–	vessel

superscripts:

b	–	bulk liquid phase
g	–	gas phase
I	–	gas-liquid interface
$*$	–	equilbrium value

Acknowledgement

I would like to thank my supervisor Dr. Ernest Peters for the guidance, insights, encouragement, support and patience he provided over the course of my program. It has been a privilege to work under his direction.

I would also like to thank Dr. David Dreisinger for his helpful comments and interest in the project. The fine work of Horst Tump and Ross McLeod in fabricating many pieces of the apparatus is greatly appreciated.

Thanks go to the many fellow students and staff with whom I have had contact. The suggestions of Mijai Talaba and Grant Morgan were always helpful (especially the sandbox, Grant). Ben Saito and Ed Chong offered valuable criticism in their diligent proofreading of the manuscript. Joan Kitchen handled long-distance problems with aplomb and a friendly voice. I trust the friendships with Mike Bouliane, Lorraine Brendzy, Mike Carriere, Mike Grant, Geoff Lowe, David Tripp and many others will continue though miles will come between us. And I thank St. Jude for his help.

I thank Colin Edie, Bernardo Hernandez-Morales and Andrew Wong for setting me on the road to computer literacy. On this note I am indebted to Chris Parfeniuk, who was always available and willing to help in an emergency—a steadfast friend.

Financial support received from NSERC and the Cy and Emerald Keyes Foundation is gratefully acknowledged.

Finally, I would like to thank my family, especially my parents to whom this is dedicated. Without their unending support, prayers, encouragement and love this all would not have been possible.

Chapter 1

Introduction

1.1 Oxygen Pressure Leaching

1.1.1 Process Development

The pursuit of hydrometallurgical processes which utilize elevated pressures (most always in association with elevated temperatures) is common today but hardly a new phenomenon. As far back as 1859, Béketoff [1] precipitated metallic silver from a solution of silver nitrate with heat under hydrogen pressure.

Reaction under pressure was exploited by Bayer [2] in 1892 to dissolve alumina and separate it from most bauxite impurities *via* :

$$Al_2O_3 \cdot xH_2O + 2NaOH \rightarrow 2NaAlO_2 + (x+1)H_2O \tag{1.1}$$

The reaction occurs at a temperature between 140 and 220°C and pressure of 1000 to 1200 kPa. Bayer digesters continue to be used in the production of purified alumina for the Hall-Héroult process.

The genesis of modern pressure leaching systems can be traced back perhaps to Malzac [3] who, in 1903, patented a process for the pressure leaching of copper, nickel and other sulphides with ammonia and air at high temperature. Indeed the first successful application of the technology was the Sherritt Gordon ammonia pressure leach process in the early 1950's.

This process was founded on a feature of ammonia chemistry, where cobalt, nickel, copper, zinc and ferrous iron form complex ions of the form $[Me(NH_3)_x]^{z+}$ in aqueous

ammonia solution [4].

The Caron process [5] had made use of that feature during the Second World War. Reduced nickel and cobalt from nickeliferous laterite ores were leached with ammonia-ammonium carbonate solutions and air under ambient conditions. The pregnant solution was steam stripped of ammonia (which was recycled) to precipitate basic nickel carbonate ($NiCO_3 \cdot 2Ni(OH)_2$). This precipitate was calcined to nickel oxide (NiO) containing some cobalt oxide. Operations were interrupted by Cuban nationalization and later resumed on the Major Ramos Latour (formerly Nicaro) ores of Cuba.

Sherritt initially proposed in 1948 roasting their domestic pentlandite concentrates to remove the sulphur (as SO_2), reducing the calcine, and then digesting and leaching via the carbonate route [6]. But this flowsheet proved unwieldy and was not pursued commercially.

Subsequently it was found by Professor Frank Forward that the concentrates could be leached *directly* in an aqueous solution of ammonia in the presence of oxygen [4]. The chemistry of the batch tests demanded a large initial oxygen requirement for the oxidation of sulphide minerals and sulphur oxyanions. An important observation from the 1948 testwork was the dramatic increase in nickel leaching rate as the oxygen partial pressure was increased from 21 kPa (ambient air) to 203 kPa. This was applied to the newer process and a similar (yet less profound) effect was demonstrated with partial pressures between 70 and 280 kPa. As well, the reaction rates were expected to be influenced by temperature and this was examined in the range 50 to 104°C.

From this work, a successful two-stage leaching process at 80°C and oxygen partial pressure of 90 kPa (using air and ammonia) was incorporated into a commercial flowsheet which has operated since 1954.

The Sherritt ammonia process serves as a landmark in the evolution of pressure leaching technology because it was developed in direct response to the difficulty in adapting

an existing ambient process. It realized at least three important advantages over the Caron approach:

- **Simplification**: It eliminated two unit operations (roasting and reduction) ...
- **Materials Handling**: ... which were high-temperature processes
- **Pollution**: It treated sulphide concentrates yet produced no SO_2.

1.1.2 Chemistry of Modern Processes

Several processes and flowsheets have been developed during and since the 1950's. For example, alkaline (Na_2CO_3) pressure leaching was adapted for tungsten-molybdenum and arsenide concentrates in the USSR [7] and by Sherritt for uranium ores [8]. Sulphuric acid pressure leaching was developed by Chemico for cobalt concentrates [9], and for the low-magnesium Cuban laterite ores[1] [10] and their resultant sulphide precipitates [7]. It was also applied to lead [11], zinc [12], complex sulphide [13] and copper concentrates [14].

Sarkar [15] classifies five separate systems based on chemistry:

(a) Acid Pressure Leaching Metal sulphides and oxygen react in strong acid solution to produce metal sulphates and elemental sulphur. Examples of over-all reactions:

$$ZnS + H_2SO_4 + \tfrac{1}{2}O_2 \rightarrow ZnSO_4 + H_2O + S^0 \tag{1.2}$$

$$PbS + H_2SO_4 + \tfrac{1}{2}O_2 \rightarrow PbSO_4 + H_2O + S^0 \tag{1.3}$$

$$Cu_2S + 2H_2SO_4 + O_2 \rightarrow 2CuSO_4 + 2H_2O + S^0 \tag{1.4}$$

$$UO_2 + H_2SO_4 + \tfrac{1}{2}O_2 \rightarrow UO_2SO_4 + H_2O \tag{1.5}$$

[1] The ores were concentrated to a small degree by screening off the practically barren +20 mesh fraction.

(b) **Alkaline** As used in the processing of uranium ore (e.g. Eldorado Beaverlodge), incorporating bicarbonates:

$$U_3O_8 + \tfrac{1}{2}O_2 \rightarrow 3UO_3 \tag{1.6}$$

$$UO_3 + Na_2CO_3 + 2NaHCO_3 \rightarrow Na_4UO_2(CO_3)_3 + H_2O \tag{1.7}$$

(c) **Aqueous Ammonia** Applied to copper and nickel sulphides found in association with iron sulphides:

$$NiS{:}FeS + 3FeS + 7O_2 + 10NH_3 + 4H_2O \rightarrow Ni(NH_3)_6SO_4 + 2Fe_2O_3{\cdot}H_2O + 2(NH_4)_2S_2O_3 \tag{1.8}$$

$$2(NH_4)_2S_2O_3 + 2O_2 \rightarrow (NH_4)_2S_3O_6 + (NH_4)_2SO_4 \tag{1.9}$$

$$(NH_4)_2S_3O_6 + 2O_2 + 4NH_3 + H_2O \rightarrow NH_4{\cdot}SO_3{\cdot}NH_2 + 2(NH_4)_2SO_4 \tag{1.10}$$

(d) **Ammonia-Ammonium Sulphate** For the treatment of metal sulphides in mattes:

$$MeS \text{ (Matte)} + 2O_2 + 2NH_3 \rightarrow Me{\cdot}(NH_3)_2SO_4 \tag{1.11}$$

The metallics associated with mattes react to form diammine sulphates also:

$$Me \text{ (Metallics)} + \tfrac{1}{2}O_2 + (NH_4)_2SO_4 \rightarrow Me{\cdot}(NH_3)_2SO_4 + H_2O \tag{1.12}$$

The metal diammine sulphates are reduced by hydrogen, producing pure metal precipitates and ammonium sulphate for recycle.

(e) **Aqueous** The oxidation of metal sulphides in water with air, generally at low temperature (< 130°C) and high acidity:

$$2FeS + 2H_2O + \tfrac{9}{2}O_2 \rightarrow Fe_2O_3 + 2H_2SO_4 \tag{1.13}$$

$$4FeAsS + 5O_2 + 4H_2SO_4 \rightarrow 4HAsO_2 + 4FeSO_4 + 2H_2O + 4S^0 \tag{1.14}$$

$$2FeAsS + 7Fe_2(SO_4)_3 + 8H_2O \rightarrow 16FeSO_4 + 2H_3AsO_4 + 5H_2SO_4 + 2S^0 \tag{1.15}$$

1.1.3 Merits of Pressure Leaching Processes

The direct leaching of concentrates offers certain advantages over 'conventional' processes. A practical example is the treatment of zinc sulphide concentrates, where the traditional roast-leach process has onerous consequences stemming mainly from the disposition of sulphur.

The roasting process dispels sulphur by the formation of SO_2 gas, with as much as one quarter of the initial feed borne in dust-laden roaster off-gases. Secondary roasting of partially oxidized material may require energy input due to low sulphur content levels. Iron in the concentrate reacts to form zinc ferrite, which is insoluble in the leach and requires additional processing to recover the zinc.

Electrostatic precipitators are required to remove dust from off-gases, but capture is never entirely complete so heavy metal particulates escape to the atmosphere. The practice of simply allowing SO_2 gases to escape up the stack is no longer prudent and faces increasing legal restriction [16]. Thus, the captured SO_2 gas must be fixed in a marketable or disposable form.

Liquid SO_2 can be produced from SO_2 gases which must be absorbed and then acidified to attain commercial purity. It is less expensive to capture the SO_2 from zinc roaster off-gases as sulphuric acid. However, sulphuric acid is very costly to transport to market, and though it and ammonium sulphate can be generated as feedstock for fertilizers, this requires nearby facilities and ties metallurgical operations to agricultural commodities which are subject to their own market conditions.

Oxygen pressure leaching, as described in Reaction 1.2, is an attractive means of addressing the problems just cited:

1. The hygiene and environmental concerns associated with roaster off-gases and their contained dusts are eliminated.

2. SO_2-containing gases are not released into the atmosphere, averting 'acid rain' production.

3. Zinc ferrite is not formed, so first-pass recovery of zinc may approach 100 per cent.

4. The link between production of zinc and of liquid SO_2, sulphuric acid or fertilizers is broken.

5. Sulphur recovered in elemental form may have greater market appeal (if appropriate purity can be achieved). Alternative handling strategies include impoundment, or combustion to generate plant acid.

1.2 Pressure Leaching of Zinc Sulphide Concentrates

1.2.1 Process Development

Early investigation into the treatment of zinc sulphides was reviewed by Forward and Warren [17]; patents were awarded as early as 1927 but no system was applied commercially.

Reaction 1.2,

$$ZnS + H_2SO_4 + \tfrac{1}{2}O_2 \rightarrow ZnSO_4 + H_2O + S^0$$

was reported by Björling [18] to occur under pressure but impractically slowly in the absence of nitric acid (a catalyst). The nitric acid would have a negative impact on the electrolysis of the $ZnSO_4$ so the process was not seen as promising.

Forward and Veltman [12] achieved remarkably different results with zinc-lead concentrates. If H_2SO_4 was supplied stoichiometrically to react with the ZnS and PbS according to Reactions 1.2 and 1.3, near complete conversion of the sulphides was observed.

1.2.1.1 Reaction Temperature and Piloting

There were two important observations regarding the rate of the reaction, which spawned parallel paths of development. The first was a temperature limit of about 115°C, just below the melting point of sulphur. In excess of this point the reaction was initially very rapid but then ceased almost completely within minutes, as molten elemental sulphur encapsulated the unreacted sulphide particles and prevented further reaction. Thus, a typical batch test required four hours for 97 per cent conversion when limited only to 110°C.

This constraint was solved [19] by use of lignin sulphonate salts: surface active agents which disperse the molten sulphur by lowering the work of adhesion between the molten sulphur and the mineral surface [20]. The upper bound was pushed to about 158°C, and is now likely linked to the minimum viscosity range of molten elemental sulphur [21,22] or the diminishing solubility of $FeSO_4$ [23].

Since faster leaching rates can be realized with increased temperatures, retention times are of course reduced. This translates directly to smaller autoclave volumes or larger throughputs and in turn, reduced capital costs for the vessels, which adds to the competitiveness of pressure leaching as a process alternative. A 30 per cent advantage in capital cost (relative to a roast-leach plant) has been estimated [24].

Pilot plant demonstration was first attempted jointly by Cominco and Sherritt in 1961 [25], but only at 110°C. This obtained zinc extraction of 70 to 80 per cent with a mean residence time of eight to twelve hours. At this throughput the capital costs for pressure leaching were not advantageous. Plans to run a pilot plant at Hudson Bay Mining & Smelting [26] were discontinued in 1971 after preliminary testwork was not encouraging, due to constraints similar to those encountered in 1961. Cominco and Sherritt piloted a single-stage leach in 1977, following discovery of the surfactant (as cited) and two

techniques for separating elemental sulphur (in the molten or solidified state) from the leach product [21].

The results of the latter testwork were incorporated into modernization plans by Cominco and the process was established commercially in 1980, with the capacity to treat up to fifteen per cent of their zinc capacity [24,27,28]. In 1983 the process was installed at Kidd Creek Mines [29], but presently it runs only intermittently. Hudson Bay plans in 1994 to be the first to apply the process to treat 100 per cent of its zinc concentrates.

1.2.1.2 Iron and the Reaction Mechanism

The second observation in the work of Forward and Veltman concerned the presence of iron in the leach solution. (Björling's 'natural' sphalerite must have been iron-free.) Although the role of iron species was not determined in their work, it was noted that some iron in the concentrate dissolved as $FeSO_4$, with subsequent oxidation of Fe^{2+} to Fe^{3+}.

Continued research by Mackiw and Veltman [13] established the source of iron as being FeS from pyrrhotite or the iron sulphide component of marmatitic ZnS concentrates. (Pyrite and chalcopyrite oxidized very slowly in comparison.) They proposed a dissolution mechanism,

$$FeS + H_2SO_4 + \tfrac{1}{2}O_2 \rightarrow FeSO_4 + H_2O + S^0 \tag{1.16}$$

$$2FeSO_4 + H_2SO_4 + \tfrac{1}{2}O_2 \rightarrow Fe_2(SO_4)_3 + H_2O \tag{1.17}$$

which would act in concert with a proposed leaching mechanism:

$$ZnS + H_2SO_4 \rightarrow ZnSO_4 + H_2S \tag{1.18}$$

$$Fe_2(SO_4)_3 + H_2S \rightarrow 2FeSO_4 + H_2SO_4 + S^0 \tag{1.19}$$

with regeneration of ferric iron by Reaction 1.17. The rates of leaching and S° production were very dependent on the presence of iron, which was proposed to be an oxygen carrier. Assuming the sulphur in the H_2S comes from the ZnS, the change in oxidation state of sulphur is seen to occur not in Reaction 1.18 but in Reaction 1.19.

Later work [30,31,32] suggested a basic electrochemical leaching model, analogous to the corrosion of metals, with

$$ZnS = Zn^{2+} + S^0 + 2e^- \tag{1.20}$$

being the anodic reaction and

$$2H^+ + \tfrac{1}{2}O_2 + 2e^- = H_2O \tag{1.21}$$

the cathodic reaction.

The first two of these studies also proposed the existence of the H_2S intermediate product. Although the formation of H_2S from most metal sulphides (e.g. Reaction 1.18) is not thermodynamically favoured and its oxidation is known to be slow [33], Scott and Dyson [30] detected it and suggested the oxidation may be subject to catalysis. However, they offered no mechanism for its formation nor oxidation. (If the 3.1 per cent impurity in their 'pure' ZnS contained FeS, then the origin could have been

$$FeS + H_2SO_4 \rightarrow FeSO_4 + H_2S \tag{1.22}$$

reported in 1955 by Downes and Bruce [34] and shown to be thermodynamically favourable by Majima and Peters [33].)

They postulated that catalyst ions (Cu, Bi, Ru, Mo and Fe in descending order of effectiveness) displace zinc from the surface layers of ZnS, making it more electrically conducting and accelerating the reduction of dissolved oxygen on the ZnS surface.

Pawlek [31] used H_2S to suppress ZnS dissolution, which would be predicted by Reaction 1.18 in an enclosed environment.

Niederkorn [32] evaluated Co^{2+} and Ag^{+} as catalysts acting in the same vein as those of Scott and Dyson. He did not mention a role for or the presence of H_2S in his experiments.

Jan *et al.* [35] cited deficiencies they believed detracted from the electrochemical model and returned to the Mackiw-Veltman model. They assumed ferric oxidation of H_2S (Reaction 1.19) to be the rate-controlling step of 1.18, 1.19 and 1.17. However, they preferred the non-oxidative Reaction 1.22 to Reaction 1.16 for the dissolution of pyrrhotite.

Verbaan and Crundwell [36] proposed an electrochemical charge-transfer model consisting of the non-oxidative dissolution of ZnS (equivalent to Reaction 1.18)

$$ZnS + 2H^{+} \rightarrow Zn^{2+} + H_2S \tag{1.23}$$

followed by the oxidation of H_2S,

$$H_2S \rightarrow S^{0} + 2H^{+} + 2e^{-} \tag{1.24}$$

$$2Fe^{3+} + 2e^{-} \rightarrow 2Fe^{2+} \tag{1.25}$$

1.2.1.3 Current Reaction Mechanism

The present understanding of the leaching mechanism in the commercial process no longer views H_2S as being critical or rate-controlling. While indeed it may be generated and oxidized as described, the leaching rate it would sustain has been shown by Dreisinger and Peters [37] to be too slow to explain observed industrial leaching rates.

The over-all reaction mechanism is now generally accepted to consist of three simultaneous physicochemical steps [37]:

1. Mass transfer of oxygen from the gas to the leach solution,

$$O_{2\ (g)} \rightarrow O_{2\ (aq)} \tag{1.26}$$

$$R_1 = k_1([O_2]^I - [O_2]^b)$$

2. Homogeneous oxidation of Fe^{2+} to Fe^{3+} by dissolved oxygen,

$$4Fe^{2+} + 4H^{+} + O_2 \rightarrow 4Fe^{3+} + 2H_2O \tag{1.27}$$

$$R_2 = k_2[Fe^{2+}]^2[O_2]$$

3. Leaching of ZnS by the ferric ion,

$$4Fe^{3+} + 2ZnS \rightarrow 4Fe^{2+} + 2Zn^{2+} + 2S^0 \tag{1.28}$$

$$R_3 = k_3 a_{ZnS}[Fe^{3+}]$$

1.2.2 Process Optimization

Dreisinger and Peters [37] used Cominco plant data to model the zinc pressure leach and showed how rate control is different in each of the compartments of the four-stage autoclave.

In the second through fourth stage the rate is governed by ferric ion leaching, and the rate constant for Reaction 1.28 in each stage declines from first to last. This could be attributed to the increased relative abundance of less reactive zinc minerals, or to a molten sulphur encapsulation problem caused by decreased surfactant activity. The role of the surfactant was investigated separately by Owusu [20].

Their model also showed that in the first stage, the over-all reaction rate probably is controlled by the rates of all three reaction steps. An improvement in the rate constant for any of Reactions 1.26, 1.27 and 1.28 would result in an over-all improvement in performance. Since greater than 80 per cent of the leaching occurs in the first compartment[2], these are fruitful areas of investigation.

[2]This is true for a single-autoclave circuit; when two countercurrent autoclaves are employed, about 80 per cent of the leaching occurs in the first autoclave [38].

Parker and Romanchuk [21] had reported that under standard pilot plant conditions in 1977, concentrate surface area was found to be the rate-limiting factor; but when concentrate was fed at 150 per cent of the standard rate, the ferric ion concentration dropped to zero, which would mean the rate-limiting factor shifted from a_{ZnS} in the rate equation for Reaction 1.28 to the oxidation of ferrous ion (Reactions 1.26 and 1.27).

This oxidation has been the subject of much previous work, which was reviewed by Dreisinger and Peters as part of another investigation [39], where the oxidation of the ferrous sulphate ion pair under pressure leach conditions was evaluated.

Finally, the absorption of oxygen (Reaction 1.26) is left for scrutiny. The model showed that of the three rate constants, the greatest benefit in extraction would be derived from an increase in k_1. This can be expressed more appropriately by

$$k_1 \equiv K_g = k'_g \cdot a = k^o_L \cdot a \tag{1.29}$$

where K_G is the product of the gas phase mass-transfer coefficient and the volumetric gas-liquid interfacial surface area. Either or both of these can be influenced to produce an increase in K_G.

DeGraaf [40] investigated the effect upon oxygen transfer rate of:

- agitator type, speed, configuration
- depth of immersion
- baffles
- and gas sparging

in gas-liquid models at several volumetric scales. The power input of agitation also was measured.

The work presented in this thesis builds upon that of DeGraaf, examining in greater detail:

- agitator design
- agitator type, speed, configuration
- depth of immersion
- and effect of baffles

at one tank volume (200 ℓ). As with the previous work of DeGraaf and subsequent work of Dawson-Amoah [41], it will provide an understanding into the means by which physical factors can be exploited to maximize K_G and, in turn, over-all pressure leaching rates.

Chapter 2

Study of Gas-Liquid Mass Transfer in Agitated Systems

The practical approaches for increasing the rate of oxygen absorption usually are based on increasing the partial pressure of oxygen, increasing the volumetric gas-liquid interfacial area, and increasing the efficiency of agitation. Each of these has theoretical considerations.

2.1 Gas-Liquid Mass Transfer

The phenomenon of mass transfer with chemical reaction is generally described by four elementary steps [42]:

1. Diffusion of one or more reactants from the bulk of phase 1 to the interface between phases 1 and 2;
2. Diffusion of the reactant(s) from the interface towards the bulk of phase 2;
3. Chemical reaction within phase 2;
4. Diffusion of reactants and reaction products within phase 2, due to concentration gradients established by the chemical reaction.

Steps 2, 3 and 4 may take place simultaneously, in series with step 1. If 1 is the rate-controlling step, the over-all rate is not influenced by chemical reaction and the phenomenon reduces to simple mass transfer, independent of the reaction rate. Alternatively,

the over-all effect of 2, 3 and 4 may be rate-controlling. In this case each of these three steps may be analysed for their respective contributions.

This sequence is acceptable for the specific example of pressure leaching described by Reactions 1.26 and 1.27. Phase 1 is the gas containing the reactant oxygen (as pure oxygen or air), phase 2 is the liquid containing the Fe^{2+}, Fe^{3+} and H^{+} ions, and the chemical reaction occurring in step 3 is the homogeneous reduction of oxygen by ferrous ions (Reaction 1.27).

2.1.1 Gas Absorption

Various models have been advanced to describe the absorption of a gas into a liquid. Historically the most prominent have been the film, penetration and surface renewal theories.

Film Theory

In the film theory of Lewis and Whitman [43], there exist layers or films of gas and liquid respectively on each side of the gas-liquid interface, in which motion by convection is slight. Thus, any transfer of solute through the layers must occur by diffusion, and the films offer resistances to transfer of a material from one phase to another.

The gas film is likely the thicker of the two since film thickness probably depends on the ratio of viscosity to density, which is greater for gases. But resistance to diffusion owing to intermolecular collision is much greater for the liquid.

The rate of gas absorption by diffusion through the two films is then given by:

$$R = k_g a(P^g - P^I) = k_L^o a(C^I - C^b) \tag{2.1}$$

where P and C are gas and liquid concentrations and the superscripts I, g and b refer to conditions at the interface and at the outside of the gas and liquid films respectively.

With film thickness of δ and no generation (*i.e.* no chemical reaction),

$$-\left(\frac{\partial c}{\partial x}\right)_{x=0} = \frac{C^I - C^b}{\delta} \tag{2.2}$$

and the coefficient for physical absorption, k_L^o, is defined as

$$k_L^o = \frac{\mathcal{D}_A^n}{\delta} \tag{2.3}$$

where the exponent n equals unity. Thus at constant hydrodynamic conditions (effecting no change in δ), the absorption coefficient is seen to be proportional to molecular diffusivity. This is contrary to experimental values for n for turbulent flow which range from nearly zero to 0.8 or 0.9 [44], with 0.5 being a reasonable estimate [42, p. 4].

Penetration Theory

The film theory assumes diffusion *via* a steady concentration gradient in the liquid film. However, at the instant gas and liquid are first brought into contact, the concentration in both liquid film and bulk liquid are identical. If the time of contact between gas and liquid is shorter than the time required for the diffusing gas to 'penetrate' and establish the liquid film gradient, the film theory is not applicable.

Higbie [45] believed contact time to be in the order of only 0.01 second for bubbler absorbers, and described the liquid surface about an ascending bubble as being continually formed at the top, passing around it and then being destroyed at the bottom when taken into the bulk liquid, all of which shared the same life t_e. In this way the absorption coefficient would be

$$k_L^o = 2\sqrt{\frac{\mathcal{D}_A}{\pi t_e}} \tag{2.4}$$

and would vary as the inverse root of contact or penetration time. It would asymptotically approach the value given by the film theory to the time the concentration gradient had been established in the film.

Surface Renewal Theory

The penetration theory was later modified to consider the liquid surface as being composed of surface *elements*, with constant life t_e. Danckwerts [46] viewed the surface elements as being exposed to the gas for different lengths of time before being replaced by fresh elements of bulk composition. Thus the absorption rate in an element is a function of its age, while the chance of an element being replaced is independent of its age. The distribution function of ages, $\psi(t)$, is given by

$$\psi(t) = s \cdot \exp(-st) \tag{2.5}$$

where s is the fractional rate of surface renewal. The system hydrodynamics and geometry affect the value of s.

The absorption coefficient computes to

$$k_L^o = \sqrt{\mathcal{D}_A s}. \tag{2.6}$$

If $1/s$ is considered to be the average life of the elements, Equation 2.6 takes the form of Equation 2.4, with a different distribution of surface ages about the mean value.

The surface renewal model is perhaps the most realistic, but all three models have been shown to give close agreement in their predictions of the effect of chemical reaction and physicochemical factors on absorption rates [47].

Theory development continues; several newer models have been proposed (e.g. film-renewal, potential flow, surface rejuvenation, molecular and eddy diffusivity) and reviewed [44, pp. 62-64], [48].

2.1.2 Mass Transfer with Chemical Reaction

When the concentration of the liquid phase reactant is practically equal in the bulk and in the vicinity of the gas-liquid interface, and is much larger than the concentration of

the absorbing gas, simultaneous diffusion and chemical reaction can be expressed as:

$$\mathcal{D}_A \frac{\partial^2 c}{\partial x^2} = \frac{\partial c}{\partial t} + r(c)\,. \tag{2.7}$$

In Section 2.1, step 3 cites chemical reaction of the dissolved gaseous reactant within the liquid phase, but is indeterminate about its rate relative to the rate of absorption and about the proximity of its occurrence relative to the gas-liquid interface. The characterizations of the possibilities are many, but may be limited to three practical reaction regimes [42]:

(a) Slow

(b) Fast

(c) Instantaneous

A **slow** chemical reaction can be defined as one where the amount of gaseous reactant consumed within the liquid film is negligible compared to the amount which diffuses through (film theory), or where the reaction is negligible during the life of a liquid surface element (surface renewal theory). In this case the chemical absorption coefficient, k_L, is equal to that for physical absorption, k_L^o.

A system operating in this regime with chemical reaction rate much greater than absorption rate can have the absorption rate enhanced through increases in both the absorption coefficient and gas-liquid interfacial area. When the rate of chemical reaction is much less than that of absorption, the over-all rate is independent of k_L^o and a but depends on the reaction rate; rate improvement would require catalysis or other factors making the kinetics more favourable.

A **fast** chemical reaction is a reaction which occurs to an appreciable extent during the element life. The term $r(c)$ is much larger than $\partial c/\partial t$ and the reaction is sufficiently fast to keep the bulk liquid concentration C^b practically equal to the equilibrium concentration C^*.

The total absorption rate does not depend on δ, t_e or $1/s$, *i.e.* it is independent of the hydrodynamic conditions of the liquid phase. It is independent of k_L^o but depends on a and the reaction rate.

A reaction which takes place in the liquid phase such that neither the gaseous nor liquid-phase reactant can coexist in the same region is termed **instantaneous**. The two reactants diffuse through the liquid film to a reaction plane a distance λ from the gas-liquid interface. Equation 2.7 extends to:

$$\mathcal{D}_C \frac{\partial^2 c}{\partial x^2} = \frac{\partial c}{\partial t} \tag{2.8}$$

$$\mathcal{D}_B \frac{\partial^2 b}{\partial x^2} = \frac{\partial b}{\partial t}. \tag{2.9}$$

This leads to

$$-\mathcal{D}_C \left(\frac{\partial c}{\partial x}\right)_{x=\lambda} = \frac{1}{q}\mathcal{D}_B \left(\frac{\partial b}{\partial x}\right)_{x=\lambda} \tag{2.10}$$

for the surface renewal theory or

$$\mathcal{D}_B \frac{B^b}{\delta - \lambda} = q\mathcal{D}_C \frac{C^I}{\lambda} \tag{2.11}$$

for the film theory, where q describes the stoichiometry (moles of liquid-phase reactant per mole of gaseous reactant).

The absorption rate in the instantaneous regime is dependent upon both k_L and a and of course is independent of the reaction rate.

2.1.3 Optimization

It is seen in Equation 2.1,

$$R = k_g a(P^g - P^I) = k_L^o a(C^I - C^b),$$

that the rate R of transfer of gas into a liquid is the product of three terms: the absorption coefficient, the interfacial area across which the gas is transferred, and the driving force presented by the difference in concentration.

Recalling the result of Dreisinger and Peters in Section 1.2.1.3 that an increase in the rate constant for oxygen absorption,

$$R_1 = k_L^o \cdot a \cdot (C^I - C^b), \tag{2.12}$$

would yield the greatest benefit in the oxidative pressure leaching of sphalerite, each of the three terms is subject to optimization.

The concentration gradient is of course exploited through the use of oxygen overpressure: the difference between the concentration of oxygen at the interface (C^I or $[O_2]^I$) and in the bulk liquid.

The absorption coefficient and interfacial areas may be addressed through principles of mixing and agitation. It should be possible to realize an increase in the rate of Equation 2.12 by creating turbulent shear to reduce the thickness of the liquid film; through the increase in gas-liquid interfacial area, *i.e.* more bubbles and/or smaller bubbles per given gas rate; and by lengthening the time of passage through the slurry before the gas bubble escapes.

2.2 Mixing and Agitation Theory

The industrial practice of mixing and agitation is applied to many operations, ranging from the simple bulk mixing of two dissimilar liquids, to promotion of chemical reaction and heat and mass transfer, to the more complex three-phase systems where solids suspension, gas entrainment and interphase contact must be achieved simultaneously.

In these complex systems the optimization of one function may be at odds with that of another: an improved agitation system for solids suspension might provide inferior gas dispersion. While this stands as an impediment in the pursuit of more universal design criteria, it should not prevent study into the fundamentals of the individual objectives, which may then be extended carefully into problems of greater dimension.

2.2.1 Early Work

The first detailed studies into agitation centred on impeller power consumption in liquid mixing, as this was needed to size the motors and drives for design purposes. With the extensive data generated by White *et al.* [49] with paddle agitators, White and Brenner [50] used dimensional analysis to correlate power to significant variables[1] with the form[2]

$$\frac{P}{\rho_L N^3 D^5} = K \left(\frac{\mu}{ND^2\rho_L}\right)^a \left(\frac{W}{D}\right)^b \left(\frac{H_L}{D}\right)^c \left(\frac{T}{D}\right)^d \tag{2.13}$$

where the term $ND^2\rho_L/\mu$ is a modified Reynolds number. The results reduced to

$$P = 0.000\,129 \left(\frac{ND^2\rho_L}{\mu}\right)^{0.86} N^2 D T^{1.1} W^{0.3} H_L^{0.6} \mu \tag{2.14}$$

or after rearrangement,

$$P = 0.000\,129\, N^{2.86} D^{2.72} T^{1.1} W^{0.3} H_L^{0.6} \rho_L{}^{0.86} \mu^{0.14} \tag{2.15}$$

with P being the power requirement of the impeller in Hp; N the agitator speed in rev/sec; D the impeller diameter, T the tank diameter, W the impeller width and H_L the liquid height from tank bottom, all in ft; ρ_L the density of the liquid being mixed in lbs/ft^3; and μ the absolute viscosity of the liquid in lbs/sec-ft.

Hixson and Luedeke [52] measured the friction drag at the tank wall for liquids of varying viscosities, and examined the effects of turbine impeller pitch and clearance and liquid height. They grouped the length dimensions and their correlation was similar to that of White and Brenner.

Hixson and Baum [53] later measured the power input to the impeller. A wide range of variables was evaluated, but each independently of the others. Stoops and Lovell [54] began with a modified correlation which included a Froude number, $Fr = N^2D/g$, though

[1] Nomenclature for variables relating to mixing vessels and impellers is defined in Figure 2.1.

[2] Thomson in 1855 first related the work consumed in friction of a rotating disc by $P = k\,N^3D^5$ [51].

Figure 2.1: The Mixing Vessel and Impellers

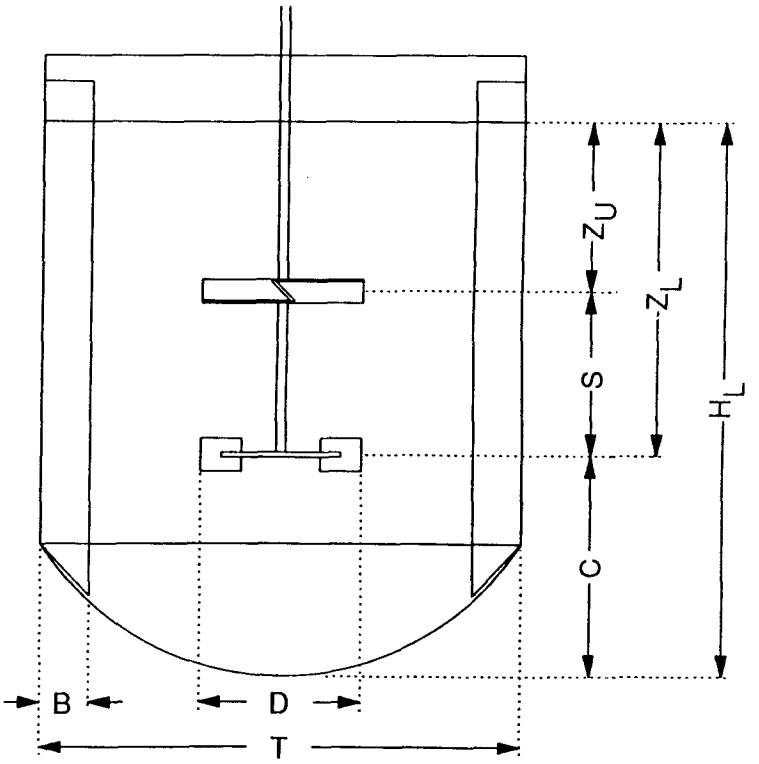

Following recommended nomenclature for mixing [55].

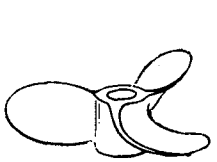

marine propeller

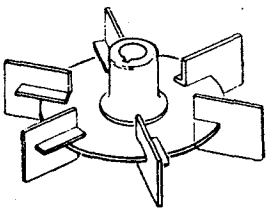

radial disc
(Rushton) turbine

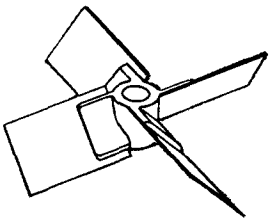

axial turbine
(pitched blade)

Figures from Oldshue [56].

their data with a marine propeller gave the term an exponent of zero. They also found liquid height and off-bottom clearance to have negligible impact on power consumption.

Miller and Mann [57] studied the mixing of two immiscible liquids. They introduced an agitator power function ϕ_μ,

$$\phi_\mu = \frac{P}{\rho_L N^3 D^5} \cdot Re \tag{2.16}$$

and used the 'mixing index' concept [58] to evaluate not only the power requirement but also the degree of mixing achieved by several different impeller types and settings.

Hixson and Baum found it necessary to compose a cluttered 'correction factor' graph to make their mass of results predictive for a change in two or more variables [53]. Hooker [59] attempted to correlate the data published up to 1948 for axial, tangential and radial flow impellers but, likewise, still was forced to generate a series of design factor constants to account for blade geometry plus the effects of tank diameter and liquid depth.

Rushton, Costich and Everett [60,61] recognized some of the shortcomings of these pioneering methods. Most investigators used several different impellers and settings but, as Table 2.1 shows, offered a correlation only to one 'standard' impeller[3] and configuration, thus much of their data was not represented, nor did each conform to an identical 'standard'. They too saw advantage in using an agitator power function, and wrote theirs to include the Froude number but not the Reynolds number (to isolate the functional dependence upon Re). The term Po,

$$Po = Pg/\rho_L N^3 D^5 \tag{2.17}$$

was called the 'power number'[4], and is a measure of inertial forces and basic flow patterns.

[3]White *et al.* did account for paddle dimensions, Equation 2.15.

[4]The power number was originally denoted by the symbol N_P.

Table 2.1: Summary of Exponents to Original Power Correlations

Investigators, year	std. impeller: pitch, blades	k x 10^5	Exponents to: N	D	ρ_L	μ
White *et.al.*, 1934	90° 2-flat	12.9	2.86	4.72	0.86	0.14
Hixson & Luedeke, 1937	45° 4-flat	···	2.8	4.6	0.8	0.2
Hixson & Baum, 1942	45° 4-flat	6.34	2.88	4.76	0.88	0.12
Stoops & Lovell, 1943	3-prop	3.16	2.8	4.6	0.8	0.2
Miller & Mann, 1944	90° 2-flat	5.74	2.78	4.56	0.78	0.22

Correlations of the form $P = kN^a D^b \rho_L^c \mu^d$, in Hp.
All investigations in right-cylindrical flat-bottomed unbaffled mixing vessels.

They defined $\Phi = Po \cdot Fr^n$ where

$$n = \begin{cases} 0 & \text{with baffles,} \\ 0 & \text{without baffles and } Re < 300, \text{ and} \\ \frac{(\log Re) - a}{b} & \text{without baffles and } Re > 300. \end{cases} \tag{2.18}$$

When required, the exponent n of Fr was found by plotting the logarithm of Re *vs.* the slope of the lines of a plot of Po *vs.* Fr for a particular impeller at constant Re. Thus a and b are empirical constants for a specific impeller. It was found that a (and hence, n) varied with the impeller-to-tank diameter ratio D/T.

Using Φ instead of the power measurement as the ordinate in the usual log-log plots *vs.* Re, they could plot literally hundreds of test results on a single chart. While this technique greatly simplified the graphical presentation of design data[5], it required a significant amount of calculation to produce the value of Φ for a given configuration.

Others later modified Po to correlate to the number of impeller blades [62], and extended it to account for impeller blade geometry [62,63,64]. In the last case, Nagata

[5]The graphs from [60] still appear in the *Chemical Engineers' Handbook.*

and co-workers developed a remarkably complex relation:

$$Po = \frac{a}{Re} + b\left(\frac{10^3 + 1.2Re^{0.66}}{10^3 + 3.2Re^{0.66}}\right)^p \left(\frac{H_L}{T}\right)^{(0.35+\frac{W}{T})} (\sin\alpha)^{1.2} \tag{2.19}$$

with

$$a = 14 + \frac{W}{T}\{670\left(\frac{D}{T} - 0.6\right)^2 + 185\}, \tag{2.20}$$

$$b = 10^{\{1.3 - 4\left(\frac{W}{T} - 0.5\right)^2 - 1.14\left(\frac{D}{T}\right)\}} \tag{2.21}$$

and

$$p = 1.1 + 4\frac{W}{T} - 2.5\left(\frac{D}{T} - 0.5\right)^2 - 7\left(\frac{W}{T}\right)^4. \tag{2.22}$$

Nagata and co-workers continued their study of one-phase systems. They evaluated the flow patterns within unbaffled [65] and baffled tanks [66], and from a Rushton-Oldshue relation [67] developed the discharge number for impellers,

$$N_D = Q_L/ND^3, \tag{2.23}$$

where Q_L is the volumetric flow rate of liquid from the impeller.

The general thrust of this initial body of research, though extensive and meritorious, suffered from two major limitations in scope:

- Work was restricted almost entirely to liquid mixing; aeration from the freespace was prevented through the use of baffles and/or curtailed impeller speeds. This precluded the application of results to gas-liquid mixing, or even the results of unbaffled testwork to baffled systems;

- Correlation of data into dimensionless groups could never account for all variables and this hindered insight into the fundamental factors of mixing. Power input was the usual objective function, but good experimental designs were rare. 'Standard' configurations were adopted and while they facilitated the comparison of different investigations, they prevented examination of the interaction of the many variables that exist in mixing and agitation systems.

2.2.2 General Directions of Later Work

Three areas of investigation of profound importance in mixing applications have been: the effect of dispersed gas on impeller power consumption; the existence of a critical impeller tip speed for effective gas distribution; and the nature of gas behaviour at the impeller and the distribution of bubbles throughout the vessel.

2.2.2.1 Power Consumption in Aerated Systems

When an agitator disperses gas in a liquid, it consumes less power than in an identical but gas-free system as was first demonstrated by Cooper *et al.* in 1944 [68]. The magnitude of this reduction depends on impeller type, tank geometry, physicochemical properties of the liquid and gas sparging rate. The difference in effective density is obvious, but simple replacement of ρ_L in Equation 2.17 with the density of the dispersion ρ_D is insufficient to account for the entire reduction, since ρ_D is not uniform throughout the dispersion and is usually lowest at the impeller [69]. Thus, Rushton-type correlations to a Reynolds number can no longer be used for gas-liquid systems.

Many investigators have proposed correlations to account for this reduction. Ōyama and Endō [70] developed the flow number[6], $Fl = Q_G/ND^3$, analogous to Nagata's subsequent N_D but with Q_G the volumetric gas sparging rate. Michel and Miller [71] correlated impeller power to impeller speed and the gas rate in sparged systems. They fitted their data and that of three others to

$$P_g = c\left(\frac{P_u^2 N D^3}{Q_G^{0.56}}\right)^{0.45} . \tag{2.24}$$

The coefficient c accounted for the impeller and other geometric factors. They demonstrated that a plot of P_g/P_u *vs.* Fl is discontinuous—a clustered family of curves for each Q_G arises instead—but this result was largely ignored.

[6]This was originally called the Aeration Number, N_A.

Uhl *et al.* [72] found their data fit Equation 2.24 if P_u was used in place of P_u^2. Brown [73] found his own data fit

$$P_g = \alpha P_u \cdot \exp(-\beta Q_G) \tag{2.25}$$

and Equation 2.24 within similar error. However, the constants α and β were empirically derived from his data so his correlation is descriptive only.

Effect of Solution Properties

Michel and Miller found interfacial tension had an unpredictable effect on power consumption of gassed liquids with different Weber numbers ($We = N^2D^3\rho_L/\sigma$) [71], while Lee and Meyrick [74] and Bruijn *et al.* [75] each observed little effect on power, only on bubble size, which suggests an effect on the bubbles which break away from the impeller cavities but not on the cavity structure itself. Hassan and Robinson [76] proposed

$$P_g = c_1 P_u\, We^m\, Fl^{-0.38} \left(\frac{\rho_L}{\rho_D}\right) \tag{2.26}$$

where the constant c_1 depended on impeller type, tank size and ionic nature of the liquid, while the exponent m varied only with impeller type. But since the density ratio is related to gas hold-up ϵ_G, power consumption cannot be predicted without knowledge of ϵ_G. This requires another correlation which includes gas flow rate and surface tension.

Impeller clearance C/H_L was always held constant by each author, yet varied amongst authors: 0.67 [71], 0.175 [72] and 0.33 ($D/3$) [73,76]. It was later shown that P_u depends on the clearance [77] and liquid height H_L/T [78].

2.2.2.2 Critical Tip Speed

Research into gas-liquid systems began to correlate superficial sparged gas velocity v_s, agitator speed N and volumetric power input ϵ_T ($\equiv P/\epsilon_L V$) to $k_L a$. This shifted the objective function from a process requirement to the process result.

Westerterp *et al.* [79] fixed the vertical position of the impeller at $C/T = \frac{1}{2}$ and varied the liquid height H_L. At constant N their volumetric mass transfer term decreased with increasing H_L; when plotted as $(k_La\big|_{H_L=T})/(k_La)$, it varied linearly with H_L/T.

They also studied the creation by agitators of interfacial area and found two regions: a sparging regime below a minimum agitation rate N_oD where area depends only on sparger design and gas velocity; and an agitation regime above N_oD, where area depends only on the stirring rate. A plot of mass transfer rate *vs.* N shows the transition; extrapolation of the linearly dependent (agitation) regime to the abscissa yields N_o. In the agitation regime the superficial gas velocity has no effect, since the volume of gas circulated in the dispersion [80] or that provided by surface aeration[7] [81] was shown to be about an order of magnitude larger than that supplied by the sparger at $N = 1.8N_o$.

They proposed the relationship

$$k_La \propto (N - N_o)\, D \left(\frac{T}{H_L}\right) T^{-0.5} \tag{2.27}$$

and further correlated the minimum agitation speed N_o to

$$\frac{N_oD}{(\sigma g/\rho_L)^{0.25}} = A + B\left(\frac{T}{D}\right) \tag{2.28}$$

where A and B are constants characteristic of the impeller. They intrepreted Equation 2.28 to mean πN_oD should be at least 8 to 30 times higher than the rising velocity of gas bubbles for a good dispersion.

The existence of a critical tip speed has been confirmed by Mehta and Sharma [82] and DeGraaf [40]; others have confirmed the result of Equation 2.28 [83,84]. The sparging regime $N < N_o$ was defined as a condition of 'flooding' by Nienow and Wisdom [85].

[7]By definition, *surface aeration* refers to the transfer of gas through the cross-sectional tank interface between the liquid in the tank and the gas above, and is the mechanism associated with (though not exclusive to) baffled tanks. *Vortex aeration* occurs when the forced vortex reaches the impeller allowing gas to be dispersed by contact with the impeller blades; this is the principal form of such transfer in unbaffled tanks. *Gas pumping* agitators may use either or both methods.

Boerma and Lankester [86] extended some of Westerterp's work to an unsparged system, and confirmed Westerterp's claim of a minimum agitator speed for absorption to occur, with absorption rate a function of N_o. They too found N_o to be dependent upon T/D, but also showed a dependence upon H_L by using variable liquid heights.

Westerterp's linking of N_o to gas bubble ascension rate should not apply to an unsparged system, yet Boerma and Lankester also found a dependence upon a minimum tip speed. From this they concluded that aeration from freespace gas, even surface aeration in a baffled tank, contributed far more to mass transfer than sparged bubbles.

In concert with the observations on the volume of gas being circulated relative to that being sparged, this suggests the impeller is most effectively used for both the dispersion *and* entrainment of gas.

2.2.2.3 Gas Deportment and Distribution with Impellers—Baffled Vessels

The distribution of sparged gas has now been studied extensively ([69,75,83], [87] to [92]). The phenomenon consists of the bubble behaviour about the impeller, the flow and discharge from the impeller, and the distribution of the gas-liquid dispersion throughout the mixing vessel.

Cavity Development and Bubble Deportment—Radial Flow Impellers

De-rotational prisms have been used to produce a stationary image of the rotating impeller [93], and this has permitted the observation of cavity initiation and growth. Greaves and Kobbacy [77] have summarized this mechanism: when gas is sparged to a rotating turbine impeller, it fills the low pressure regions behind the blades, forming gas cavities. The cavity begins at the lower part of a blade back, and will cover the upper part as gas flow increases. If the impeller speed is adequate to cause gas and liquid to flow from both the top and bottom of the blade into the discharge stream, large

gas cavities can then form behind both the top and bottom of the blade, causing some hydrodynamic smoothing of the blade, which decreases the drag effect and reduces the power consumption.

An increase in gas rate leads to full coverage of the blade; with the formation of each cavity there follows a step-wise drop in impeller power. (This is most notable upon the formation of the first three cavities, and less distinct for the final blades.) On the other hand an increase in speed can change the number and shape of the trailing cavities, so that less of the blade is covered by gas and the power again increases.

There is visual evidence of coalescence of sparged gas bubbles into an inner vortex within the cavity, followed by dispersion from a cavity tip or edge [87], due to flow instabilities and turbulence. Four distinct cavity structures have been described for six-blade Rushton impellers [95]: (a) small *vortex cavities*, which cling to the blade at higher gas rates; gas is dispersed from the vortex ends; (b) larger *clinging cavities*, with gas departing from the cavity edge; (c) *ragged cavities*, with gas broken away from the trailing end; and (d) a highly *stable* alternate larger-smaller structure where gas is again dispersed from the trailing end.

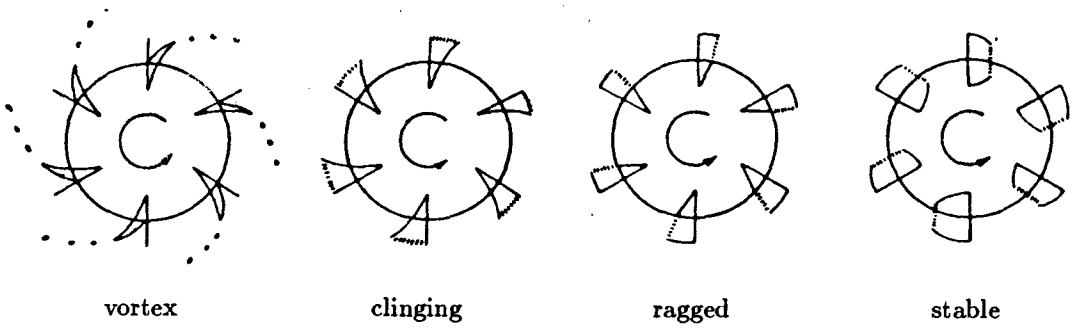

Figure 2.2: Characteristic Cavity Shapes Behind the Impeller Blades
From Nienow, Konno and Bujalski [94].

There exists some uncertainty about the nature of cavity development, however. For large Q_G and small N the progression follows (a)–(b)–(c) as the flow number Fl increases. There is a drop in power as the impeller becomes flooded at (c). But for small Q_G and large N the impeller should always be able to disperse sparged gas and will not flood; the progression with Fl then follows (a)–(b)–(d)–(c) with a step *increase* in power at (c), thought to be due to the decreased blade coverage by ragged cavities[8].

Most of the researchers attempted to describe these mechanisms in terms of the Fl group. But the number of large cavities was shown to be a function of the impeller diameter [75], and since gas reaches the cavities not only by sparging but through recirculation from the bulk liquid and from surface aeration as well, the gas sparging rate Q_G does not always describe total gas feed. Thus the power and gas dispersion phenomena of an impeller are a very complex function of N, D, and total gas flow, and are insufficiently described by correlations to Fl, which had been the conclusion of Michel and Miller much earlier.

The impeller blade region has long been considered to be the area of greatest mixing [96,97,98]. Though it occupies only a small fraction of the vessel volume, it also may be the site of most of the gas-liquid mass transfer for certain systems. The absorption of an ammonia-air mixture by dilute HCl with indicator showed initial colourization only in the impeller vortex region, but not in the vicinity of the sparger orifice nor in the remainder of the tank [83]. A similar result was found earlier for the absorption of chlorine by benzene [99][9].

[8]A cavity 'stability map' has been proposed [92] for an $N-Q_G$ plot, but even this must be interpreted with a companion $Po_g/Po_u - Q_G$ graph.

[9]It must be recognized that since both chlorine and ammonia are much more soluble in said solvents than is oxygen in sulphuric acid solutions, the interfacial area in the impeller region of a pressure leach autoclave will not be so dominant or exclusive a reaction site.

Cavity Development and Bubble Deportment—Axial Flow Impellers

Since axial flow impellers have been restricted mainly to blending operations, little attention was paid to their gas pumping capacity until very recently [100,101,91,102].

The cavity types with downward pumping axial impellers are quite similar to radial disc impellers [91]. The cavities attach towards the outer part of the blade and ultimately grow inward, to about the blade mid-point, as they become more stable. They follow a rough (a)–(b)–(d) progression, where the vortex (a) and clinging (b) cavities are long and trailing, while the stable (d) cavity ends more abruptly. In all instances gas is dispersed from the trailing end of the cavity. The power drop at (d) is much sharper than for radial flow impellers, since stable cavities for the radial impeller develop more gradually and are subject to more interaction between cavities.

Gas sparged from beneath an axial impeller approaches it in two ways. For large N and small Q_G the strong downward flow beneath the impeller sweeps the bubbles outward, and they will reach the impeller from above only if recirculated liquid carries them there. At smaller N and larger Q_G the ascending bubbles can overcome the downward flow and rise into the impeller region *directly*, in addition to whatever contribution from recirculation occurs above.

This transition has been shown to correlate very well with blade pitch angle at $\alpha = 30$, 45 and 60° by

$$N_T \sin\alpha = c_S Q_G^{0.5} ; \tag{2.29}$$

gas supply becomes 'direct' with an increase in Q_G, while the constant c_S becomes smaller (*i.e.* a larger Q_G is required) as the sparger is moved further beneath the impeller [91].

Upward pumping axial impellers have been the subject of less study. A maximum in power number is observed when recirculation loops (reaching the impeller from below) are formed. Cavity formation has not yet been well-documented [101].

Distribution Within the Vessel

The macroscopic distribution of sparged gas by radial disc impellers was defined [89] as progressing through five stages, at constant Q_G and increasing N (or N constant and Q_G decreasing from a large value): (a) N too small to disperse any gas; (b) mild dispersion only above the impeller plane, similar to a bubble column ('flooded' impeller); (c) circulation above the impeller plane but with little or no movement below; (d) circulation throughout the vessel ('loaded' impeller); (e) formation of secondary circulation loops depending upon vertical positioning of the impeller.

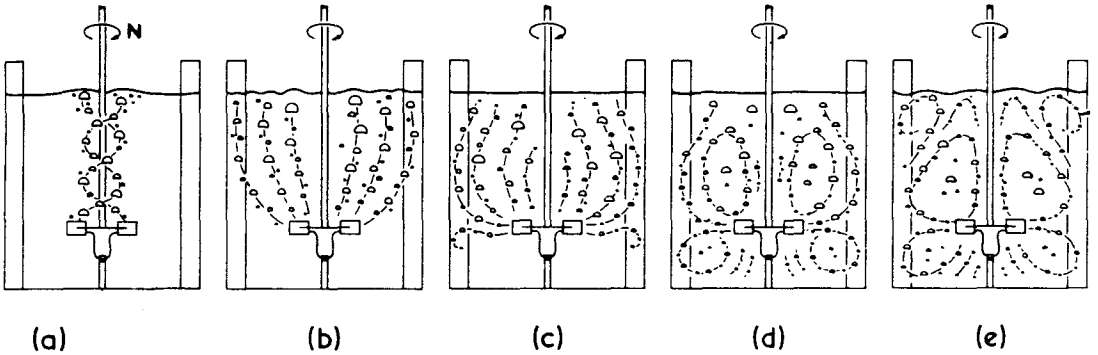

Figure 2.3: Bulk flow patterns with increasing $N \rightarrow$ or decreasing $Q_G \leftarrow$.
From Nienow, Wisdom and Middleton [89].

The degree of recirculation was described as a step function dependent upon the existence of recirculation loops below and above the impeller [90]. However, evidence in that paper suggests recirculation commences with the emergence of the first triad of large cavities. Once this occurs, the degree of recirculation would then become a function of the impeller speed required to establish the flow loops, and the vertical positioning of the impeller which modifies those flow loops. The effect of impeller speed was illustrated therein [90], and subsequent work by the principals [103] has demonstrated the important effect of vertical positioning.

A good treatment of the patterns of liquid flow in a baffled stirred tank was given by Reed *et al.* [104]. Small, neutrally buoyant spheres were tracked using laser Doppler

anemometry with optical frequency shifting. This technique is superior to previously used methods which required insertion of measuring devices (pitot tubes, flow propellers, conductivity meters); which were unsuitable for the high turbulence intensities at $Re > 10^6$ (hot wire and hot film anemometry); or which biased against negative velocities (conventional LDA). A number of (r, θ, z) maps for the velocity profiles were presented which illustrate the complex, pronounced three-dimensionality of the flow; the observed flow of some bubble streams assisted in the practical interpretation.

Surface Aeration

The results cited in Section 2.2.2.2 [81,79,86] indicate surface aeration may be very useful, yet relatively little attention has been paid to this process. Its mechanism in baffled vessels has been summarized generally [105,106]: gas is drawn in at the surface by cylindrical eddies; bubbles detach from the surface vortices which form; the entrained bubbles then are carried down to the impeller region by circulating liquid. As impeller speed increases, the eddies become stronger and draw more gas, and circulation velocities increase as well. The number of bubbles increases, as does the average diameter (although this effect is less pronounced in electrolytes). As expected, power consumption drops as stable clinging cavities develop behind impeller blades.

The rate determining step is the ability of the circulating liquid to carry the gas to the impeller. If sparged gas is added to the system it will (a) reduce the discharge capacity of the impeller and (b) induce quite different flow patterns in the vessel. The bulk upflow of the sparged gas may physically oppose downflow from the surface. Nienow and coworkers [107,108] claimed typical gas sparging rates can reduce the surface aeration rate to neglible levels, but this was only true when their impeller tip speeds were slower than the industrial norm (about 2.0 m/sec). In fact, their data[10] indicate the surface aeration

[10]Cf. Figure 2, p. 987 [108].

rate may be as high as 28 per cent of the sparging rate at the more realistic tip speed of 4.0 m/sec, and that this value will continue to *increase* with N.

Earlier work also reflected such a trend with N. Reith and Beek [109] proved freespace gas was drawn down and then became mixed with sparged gas bubbles by coalescence. The volumetric fraction of freespace gas in the dispersed bubbles increased with N but decreased when v_s was increased. The data of Fuchs *et al.* [110], though confounded by severe geometric dissimilarity, showed the same increase with N though they did indicate a diminishing contribution from the freespace with increasing vessel scale. Nonetheless, under these conditions the impeller still is able to overcome the effects of the sparged gas.

Clark and Vermeulen [111] found the onset of surface aeration depended upon impeller location:

$$N_{SA1} = c_2 \frac{T}{D} \left(\frac{H_L}{WD}\right)^{0.5} \cdot \left(\frac{H_L}{C}\right)^{0.33} . \tag{2.30}$$

Greaves and Kobbacy [105] found smaller impeller diameters required larger impeller speeds (both in Hz and m/sec) to detach bubbles from the surface vortices. They suggested

$$N_{SA1} = c_3 \left(\frac{H_L T}{D^3}\right)^{0.67} \cdot \left(1 - \frac{C}{H_L}\right)^{0.33} \cdot \left(\frac{\mathcal{P}}{\mathcal{P}_a}\right)^{-0.13} \tag{2.31}$$

where c_3 is specific to the electrolytic nature of the liquid, and $\mathcal{P}$ and $\mathcal{P}_a$ are the vessel operating and atmospheric pressures. Heywood *et al.* [106] defined two other critical tip speeds in this phenomenon: N_{SA2}, where bubbles are first drawn into the impeller region; and N_{SA3}, the point at which Po drops with increasing Re. They could correlate each N_{SA} to D, T, C and H_L, but each impeller or different electrolyte required a different correlation, with vastly different exponents.

2.2.2.4 Flow Phenomena and Vortex Characteristics—Unbaffled Vessels

The height of the free surface of the vortex can be related to the impeller Froude number by

$$\frac{Z_v}{D} = c_4 \left(\frac{N^2 D}{g}\right), \tag{2.32}$$

where Z_v can be the height of the vortex below (Z_b) or above (Z_a) the static gas-liquid interface, or the total vortex height $Z' = Z_b + Z_a$. Tsao's log-log plots of Z'/H_L *vs.* N aligned well to a slope of 2 for water and simple polar solvents, but the slope changed to 2.5 for glycerol and sulphuric acid, at about $\nu > 0.01$ cm^2/sec and $Re < 3500$ [112]. This less turbulent range could be accounted for by multiplying Equation 2.32 by $Re^{0.5}$. Alternatively, Zlokarnik [113] fit all his low- and high-viscosity data with the help of the Galileo number ($Ga = Re^2/Fr = D^3 g/\nu^2$),

$$\frac{Z_v}{D} = c_5 \left(\frac{N^2 D}{g}\right) \cdot (0.1 - Ga^{-0.18}) \cdot \left(\frac{Z}{D}\right)^{-0.16}. \tag{2.33}$$

Tsao also proposed that the difference in potential energy between the top edge of the vortex and its base was maintained by the continuous conversion of the kinetic energy of the impeller into potential energy. Hence the energy balance is

$$Z' \rho_L g = \tfrac{1}{2} c_6 \rho_L (\pi N D)^2, \tag{2.34}$$

which yields

$$Z' = \frac{c_6}{2g} (\pi D)^2 N^2, \text{ or} \tag{2.35}$$

$$N = c_6 \sqrt{\frac{Z' 2g}{\pi^2 D^2}}. \tag{2.36}$$

A plot of potential energy *vs.* kinetic energy (Equation 2.34) will give unity slope ($c_6 = 1$) for the ideal case of perfect conversion of energy. Tsao found some departure from unity depending on impeller size, but his data are not well documented *vis-à-vis* impeller

position, and are only cursory in scope. Equation 2.36 thus will define the impeller speed N_V at which the vortex reaches the impeller, $Z' = Z_a + Z$. This has been illustrated by theory and experiment [114,115].

Nagata *et al.* [116] defined the onset of vortex aeration as $N_V \propto T^{-0.67}$. But they fixed D/T at $\frac{1}{2}$, and the impeller diameter would be a more appropriate variable than vessel diameter. There also was a distinct effect of impeller clearance which was not accounted for.

The 'competition' between gas sparging and freespace aeration as described in Section 2.2.2.3 for baffled systems is resolved somewhat differently in unbaffled systems. Chain *et al.* showed the contribution by vortex aeration in a Waldhof fermenter was some 80 per cent of the total oxygen transfer; the sparged gas supplied the minority [117]. In fact, the central draught-tube (which prevents foaming by promoting spill-over onto the impeller) impeded the success of the vortex. Although Chain wrote very favourably of its promise, vortex aeration never was embraced in preference to sparging.

2.2.3 Effect of System Design Elements on Power and Flow

The collected knowlege of the interrelations amongst power consumption, bubble behaviour and impeller operation presented in Section 2.2.2 has fostered much more detailed study into the effects of the many individual geometric and physical variables in the mixing vessel. These factors define the physical environment in which mass transfer takes place.

2.2.3.1 Vessel Shape

The bulk of research over the last two decades has retained the 'standard' tank configuration which evolved by mid-century. This featured a right cylindrical vessel with a flat bottom, which provided a stable basis of support.

When scaling up from bench-scale to pilot plant through to industrial scale, it is standard practice to fix dimensions to certain ratios to preserve geometric similarity. However, as mixing techniques have become more sophisticated the shape of industrial vessels rarely features a flat bottom, and dish-shaped or rounded-out bottoms are the norm. Zwietering used both flat- and dish-shaped bottoms in his work on solids suspension [118], and an increasing number of investigators are adopting a dish-shaped bottom for laboratory vessels ([73,78,79,84,89,102], [119] to [132]). In the case of pressure leaching the scaling process is made difficult by the unique 'cigar' shape of horizontal autoclaves, especially the bulged end of first compartments[11].

While it is encouraging to see that recent investigations into three-phase systems are being interpreted in terms of the well-studied gas-liquid and liquid-solid phenomena, the continued disregard for vessel geometry effects is unfortunate. The most notable omission in this respect is in the study of gas-liquid mixing, where a thorough comparison has not been reported. The added complexity in fabricating and manipulating dish bottomed mixing vessels for use in the laboratory no longer is so great that future investigations can simply ignore vessel shape effects when generating scale-up criteria. As well, these effects must be better understood, in order to make the vast body of data generated with flat bottomed vessels truly useful for scale-up to vessels of industrial size and shape.

Flat Bottom *vs.* Dish Bottom

The *comparison* of performance of flat and dish bottoms is very limited, and surprisingly the effect on gas-liquid mixing has not been reported in the literature. However, in the work that has been done the influence of these geometries on power consumption, and the interrelation with other physical parameters has been demonstrated. Novak *et al.* [128] used three- and six-blade axial turbines to stir only liquid in unbaffled vessels and

[11]Vertical autoclaves, in comparison, are very well-served by a dish-bottomed model.

found power consumption lower for dish and cone bottoms than for flat. Zwietering [118] reported the impeller speed required to 'just suspend' solids off the bottom of the vessel, N_{JS}, to be lower for a dish bottom for two-blade paddle impellers but practically equal for marine-type propellers. Cliff *et al.* [127] used a marine propeller in a flat-bottomed tank with a dish insert and found N_{JS} was lower with the dish when the impeller was $C/T = \frac{1}{3}$ from the tank bottom, but was comparable when the impeller was lower. The dish case consumed more power, especially at the lower clearance. As well, dropping the clearance in the flat bottomed tank required lower N_{JS} and power, while with the dish this was reversed, suggesting a narrower effective T in the dish.

The smaller tanks of Westerterp *et al.* [79] had flat bottoms while their larger tanks had dish bottoms, but the authors chose not to consider this in any difference between test results. Connolly [121] designed from a smaller dish-bottomed tank to a larger flat-bottomed tank to demonstrate the universality of certain scale-up principles. The power savings realized by using fillets (either built-in or from settled solids) in flat-bottomed tanks was illustrated by Oldshue [56].

2.2.3.2 System Geometry

Impeller Location—Off-Bottom Clearance

The 'standard' mixing tank uses a liquid height H_L equal to T, the tank diameter. The impeller clearance usually is at half liquid height, $C/T = \frac{1}{2}H_L = \frac{1}{2}T$. Liquid mixing homogenization time was reported to be minimized at the half-height location [114], although a relation of $C/T = D/T$ often was recommended [133]. Since the standard impeller-to-tank ratio D/T then was $\frac{1}{3}$, this led some investigators to set $C/T = \frac{1}{3}$ and occasionally this is still seen.

The fact it exists as a convention unfortunately has caused most researchers to fix the impeller automatically at half-height and avoid any departures therefrom. Apart from

the results mentioned in Section 2.2.2.2, the effect of vertical location rarely has been examined rigorously. Clark and Vermeulen showed that power drawn falls more and at lower N as a flat-blade impeller is raised from the bottom of the tank [111].

The change in flow patterns induced by impeller position likely is a critical factor. Bates *et al.* [134] duplicated the power drop result for flat-blade and axial impellers in liquid mixing, but obtained the opposite trend for radial disc impellers. It was suggested at lower clearances a simpler flow pattern with less recirculation emerges, and the impeller works against itself much less [135]. For gas dispersal, Nienow *et al.* [89] found $C/H_L = \frac{1}{4}$ to be optimal, as gas was poorly circulated above the impeller at smaller clearances and below the impeller at greater clearances.

Early work by Chain *et al.* [117] offered limited results which indicated impellers in unbaffled vessels closer to the bottom gave slightly better oxygen transfer but at much greater power consumption than impellers at mid-height, beyond speeds of about 6.5 m/sec. It was over 30 years before DeGraaf revisited the subject [40], and showed how oxygen transfer can be related to impeller clearance[12] and tip speed. His work indicated conclusively that power consumption and the minimum tip speed for agitation N_o fall as the impeller is brought closer to the surface.

Some recent liquid-solid studies [135,136,137] suggested qualitatively that lower clearances ($C/T < \frac{1}{5}$) gave more efficient particle suspension (especially as $D/T \rightarrow \frac{1}{2}$). Work on three-phase systems has shown that the clearance giving the minimum ϵ_T is not the same as for two-phase systems [126], and depends greatly on the gas rate [138].

Liquid height

The practice of fixing the off-bottom clearance and increasing the liquid height is similar

[12]DeGraaf used the static gas-liquid interface instead of the tank bottom as his datum, and expressed his results in terms of *immersion depth* (Z).

but not strictly identical. Cooper *et al.* [68] reported an increase in the volumetric absorption rate of oxygen at constant ϵ_T when they increased liquid height above $H_L/T = 1$. Wilhelm *et al.* [99] found the absorption rate of a sparingly soluble gas was linearly dependent upon liquid height above the impeller. They apportioned the total absorption rate at a given volume to two sources: a finite rate delivered by the impeller region, and an incremental (variable) contribution of mass transfer from free bubbles in the remainder of the liquid. These results endorse the use of tall, thin vessels for gas absorption.

Mehta and Sharma [82] observed that k_La *decreased* as H_L/T increased, and increased with C/T up to a critical value, above which there was no longer any effect. This was true both for sparging and surface aeration, although they failed to examine clearances greater than $\frac{1}{2}$. Unfortunately they did not report their power consumption, so it is not possible to determine if their results match with the two earlier groups.

Greaves and Kobbacy [77] observed incidentally that surface aeration in a baffled tank occurred at a lower impeller speed when the C/H_L was raised to $\frac{1}{3}$ from $\frac{1}{4}$. Heywood *et al.* [106] observed that N_{SA1} increased as H_L was increased, more so with axial impellers.

Impeller-to-Tank Diameter Ratio

D/T has been used often as a dimensionless group in correlations (e.g. Equations 2.13, 2.28, 2.30, 2.31) and is frequently investigated. The range usually spans 0.20 to 0.50 (e.g. [71,134,87,73]) although this is by no means restrictive, as values of 0.15 [122] and 0.75 [139] have been reported. The industrial standard is often given as $D/T = \frac{1}{3}$ [133].

The power number relation $Po = Pg/\rho_L N^3 D^5$ defines (at least for a well mixed liquid) the inverse relationship between impeller diameter and speed for a given power delivery. The large D–small N cases often are classed as 'flow-sensitive' mixing systems, and small D–large N cases as 'shear-sensitive'. While these labels are very general, they do describe broadly the action of the impeller on its medium. Liquid mixing, blending

and solids suspension are examples of flow applications, and gas dispersion is an example of a high-shear process.

Most often D/T is discussed only qualitatively, probably due to the difficulty in decoupling the flow/shear effects of an impeller from its influence on bulk flow patterns.

Rushton and Bimbenet [140] showed that their D/T ratio for maximum gas hold-up increased as T increased. Solomon *et al.* [141] found large D/T ratios required much less power to achieve good aerated mixing of highly viscous liquids. Roustan [132] observed that P_g/P_u fell with N faster with larger D/T ratios, and attributed this to the greater ability to recirculate gas bubbles back to the impeller.

2.2.3.3 Impeller Geometry

Smith, van't Riet and Middleton [142] claimed mass transfer in aerated mixing vessels appears to depend only on the dissipation of agitator power ϵ_T and the gas flow rate v_s, and is almost independent of the D/T ratio. But this is misleading, as it suggests insensitivity to impeller size. In fact, the ϵ_T and gas dispersing ability of an impeller are determined directly by the diameter of the impeller and by the flow pattern it establishes.

The ratios for the dimensions of turbine impellers were first given by Rushton *et al.* [60] as D:L:W = 20:5:4, and these have been adopted as the standard. A convention is useful since Po and ϵ_T have been shown to be very sensitive to the minor dimensions of the impeller [62,63,64,143,144,101] (also recall Equation 2.19).

For axial impellers, D:W is fixed at 5:1 for a 45° pitch [145,56,91,146] although an equipment manufacturer gave the projected height to be $D/6$ (*i.e.* D:W = 4.24:1) [121].

Flow Characteristics

Radial flow impellers are used for mass transfer and gas-liquid processes (e.g. contacting

and dispersion) where greater shear and turbulence is required. Axial flow impellers[13] generally are used for the flow-sensitive applications, such as blending, heat transfer and solid-liquid processes, which rely upon discharge from the impeller stream and movement of the bulk vessel contents [56,91].

The power consumption of gassed downward pumping axial impellers fluctuates with the prevailing flow patterns; the impeller must also work against the rising flow of gas. The transition from axial to radial discharge reportedly can be impeded, *i.e.* more gas can be dispersed per given power input, by the use of ring spargers and increased distance between the sparger and impeller [102], and by using six blades and $D/T > 0.4$ [94].

When pumping upward, gas and liquid flows are co-current so energy efficiency is improved. The benefits of six blades, large D/T ratio and ring spargers are claimed to apply to these impellers as well.

Performance Comparisons—Freespace Aeration

Nagata, Yamamoto and Ujihara [65] showed that flat blades are superior to pitched blades for vortex formation in unbaffled tanks, by producing larger tangential velocities. Pitched blades discharge more volume of liquid but the direction of flow is away from the rotation plane of the impeller. Rieger *et al.* [147] showed that six-blade radial, six-blade radial disc, six-blade pitched and three-blade pitched turbines produced more shallow vortex depths in that order. Heywood *et al.* [106] found N_V was lower for radial disc impellers than for axial. They also found N_{SA1} increased as H_L was increased in baffled vessels, more so for axial impellers. Therefore by virtue of their characteristic discharge patterns, radial flow impellers would be expected to be the more efficient at pumping gas from the freespace.

[13]Marine propellers generate axial flow but are rarely used in gas-liquid applications. The term 'axial' impeller will be used here to denote only axial, pitched-blade turbine impellers.

Performance Comparisons—Sparged Gas Dispersion

Disc turbines are less energy efficient than downward pumping axial impellers when suspending solids in unaerated systems [118,148], and upward pumping axial impellers are the least efficient of the three [148]. But a reversal was found when gas was introduced to the system: the renowned ability of the downward axial impeller to suspend solids quickly declined and it approached the results of the disc turbines. This led Chapman *et al.* [138] to conclude that at large gas flows the upward axial impeller may be the best choice when both particle suspension and gas dispersion are required.

This unheralded ability of upward axial impellers to disperse large gas flows applies also to gas-liquid systems. Chapman *et al.* later showed $k_L^o a$ to be a function of ϵ_T and gas flow rate for radial disc and upward pumping axial impellers, but only of ϵ_T for downward pumping axial impellers [149]. They interpreted this to mean the radial disc and upward axial impellers could still effectively disperse additional sparged gas with relatively less additional power. This would disprove the opinion of Oldshue [56], who felt upward axial impellers did not give the required flow pattern for proper gas dispersion.

Warmoeskerken *et al.* plotted the dimensionless mass transfer coefficient $(k_L^o a \cdot V_L)/Q_G$ *vs.* dimensionless gassed power consumption $P_g/\left(Q_G \rho_L (g\nu)^{2/3}\right)$ at $Re > 10^5$ and showed that 45- and 60°-pitch blade downward axial impellers were equal or superior to the radial disc impellers, a remarkable result [91].

This may be explained in part by an observation—on downward axial impellers but which can be extended to upward also—that with the formation of cavities on the blades, axial flow diminishes and the discharge becomes almost completely radial [102].

Other Impeller Types

Chapman *et al.* [101] evaluated a Rushton-type impeller with blades at a 45° pitch. Its flow patterns were similar to the standard 90° model and although it needed to run

slightly faster to distribute the same flow rate of gas, it required less specific power (W/kg) than the standard Rushton, axial up or axial down impellers, and at large gas flow rates (1 v.v.m.) was four times more efficient than the axial down impeller. Pawlek [31] also used this impeller. When mounted on a hollow shaft, it induced substantially more air than its 90° counterpart.

Joshi and Sharma did extensive work with gas-inducing impellers in baffled vessels. The k_La performance at a given ϵ_T was claimed to be 'comparable' to a six-blade radial disc impeller, although their logarithmic plot of k_La obscures the quite inferior results below $\epsilon_T = 5$ kW/m^3 [150, cf. Fig. 18, p. 693]. Interestingly, in many respects the (baffled) gas-inducing impellers behaved as the conventional impeller does in an unbaffled tank. The minimum tip speed for gas induction could be related identically to Equation 2.36 for the onset of unbaffled vortex aeration,

$$N_V = c_6\sqrt{\frac{Z'2g}{\pi^2 D^2}}.$$

Blade Dimensions

Chain *et al.* [117] doubled blade width and obtained oxygen efficiencies (oxygen transfer rate/power consumption) almost identical to their reference impeller. Nagata, Yokoyama and Maeda [63] varied blade length ratios and observed an increase in Po as D/T decreased, or W/D increased. Bruxelmane [151] obtained a power dependence of 1.3 on the width ratio. Bates *et al.* [134] give $P_\alpha/P_{90^\circ} = (\sin\alpha)^{2.5}$ for four-blade axial impellers with blade angle α.

Calderbank and Moo-Young [152] varied the blade areas of six-blade disc turbines at $D/T = 0.27$ and correlated to

$$Po = c_7\frac{LW(D-L)}{D^3}. \tag{2.37}$$

The constant c_7 would appear to account for the system D/T ratio, cf. [73]. A similar

form was used to correlate to oxygen transfer [143,144], where the observed increase reached a break point. This levelling-off was attributed to a minimum bubble size being reached when bubble coalescence became a dominant factor. In the latter work, Hamer and Blakebrough [144] studied at least 36 combinations of blade and disc sizes but did not report their results or trends apart from the $LW(D-L)$ correlation.

Studies into the effect of blade size on oxygen transfer are beset by the same problems which make correlations to the flow number Fl so difficult (Section 2.2.2.3): the impeller is able to disperse gas efficiently by developing shear and flow patterns which can adequately treat the gas stream, but gas flow and impeller discharge are 'competing' factors. Since blade area directly determines the impeller discharge, its effect cannot be isolated easily from the gas flow and impeller speed used in its application. This explains the apparently contradictory results of work from the same laboratory [143, p. A79], [144, Fig. 9], [69, Fig. 7].

Number of Blades

This is a neglected area since the industrial standard has long been the six-blade radial disc impeller. For a baffled tank Po was reported to vary with n to a power of about 0.5 for flat blade impellers [62], about 0.9 for radial disc turbines [151] and about 0.6 for axial impellers [145]. Johnson *et al.* [153] found the increase in k_La by using more blades was more pronounced at lower stirring speeds.

Bruijn *et al.* [75] also showed how the power number increased with number of blades: for their six-blade impeller, $Po = 5.6$; for nine, 8.6; for twelve, 10.0; and for eighteen, 12.0. Thus a twelve-blade impeller must have a diameter $(5.6/10)^{1/5} = 0.89$ times that of a six-blade impeller to run at the same P_u. Their data for sparging indicated that the twelve-blade impeller (with new $D = 0.89$) would pump 2.7 times as much gas as the

six-blade running at the same speed and P_g.[14] They also estimated that the proportion of recirculated gas in the discharge stream was more than doubled with twelve blades instead of six, and that the drop in power with gassing was much less severe [154].

A radial disc turbine with an odd number of blades will exhibit cavity formation similar to the six-blade model described in Section 2.2.2.3. However, for (N, Q_G) conditions leading to the alternating cavities of different sizes, symmetry cannot be established and the distribution amongst the blades changes continuously, leading to a periodic non-axial loading on the impeller shaft [90]. For this reason an odd number of blades is undesirable.

Impeller Discs

Oldshue [56] explained the role of the disc as forcing sparged gas bubbles along a path of maximum liquid contact, and toward the regions of high shear. Nienow and Wisdom [88] stated that it acts as a splitter plate to the flow about the blade. A leading edge separation bubble forms on the blade front, which is a high-pressure region; this would help explain why full-blade turbine impellers without discs draw 20 per cent less power [134]. A full-blade disc impeller draws 40 per cent less power, so clearly there is an effect associated with the disc. As well, there is the obvious complexity of flow induced by not extending the blade inward to the shaft hub. Very few investigators [68,70,118,155] have reported the use of a vaned disc impeller (*i.e.* partial blades beneath a disc of full impeller diameter). Only Yoshida *et al.* [155] gave data on their performance: they were inferior to a radial disc and the deficiency widened as N increased.

The ratio of the disc to the over-all impeller diameter has almost exclusively been reported as $D_d/D = 0.75$, though it has infrequently been set at 0.70 [118,79], 0.67 [99] and 0.65 [156]. Blakebrough [69] even used 0.19 as an extreme but did not discuss its effect. Bruxelmane [151] varied D_d/D from 0.75 to 0.65 but reported only that a

[14]Bruijn *et al.* claimed this value is over three times as great (p. 101) but their calculation, which was not given, must be in error since $Q_G \equiv Fl\,ND^3$.

smaller disc made the impeller more susceptible to flooding (or reduced its gas dispersing capacity). Industrial practice appears to favour 0.67, as this is the recommendation of Oldshue [120,56] and Bowen [157].

Thickness of Material

A reduction in Po for liquid mixing has been observed when thicker gauge material is used for radial disc impellers. The results have been attributed to a reduction in inside edge blade perimeter [139]; to a reduction in size of the leading edge separation bubble and high pressure region at the blade front [88]; and finally to the skin friction and form drag acting on the impeller [158]. This last study correlated mean peak power number[15] to the ratio of disc thickness to impeller diameter:

$$\overline{Po} = 2.5 \left(\frac{x_D}{D}\right)^{-0.2} \cdot \left(\frac{T}{1.0}\right)^{0.065} \tag{2.38}$$

for $0.01 \leq x_D/D \leq 0.05$.

2.2.3.4 Multiple Impellers

Multiple impeller systems are used often in fermentors, and in any vessel which is tall and narrow or requires specific mixing at vertical points.

Results in the literature appear contradictory and are greatly dependent upon system specifications. On the one hand, Rushton *et al.* [156] reported that depending on air flow, power input and impeller spacing, a second impeller could reduce k_La by 50 per cent or increase it by 25 per cent. They suggested dual impellers offer advantages at high v_s or at ϵ_T levels of about 700 W/m^3, and with large liquid heights ($H_L/T \simeq 4$) and impeller spacings ($3 \leq S/D \leq 7$). On the other, the mass transfer coefficient, air

[15]The power number was originally believed to be independent of Re in the turbulent regime ($Re > 10^4$) in a baffled tank with no surface aeration [60,134], but has since been shown to rise about ten per cent to a peak (near the onset of surface aeration), and then subside [89,73,78,158].

utilization and rate of extraction of nickel from matte evaluated by Queneau *et al.* [136] all were better for one radial or one axial impeller than for any combination of the two.

In a similar vein, Oldshue [120] claimed that similar mass transfer coefficients could be obtained if ϵ_T was maintained: that is, an averaging process occurs so that a weaker dispersion from two or three turbines is similar to a more intense dispersion from one. This conclusion was drawn from a $\log - \log$ plot of $K_G a$ *vs.* ϵ_T; unfortunately, some of the data were plotted incorrectly[16]. Though they are confounded somewhat by different system geometries, his data tend to indicate that a dual impeller system gives comparable results only when working in a vessel of double volume and liquid height (*i.e.* same diameter).

Impeller Spacing

A rule of thumb for vertical separation S has long been one impeller diameter [159]. This has been varied often [156,134,120] but results usually are specific to the system (impeller type, D/T, H_L/T) studied, and no universal correlations have emerged.

Power Consumption

Nagata *et al.* [63] found a dual impeller system drew the same power as a single impeller with identical blade area. Bates *et al.* [134] measured P for two ungassed impellers relative to a single flat-blade impeller. For spacings greater than one diameter, two flat-blade impellers drew almost twice the power, and for an axial above a flat-blade, the ratio was about 1.5. A single axial impeller drew one-half the power of the single flat-blade impeller, and two axial impellers drew about 90 per cent of the power.

Combinations of Impeller Types

Kuboi and Nienow [160] reported Rushton (lower) and upward pumping axial impellers

[16]Cf. Table 7 and Figure 13, pp. 18-19 *op.cit.*

(upper) are often used industrially. Oldshue [56] suggested putting most of the power into the lower radial flow impeller, and using one or more axial impellers above to pump the dispersion into the upper regions of the vessel. This was shown to be especially effective for gas distribution in a high viscosity liquid [141].

The 'additivity' rule for no sparging [161],

$$(P_u)_{\text{dual}} = 2(P_u)_{\text{single}}, \tag{2.39}$$

was shown by Kuboi and Nienow [160] to work to within about ten per cent when one or two axial impellers were used, but two Rushton impellers drew 25 per cent less power. It had also been proposed [162,161] that with sparging, the lower impeller will draw the same power as it would alone at the same sparging rate,

$$(P_g)_{\text{lower}} = (P_g)_1, \tag{2.40}$$

and the upper impeller the same power as it would alone in pumping a dispersion with the same gas hold-up,

$$(P_g)_{\text{upper}} = (P_u)_1 \cdot (1 - \epsilon_G), \tag{2.41}$$

but Equation 2.41 was shown to overestimate the power drawn. Downward pumping axial impellers performed poorly, especially at the lower position. Upward pumping impellers tended to discharge gas up to the surface. A lower Rushton and upper upward axial pair produced a hysteresis loop relative to impeller speed, which would produce a loss of gas dispersion and conceivably a loss of solids suspension in a three-phase system. The three combinations listed in Table 2.2 were judged the most efficient. Unfortunately the data were presented in P_g/P_u *vs.* Fl plots at constant gas flow, with a criterion of complete dispersal of gas in the vessel or above the upper impeller, and it is difficult to transfer their results to systems with different gas flows and impeller speeds, which permit surface aeration, or which have particular power requirements.

Table 2.2: Observations on Dual Impeller Performance

Lower	Upper	Comments
Rushton	Rushton	Good dispersion
Axial Up	Axial Down	Dispersion as above at much lower N and P_g
Rushton	Axial Up	Needs larger D/T, P falls when flow pattern changes

From Kuboi and Nienow [160].

DeGraaf's combination [40] for surface aeration drew fifteen per cent more power but its oxygen transfer rate was about four times greater than the sum of the individual impellers working alone in their same location, indicating synergy of flow patterns.

2.2.3.5 Effect of Baffles

Baffles serve to minimize the tangential component of velocity, increase the vertical mixing currents and provide a more homogeneous turbulence distribution. They help to circulate the liquid, delay gas escape and increase contact time, and by increasing turbulent shear contribute to the reduction in liquid film thickness [143].

Hixson and Wilkens [163] were perhaps the first to report the increase in P with the introduction of baffles. As well, they offered the first evidence that four ($T/12$) baffles constitute the so-called 'fully-baffled' condition. Mack and Kroll [119] claimed maximum power input into a mixed liquid could be achieved with only one baffle of width $T/16$, or four with width of only $T/32$. Obviously this represents a different definition of 'full baffling' or the purpose of baffles.

Nagata *et al.* [63] measured P_B/P, the ratio of power with and without baffles. It increased to about 15, then subsided to about 9.5 as baffle width B increased. The peak value occured at $B/T \simeq 1/12$ with six baffles, $\simeq 1/8$ with four baffles, and increased as number of baffles decreased. In the literature, $B = T/10$ is almost universally quoted now

by the European researchers, while $T/12$ is preferred by North Americans, particularly those with ties to industry [156,121].

Bates *et al.* [134] found *Po* was less sensitive to changes in D/T for baffle width $T/12$ than for $T/10$. But this is merely the overlap of similar effects: a wider baffle moves closer to the impeller, while a wider impeller moves closer to the baffle.

An off-centred impeller in an unbaffled tank suppresses tangential flow and the formation of a forced vortex. In this way its effect is akin to that of baffles, with the expected consequence of increased power dissipation. A near tripling in power consumption at equal N was observed for a downward axial impeller at an off-set $e/T = 0.3$. This corresponded to the same power consumption of a fully-baffled tank with a centred impeller [128]. A remarkable feature of this arrangement is the *reduction* in N_{SA1} which results from the initial minor departure from concentricity (typically for $e/T \leq 0.03$). Thus where an impeller is used for surface aeration, a slight off-set from co-axial alignment and removal of baffles may result in better mixing and a reduction in power consumption.

2.2.3.6 Effect of Solids on Gas-Liquid Phenomena

It would be inadequate and unwise to restrict the concern for solids deportment in a three-phase system solely to the actual solid-liquid or solid-gas mass transfer which occurs. Some degree of understanding must be achieved about the impact that solids will have upon gas-liquid processes, to prevent the expectation that such two-phase phenomena will remain entirely unchanged when a solids phase is introduced.

Mehta and Sharma [82] found the addition of solids caused an increase in a, perhaps by decreasing bubble size, and a decrease in k_L^o, attributed to a decrease in interface mobility and interference with surface turbulence. The combination of the two effects can then lead either to an increase or decrease in $k_L^o a$, depending upon the more dominant effect.

Greaves and Loh [78] investigated gas-liquid-solid suspensions and identified distinct rheological regimes depending upon solids concentration. Up to about 30 weight per cent the viscosity increased and larger stable gas cavities formed on the impeller. Between 30 and 40 weight per cent, the suspension became non-Newtonian, and the trailing gas cavities may have coalesced into one large bubble about the impeller. Beyond 40 weight per cent, the suspension was highly non-Newtonian and once formed, the stable gas bubble continued to enshroud the impeller even when the sparger gas was discontinued.

The decreased discharge capacity of the impeller with sparging and the effect of the rising gas on slurry flow beneath the impeller will alter the flow patterns within the tank. Frijlink *et al.* [102] found that at low sparging rates, downward pumping axial impellers transported solids from the bottom of the tank towards the walls and then upward, but at high sparging rates, the pattern reversed, as solids were drawn from the wall to the bottom centre and then up into suspension. In some systems the massive sedimentation of suspended solids is known to occur when a critical gas flow rate is exceeded, e.g. the Port Nickel matte leach [136]. Warmoeskerken *et al.* [129] were able to associate this occurrence with the incidence of the large cavity structure on the impeller. Thus, an (N, Q_G) operating regime which is efficient for gas-liquid contacting might not be suitable for slurry reactors, and adjustments to N and Q_G which are helpful in gas-liquid reactions may prove catastrophic for three-phase processes.

2.2.4 Factors Affecting Mass Transfer

Having gained an understanding of the factors which determine the supply of energy, gas bubbles and liquid flow within the mixing vessel, the final step leading to system design is the study of the effects of the physical environment on mass transfer itself.

2.2.4.1 Interfacial Area

Factors Affecting Bubble size

Vermuelen *et al.* [164] showed that bubble diameter decreased toward the impeller region and with increasing N, and increased as gas hold-up was increased, for air and helium bubbled into CCl_4 ($\rho = 1.595$ g/cm^3).

The results of Benedek and Heideger [165] would place the bubble size dependency at $d_b \propto N^{-0.24}$ if, as they suggested, k_L^o is approximately proportional to $d_b^{0.5}$. The d_b–N result was confirmed by others: Johnson *et al.* [153], who also found d_b independent of v_s; Westerterp *et al.* [79], who observed an intermediate range of N where d_b levelled off before decreasing further; and Pawlek [31], who found the average size decreased with increasing N until a minimum was reached, beyond which a further increase in N had no more effect.

The increase in d_b with gas hold-up may be explained by coalescence caused by the greater bubble density, which increases the frequency of collisions [166].

Factors Affecting Surface Area

Calderbank [167] correlated a to:

$$a = 230 \left[\frac{(\epsilon_T)^{0.4}\rho_L^{0.2}}{\sigma^{0.6}}\right] v_s^{0.5} \text{ cm}^{-1}. \tag{2.42}$$

He noted (as did Lee and Meyrick [74]) that interfacial area changes greatly with position relative to the impeller, and that the distribution of interfacial area near the impeller changes with a change in ϵ_T. Preen [168] observed that disintegration occurred almost exclusively in the impeller region, and coalescence further away, with coalescence the more important in determining the final value of a.

Sideman *et al.* [169] reviewed the correlations for surface area to superficial gas velocity, impeller speed and energy dissipation rate. They found ranges of exponents to

v_s of 0.33 to 0.9; to N of 0.9 to 1.5; and to ϵ_T of 0.35 to 0.40. These values reveal the sensitivities of a one might encounter, although the wide variations reported imply that individual results are very specific to the range of the variables investigated and to the physical characteristics of the system used (impeller type, vessel geometry). For that reason the correlations are not useful for predicting results in non-standard or scaled-up applications.

Matheron and Sandall [170] found a rose both with N and v_s. There appeared to be a minimum agitator speed, 200 rpm, below which a was insensitive to N, but this was only 0.53 m/sec (or $Re < \sim$10,000), while Equation 2.28 suggests the critical tip speed for their system should have been about 950 rpm (2.5 m/sec). Thus their experiments may more closely describe the mass transfer of bubbles rising almost freely in a gently stirred liquid than of those being mixed in an agitated vessel.

Solution Properties

Surface active agents (surfactants) will reduce gas-liquid interfacial tension and thus increase the interfacial area. However, they will establish an interfacial tension gradient which damps internal circulation and reduces k_L^o, so the over-all effect may be an increase or a decrease in $k_L^o a$ [165]. The action of inorganic electrolytes is not as well understood: they increase interfacial tension slightly but *hinder* coalescence, thus providing an increase in surface area. If their concentration is sufficient to decrease the diffusivity of oxygen, they will have a negative effect on k_L^o.

Rennie and Valentin [83] noted the addition of nonyl alcohol to water decreased the bubble size and enabled bubble swarms to exist throughout the tank instead of only in the impeller region. Mehta and Sharma [82] related a to the $-\frac{1}{3}$ power of surface tension. They also found larger values of a for aqueous electrolytes than for non-electrolytes, and for electrolytes with greater ionic strength and viscosity. They interpreted the effect of

viscosity as imparting a higher stability to the dispersion, further reducing coalescence.

2.2.4.2 Mass Transfer Coefficient

The literature contains contradictory results concerning the effect of agitation and power dissipation upon the mass transfer coefficient. It has been reported variously that k_L^o is independent of [81,170], rises with [171,172,173,174,175,176,177] or falls with [82,165, 178,179] stirrer speed.

Calderbank [81] found a dependence only upon liquid phase diffusivity, but not upon agitation, gas hold-up or bubble mean residence time. The dependence upon bubble size was somewhat complex: k_L^o remained constant with diminishing d_b until a critical value was reached, it fell, then ultimately became constant again. The transition region was found for 0.7< d_b <2.5 mm [180]. There also was an indirect dependence *via* diffusivity, which had a step-functional relationship upon bubble size [81, Fig. 4, p. 178]. Although he used energy dissipation rates of up to 5 kW/m^3, it is still possible he may have missed the indirect link through bubble size by not reaching conditions where d_b would decrease with N.

Matheron and Sandall [170] found k_L^o was independent of N but declined with v_s. However, they used only very low values of ϵ_T (probably not in excess of 500 W/m^3). Their maximum agitator speed, 500 rpm, was only 1.33 m/sec (or $Re \simeq$ 18,000), well below the 950 rpm suggested earlier.

The claim of a proportional increase with agitator speed and power consumption has more experimental and some theoretical support. Carpani and Roxburgh [171], Kataoka and Miyauchi [172] and Alper *et al.* [176] found k_L^o proportional to the 2.6, 1.5 and 0.75 power of N respectively (0.87, 0.5 and 0.25 power of ϵ_T). However, this work was done at low tip speeds (below 1.5 m/sec) using the freespace-liquid interface, so ϵ_T never exceeded about 1200 W/m^3. Prasher and Wills [174] worked with slightly greater tip speeds but

also used sparged gas, which reduced their power input below 400 W/m^3. Their functional dependence matched that of Alper *et al.* They recommended the addition of a D/T term for scale-up to help account for the nonhomogeneity of ϵ_T.

Koetsier and Thoenes [173] reported $k_L^o \propto N^{0.9}$ or $\epsilon_T^{0.3}$. Their closed vessel maintained gas hold-up at one per cent; they suggested it had little influence on k_L^o. They proposed the increase in k_L^o was a consequence of higher surface renewal rates caused by the increased intensity of turbulence.

Greater power dissipation was used by Gollakota and Guin [177] and Topiwala and Hamer [175] (up to 8 kW/m^3). The former authors found k_L^o increased as $N^{1.23}$ ($\epsilon_T^{0.41}$), while the latter found an increase as $\epsilon_T^{0.47}$ for weak electrolyte solutions. But stronger electrolytes yielded smaller bubbles and the exponent appeared to fall through zero and become negative.

Calderbank and Moo-Young [180] semiempirically related

$$k_L = 0.13 \frac{\epsilon_T^{1/4} D_L^{2/3} \rho_L^{5/2}}{\nu^{5/12}} \tag{2.43}$$

for mass-transfer of solid particles where turbulent forces exceed gravitational forces. Lamont [181], in his eddy cell model, derived an equation for $k_L^o \propto \epsilon_T^{1/4}$ for mass transfer from gas bubbles, or in any turbulent phase contacting situation. Thus the results of at least two groups [173,176] provide some validation of the $\frac{1}{4}$ power dependence upon energy dissipation rate.

The slight decrease ($\propto N^{-0.12}$) observed by Mehta and Sharma [82, Fig. 23] and Benedek and Heideger [165] may have been artifacts of the bubble size effect just overcoming the power dissipation effect.

Hassan and Robinson [179] more thoroughly investigated the effects of ionic strength. They reported k_L^o to be independent of power dissipation up to about 2 kW/m^3, at which point it fell as $\epsilon_T^{-0.56}$; this result qualitatively explains the inflection at a similar ϵ_T point

for a correlated $k_L a$ term Robinson and Wilke had found earlier [178]. Such a response can be accounted for if one assumes that in the 'independent' region the increase in surface area (and hence, $k_L^o a$) is achieved solely by an increase in gas hold-up, while in the 'declining' region the increased power dissipation contributes to a reduction in bubble size, which causes the characteristic decline in k_L^o reported by Calderbank and Moo-Young [180]. Although their exponent to ϵ_T was practically constant, the relative values of k_L^o increased for solutions of greater ionic strength. While this last feature was at odds with Topiwala and Hamer, who found the opposite effect on k_L^o, the general trend of an inverse relationship with power dissipation in stronger electrolytes appears to be consistent.

The apparent contradictions can be resolved simply enough: obviously the degree of uniformity of power dissipation could serve either to mask or illustrate the dependence on power. For example, a decrease in $\overline{\epsilon_T}$ but more uniform distribution of power dissipation would exert both a decreasing and an increasing influence upon k_L^o. Authors reporting an exponent to ϵ_T greater than $\frac{1}{4}$ possibly may have increased the uniformity of power dissipation at the same time $\overline{\epsilon_T}$ was increased.

2.2.5 Review of Design and Scale-Up Approaches

The basic method for the design or scale-up of mixing and agitation vessels requires identification of a certain condition or conditions which, if maintained at the next scale, should guarantee an identical process result. These scale-dependent conditions have been expressed both as dimensional (e.g. ϵ_T) or dimensionless ratios (e.g. D/T), and are determined through correlations to the objective function of the process.

Because these correlations generally are not derived from fundamental first principles, and are developed from ranges of scale much smaller than those being commissioned, they are prone to extrapolation errors. This often has led to the over-specification of

important, costly elements such as mixers [121].

2.2.5.1 Constant Power per Unit Volume

Maintenance of constant power (or energy dissipation rate) per unit volume, ϵ_T, was long observed in liquid blending and mixing. There now is some debate as to its reliability, as one equipment manufacturer (Connolly, [121]) sided against it while another (Oldshue, [56]) recently endorsed it.

A practical illustration of a deficiency of the ϵ_T method concerns gas hold-up achieved in a sparged vessel (which often is a desirable feature). Experimental evidence showed the fractional hold-up ϵ_G increased with tank diameter even though geometric similarity and ϵ_T were maintained [140].

Since surface and vortex aeration will decrease the power delivered to the vessel contents they are generally regarded as undesirable (*viz.* solids suspension), even though they may prove beneficial for gas-liquid mass transfer[17].

Another difficulty with designing to constant ϵ_T arises from the correlations for power and impeller flow. From Equations 2.17 and 2.23, $P = Po\rho_L N^3 D^5/g$ and $Q_L = N_D N D^3$. Expanding upon an example given by Rushton and Oldshue, and with the term ND being a measure of the shear produced by the impeller, Table 2.3 illustrates that for identical unit power input to a mixing vessel, impeller flow increases nearly ten-fold and shear decreases to one-third its value when impeller diameter is increased by a factor of about five. When tank volume is doubled, the shear values are slightly larger but the impeller discharge is increased only by 12/7. Thus the practice of fixing D/T to preserve geometric similarity will cause a (theoretically) smaller proportion of vessel contents to be discharged by the impeller in the larger tank. An increase in one and decrease in the other of N and D would be required to maintain shear and discharge in the larger vessel.

[17]This might not be true if the reactive gas being sparged is diluted, e.g. air instead of pure oxygen.

Table 2.3: Impeller Flow and Shear at Constant Power

N, rpm	D, relative	P/V, relative	flow Q_L, $= ND^3$	shear, $= ND$
For Vessel Volume = 1, $H_L = T$				
1680	0.44	1.00	139	731
840	0.66	1.00	241	554
420	1.00	1.00	420	420
210	1.52	1.00	731	318
105	2.30	1.00	1273	241
For Vessel Volume = 2, $H_L = T$				
1440	0.55	1.00	238	790
720	0.83	1.00	414	599
360	1.26	1.00	720	454
180	1.91	1.00	1254	344
90	2.89	1.00	2183	261

For right-cylindrical vessels at constant D/T (from Rushton and Oldshue, [67, p. 268]).

2.2.5.2 Constant Impeller Tip Speed

Constant impeller tip speed is a poor design parameter for gas-liquid contacting systems. It was noted in Section 2.2.2.2 that the gas flow rates due to recirculation can be an order of magnitude larger than the feed rate of fresh gas. If an industrial vessel is scaled to a ten-fold increase in diameter, then N must fall by a factor of ten, which will bring the two gas flow rates much closer into balance. This has important consequences when the reactive gas is borne by an inert carrier, e.g. oxygen in air. In the industrial vessel the sparged gas will be less diluted by the (depleted) recirculating gas, but since circulation times will be longer, there is more opportunity for the reactive gas to be absorbed. The gas flow phenomena are not maintained with increasing scale, and this scale-up rule

clearly is deficient. Yield loss in systems with multiple product gas-liquid reactions has been modelled to demonstrate this point [182].

Table 2.4 summarizes the variety of effects that may arise when certain ratios are held constant during scale-up.

Table 2.4: Effect of Scale-Up on Mixing Parameters

Parameter	Pilot Scale 10 ℓ	Plant Scale 10,000 ℓ (geometric similarity)			
P	1.0	125	3125	25	0.2
P/V	1.0	**1.0**	25	0.2	0.0016
N	1.0	0.34	1.0	0.2	0.04
D	1.0	5.0	5.0	5.0	5.0
Q_L	1.0	42.5	125	25	5.0
Q_L/V	1.0	0.34	**1.0**	0.2	0.04
ND (tip speed)	1.0	1.7	5.0	**1.0**	0.2
Re	1.0	8.5	25.0	5.0	**1.0**

From Oldshue [120, p. 4].

2.2.5.3 Constant Torque per Unit Volume

One means by which liquid mixers have compensated for their over-design of P and ϵ_T has been to maintain constant torque per unit volume [121,146]. Bowen [146] gave a defining relation of

$$\frac{\mathcal{T}}{V} = c_8 \frac{Po\,\rho_L N_I^2}{g} \cdot \frac{T}{H_L}, \tag{2.44}$$

where N_I, the agitation intensity, is a semiempirical group $N_I = c_9\, ND \left(\frac{D}{T}\right)^{0.7}$. Then for design, $\mathcal{T}/V$ is held constant and D/T is constant to preserve geometric similarity. With N_I constant and proportional to ND, N will decrease on scale-up. Rearranging Equation 2.44 to yield

$$\frac{P}{NV} = c_{10} \frac{\mathcal{T}}{V}, \tag{2.45}$$

the new ϵ_T (or P/V) is not constant but will decrease as scale increases. Although the inclusion of N_I prevents it from being entirely rigorous, Equation 2.45 does predict the drop in ϵ_T which is encountered by equipment designers.

Wastewater aeration is not regarded as a flow-sensitive mixing operation yet Uhl *et al.* [72] were able to correlate $k_L^o a$ to $\mathcal{T}/V$, which indicates the concept may have an expanded usefulness.

2.2.5.4 'Flooding-to-Loading' Transition Point

The flooding-to-loading transition was proposed as a design criterion: it is now defined either as the impeller speed N_F at which sparged gas no longer ascends through the impeller region (flooding) but is efficiently dispersed throughout the tank by the impeller (loading) [89], or as the (N, Q_G) condition at which the impeller begins radial flow discharge by overcoming the upward axial flow induced by the sparged gas, at $Fl = 1.2Fr$ [92]. It was found by the Nienow *et al.* [89] that the transition depends upon D and v_s, and that at equivalent gas rates, larger impeller diameters prevent flooding at lower specific power inputs; Warmoeskerken *et al.* [92] did not even attempt to account for variation in D/T, and acknowledged that the type and location of sparger exert an influence. More recently the transition was found at lower N as H_L increased [183].

This approach has two deficiencies. First, it ignores the impeller-sparger separation. An increase here may establish secondary circulation loops (which serve to carry the gas bubbles away from the impeller) depending upon the placement of the sparger. Second, the N_F transition is defined by the discontinuity in the plot of the ratio of gassed to ungassed power P_g/P *vs.* the flow number Fl. The problems with using Fl were cited in Section 2.2.2.3. While the power ratio makes for simplified correlation of data, it masks the absolute value of power itself (which is a much more useful design number). If a system is sparged, the power drawn when no gas is delivered is almost irrelevant. The

ratio is sometimes confused for power itself (see [183, p. 376]).

2.2.5.5 Correlations to k_La

Nienow and Wisdom [85] claimed that equal specific mass transfer coefficients are obtained regardless of scale at constant N and Q_G/V. While their data generally are colinear, they do not provide conclusive support since there is a persistent tendency for $k_L^o a$ to increase with tank diameter at equivalent N. Also they failed to examine if the result was independent of impeller clearance.

Smith and Warmoeskerken [184] reported correlations for $k_L^o a$ based on the prevailing cavity structure:

$$\frac{k_L^o a}{N} = 1.1 \times 10^{-7}\, Fl^{0.6}\, Re^{1.1} \tag{2.46}$$

before large cavities have formed, and

$$\frac{k_L^o a}{N} = 1.6 \times 10^{-7}\, Fl^{0.42}\, Re^{1.0} \tag{2.47}$$

after they have formed. Again, this method suffers from its dependence on Fl.

Cooper *et al.* [68] in 1944 were the first to correlate the volumetric absorption coefficient with agitator power consumption and superficial gas velocity:

$$k_La = c_{11}\, \epsilon_T^{\alpha}\, v_s^{\beta}\,. \tag{2.48}$$

van't Riet [185] reprised his earlier comment [142, Section 2.2.3.3] to claim that other factors, such as sparger type, liquid height, and number, type and placement of impellers, each have no further influence in a properly stirred tank. However, he was forced to define the scope in which this 'general' statement applies: liquid height $0.5 < T/H_L < 1.5$ and impeller clearance $D/H_L < C < H_L/2$. He also acknowledged that the reported coefficients vary widely: $0.4 < \alpha < 1$ and $0 < \beta < 0.7$. Finally, he proposed one set of (c_i, α, β) for pure water and another for 'strong ionic solutions', and these equations

could describe the published data only with scatter of 20 to 40 per cent. Such a result illustrates the sensitivity of operating conditions and gas distribution on process results.

Moreover there is a fundamental flaw with this correlation: it can only be used if the energy dissipation rate in the vessel is everywhere equal to ϵ_T. Metzner and Taylor [97] in 1960 found that local rates decreased rapidly within very short radial distances from a turbine impeller. Cutter [186] had estimated that about 20 per cent of the power input was dissipated in the impeller, about 50 per cent in the impeller stream, and about 30 per cent in the rest of the tank. The ratio of local to average energy dissipation rate, $(\epsilon_T / \overline{\epsilon_T})$ was found to vary by a factor of 270 depending upon position in the vessel. Thus, power dissipation is extremely heterogeneous. Levins and Glastonbury [187] reminded that since $0 < \alpha < 1$ then any factor—including a physical factor such as impeller placement or D/T ratio—can effect an increase in $k_L a$ simply by making the power dissipation more uniform, even though the aggregate P/V ratio may remain constant. Only if the range of turbulent energy relevant to mass transfer is uniformly distributed will $k_L^o a$ be truly independent of geometric factors.

Finally, there is a flaw in the practice of correlation *per se*: Richards [188] was able to fit the same data of Cooper *et al.* (Equation 2.48, $\alpha = 0.95, \beta = 0.67$) quite well to

$$k_L a = c_{12} \frac{\epsilon_T^{0.95} \cdot v_s^{0.45}}{N^{0.5} \cdot D^{0.52}} \tag{2.49}$$

and even to

$$k_L a = c_{13}\, \epsilon_T^{0.4} \cdot v_s^{0.50} \cdot N^{0.48}. \tag{2.50}$$

Clearly the selection of different groups of variables can result in entirely different correlations from the same data. Each equation is 'correct' insofar as it fits the given data with success, but cannot be expected to produce results congruent with the others when used for scale-up purposes. Thus there is a need for design relationships which begin to incorporate fundamental principles.

2.3 Measurement Techniques

2.3.1 Power Input to Agitated Systems

Prochazka [189] reviewed the initial measurement techniques. Essentially, four different methods were used: (a) split shaft dynamometers, using springs or torsion bars as the measuring element [54,119]; (b) differential gear dynamometers [60]; (c) freely rotating motors, where torque of the shaft is measured [53,62,60]; and (d) freely rotating vessels, where the torque transmitted by the liquid to the vessel wall is measured [52,57].

Prochazka also described his system of floating the rotating vessel in a larger second vessel and holding it in place by means of hydraulic bearings [189]. Nienow and Miles [190] described the use of an air-bearing dynamometer. Nienow and co-workers have mounted foil strain gauges on the impeller shaft. For their dual impeller system, Kuboi and Nienow [160,93] placed one strain gauge above each impeller to measure the torque due to the lower impeller and due to the pair.

2.3.2 Oxygen Mass Transfer

The rate of oxygen transfer in a mixing vessel usually is measured by one of two aeration tests. The rate is measured as the product of the mass transfer coefficient k_L and interfacial area a. Techniques are available to measure a independently, and thus k_L can be computed from the measured value of $k_L a$.

Non-Steady State Reaeration

In this method the water in the vessel first is stripped of oxygen by the bubbling of an inert gas (usually pure nitrogen), or by the addition of sufficient sulphite ion to reduce the dissolved oxygen content to a negligible level. The reabsorption is then followed with

a dissolved oxygen electrode or by Winkler titration. This gives

$$k_L^o a = \frac{1 - \epsilon_G}{t} \ln \frac{C^I - C_o}{C^I - C_t} \tag{2.51}$$

so that a plot of the natural logarithm of the normalized concentration *vs.* time should produce a straight line with slope $k_L^o a$.

Steady State Aeration

In the steady state test the rate of oxygen transfer is assumed to be constant, and is measured chemically by the rate of depletion of a reactive specie. The absorption into sodium sulphite solution was used by Cooper *et al.* [68] and since then it has been employed widely. The over-all reaction

$$SO_3^{2-} + \tfrac{1}{2}O_2 \rightarrow SO_4^{2-} \tag{2.52}$$

gives

$$\frac{d[O_2]}{dt} = -\frac{1}{2}\frac{d[SO_3^{2-}]}{dt} \tag{2.53}$$

where the sulphite ion concentration can be determined by iodometric titration.

Measurement of Interfacial Area a

Direct measurements have been made by physical methods. Vermeulen *et al.* [164], Calderbank [167,81] and Benedek [165] used a light transmission technique to measure a in liquid-solid and liquid-gas dispersions. When a probe inside the apparatus is necessary, it may interfere with flow conditions in its vicinity. The method also is limited to a maximum area of about 800 m^2/m^3, and only to local measurements of a, which is known to vary with position in the vessel [167]. Full vertical and radial traverses thus are necessary to obtain an average for the whole tank.

Preen and Valentin [168,191] used photographs of the dispersion, which requires d_b of the dispersion to be known. This technique is liable to the overestimation of surface

area due to the disproportionate detection of small bubbles which may, under certain conditions, form a thin 'curtain' at the vessel walls [192]. An alternative technique involved the induction of a sample of the dispersion through a tube to an external column where the bubbles were photographed [109]. This also is limited only to measurement of local samples and may cause disruption of the hydrodynamics in the vicinity of the tube.

Chemical methods have been used more often to determine a. The primary requirement of a chemical system is a chemical reaction in the fast regime (Section 2.1.2). So long as k_L is independent of the hydrodynamics and will not be subject to the bubble size effect (Section 2.2.4.2), the observed changes in $k_L a$ will be caused only by the effects of the mixing system on a.

Sulphite oxidation with appropriate catalyst and Na_2SO_3 concentrations and oxygen partial pressure is commonly used. Other requirements of this system are a constant temperature, and negligible gas phase resistance and oxygen depletion in the gas phase.

The absorption of CO_2 in hydroxide solutions also has been employed [79,82]; the difficulties and precautions have been outlined by Westerterp *et al.* [79, p. 171]. Other systems have included the absorption of CO_2 (diluted with air) in aqueous solutions of alkanolamines, and oxygen (in air) in neutral and acidic solutions of CuCl [82] and aqueous alkaline solutions of $Na_2S_2O_4$ [82,150].

An estimate of a (and hence, k_L) in any system can be made *via* the relation

$$a = \frac{6\epsilon_G}{\overline{d_b}}. \tag{2.54}$$

This requires knowledge of gas hold up ϵ_G, which is either calculated by measurement of the vessel liquid volumes when gassed and when static,

$$\epsilon_G = \frac{V - V_L}{V}, \tag{2.55}$$

or estimated from

$$\epsilon_G = \frac{v_s}{v_t - v_s} \tag{2.56}$$

where v_t is the terminal velocity of bubble rise [84].

Measurement of Mass Transfer Coefficient

In the slow chemical reaction regime, $k_L = k_L^o$. The absorption of diluted CO_2 by carbonate-bicarbonate buffers was used by Mehta and Sharma [82] as a slow reaction. They then absorbed CO_2 in monoethanolamine solution (a fast reaction) to determine a. Under identical agitation conditions, and keeping solution properties (ionic strength, viscosity, density) as constant as possible, k_L^o for the slow chemical reaction was obtained by dividing $(k_L^o a)_{\text{slow}}$ by a.

2.3.2.1 Sulphite Oxidation

The catalysed oxidation of sodium sulphite, as described in Reaction 2.52, has gained broad acceptance by researchers measuring $k_L a$ and/or a. The reactants are inexpensive, relatively harmless, and can be used under ambient conditions. Potassium and ammonium sulphite also have been used but much less frequently.

In spite of its wide-spread use its reaction mechanism still is not entirely clear; and its kinetics, still not well defined, are sometimes misunderstood.

The Reaction Mechanism

Titoff [193] in 1903 suggested that sulphite and cupric ions formed a complex ion which reacted quickly with oxygen. Bäckström suggested [194] and then developed [195] a chain reaction mechanism, activated either by molecular activity or absorption of a light quantum $h\nu$. The free-radical chain mechanism, adapted below for a cobalt catalyst,

now is generally accepted [196,197,198,199] to follow:

$$SO_3^{2-} + [Co(H_2O)_6]^{3+} \xrightarrow{k_1} .SO_3^- + [Co(H_2O)_6]^{2+} \tag{2.57}$$

$$.SO_3^- + O_2 \xrightarrow{k_2} .SO_5^- \tag{2.58}$$

$$.SO_5^- + SO_3^{2-} \xrightarrow{k_3} SO_5^{2-} + .SO_3^- \tag{2.59}$$

$$SO_5^{2-} + SO_3^{2-} \xrightarrow{k_4} 2SO_4^{2-} \tag{2.60}$$

Reaction 2.57 is the initiation step whereby cobaltic hexaquo complex ions abstract an electron from sulphite ions to produce active centres. Reactions 2.58 and 2.59 generate more active centres plus SO_5^{2-}, which oxidizes the sulphite to sulphate ions.

The above sequence provides no mechanism for the *regeneration* of the cobaltic specie, however. In the absence of complexing agents, the oxidation back to Co^{III} is very unfavourable [200]. A possible mechanism could be oxidation *via* the SO_5^{2-} which would be generated in Reaction 2.59. The unique oxidizing capability of the SO_2–O_2 (*i.e.* SO_3^{2-}–O_2) system has been demonstrated industrially (e.g. the INCO–SO_2 cyanide oxidation process). Applying the mechanisms proposed by DeVuyst *et al.* [201], an activated complex of $CoSO_5$ might react with Co^{II} according to:

$$CoSO_5 + Co^{II} + 2H^+ \rightarrow 2Co^{III} + SO_4^{2-} + H_2O. \tag{2.61}$$

Hayon *et al.* [202] suggested a role for the radical $.SO_4^-$ in place of SO_5^{2-} in Equations 2.59 and 2.60, but they could not detect it by its electronic spectrum.

Barron and co-workers observed that in homogeneous solutions Equation 2.58 was rapid and thus not rate-limiting [196,197]. They also assumed that free radical termination occurred through the formation of inert products, with $.SO_5^{2-}$ being rate-limiting:

$$.SO_3^- + .SO_3^- \longrightarrow \ldots \text{terminal products} \tag{2.62}$$

$$.SO_3^- + .SO_5^- \longrightarrow \ldots \text{terminal products} \tag{2.63}$$

$$.SO_5^- + .SO_5^- \longrightarrow \ldots \text{terminal products.} \tag{2.64}$$

Catalysis and Inhibition

The catalytic effects of copper [193,194], cobalt [203,204,205] and nickel [205] were observed very early. The results of Reinders and Vles [205] showed copper to be most effective in neutral and acidic solutions, and nickel and cobalt only in alkaline.

Alcohols [206] and hydroquinone [207] are known to inhibit the reaction. Titoff [193] believed inhibitors acted by complexing with and rendering inactive the positive catalysts.

Use of Sulphite Oxidation as a Model Reaction

Benedek [208] investigated the effects of the sulphite solution on oxygen solubility, oxygen diffusivity, viscosity and surface tension. Below 0.8M Na_2SO_3, only the change in surface tension influenced the mass transfer rate (by altering coalescence and dispersion behaviour).

Cooper *et al.* [68] used a 1.0M solution of Na_2SO_3 but by the mid-1960's a standard concentration of 0.8M Na_2SO_3 (100 grams per litre) became popular. Kountz [209], on the other hand, recommended only 0.004 to 0.008M for reaeration device testing. A smaller group of researchers has used lower concentrations: Astarita *et al.* [210], down to 0.00375M; Bengtsson and Bjerle [211], 0.01M; and DeGraaf [40], 0.005 to 0.03M.

Cobalt now is used as a catalyst more frequently than copper. Linek and Beneš [212] gave results indicating the reaction with copper catalyst (10^{-3}M $CuSO_4$, 0.5M Na_2SO_3) was not always sufficiently fast to keep k_L independent of the hydrodynamics. The results of Schultz and Gaden [213] are ambiguous but it appears that under their conditions (10^{-4}M $CuSO_4$, 0.075M Na_2SO_3) the chemical reaction was made slower than the absorption rate: thus the over-all rate was independent of both k_L^o and a. Either case

would make a copper catalysed reaction system unsuitable for determination of interfacial area.

Reinders and Vles [205] noted a decrease in reaction rate with decreasing pH and postulated this was due to the increasing solubility of their proposed insoluble $Co(OH)_2$ catalyst. A more certain concern would be the effect upon dissociation equilibria such as

$$HSO_3^- \rightleftharpoons H^+ + SO_3^{2-} \tag{2.65}$$

which are dependent upon $[H^+]$.

Linek and Vacek [199] reviewed some proposed correlations which account for pH, temperature, cobalt concentration and activation energy. However, they are valid only within the particular ranges of the variables in which they were defined, and some extrapolate poorly at values beyond.

For use in determining the volumetric mass transfer coefficient, the gas phase resistance has been determined to be negligible [213,155,79,214].

Reaction Kinetics

The rate equation for the over-all reaction described by Reaction 2.52,

$$SO_3^{2-} + \tfrac{1}{2}O_2 \rightarrow SO_4^{2-}$$

can be expressed as

$$-\frac{d[O_2]}{dt} = k_n\, C_{CoSO_4}^r\, C_{O_2}^m\, C_{Na_2SO_3}^n \tag{2.66}$$

where m is the reaction order with respect to oxygen, n with respect to sulphite and r with respect to the catalyst. But as Linek and Vacek [199] have reviewed, the values of m, n and r vary widely with concentration ranges and experimental conditions. Thus, for the commonly used heterogeneous reaction, reaction orders of zero and one have been reported for all three species, and for oxygen (m) an order of two as well.

Generally, the reaction is of zero order in sulphite, although there is wide disagreement about the concentration below which the order becomes one.

For oxygen, Linek and Vacek give the empirical rule:

$$\begin{aligned} m &= 2 \qquad \text{for } C^I_{O_2} \leq 3.6 \times 10^{-4}\text{M; and} \\ m &= 1 \qquad \text{for } C^I_{O_2} \geq 7 \times 10^{-4}\text{M.} \end{aligned} \tag{2.67}$$

Thus under most instances, oxygen in air under ambient conditions will obey a reaction order of two. At low concentrations of Na_2SO_3, an order of zero was found by Astarita *et al.* [210] (10^{-4} to 10^{-3}M $CoSO_4$, 0.2 to 1 atm O_2, and 0.06M Na_2SO_3) and by Bengtsson and Bjerle [211] (10^{-8} to 10^{-4}M $CoSO_4$, 0.04 to 0.2 atm O_2, and 0.01M Na_2SO_3).

An order of one in cobalt catalyst is almost always observed, although Bengtsson and Bjerle [211] reported zero ($C_{CoSO_4} \leq 10^{-7}$M) and one-half orders ($C_{CoSO_4} \geq 5 \times 10^{-6}$M).

The reaction orders for the homogeneous[18] reaction have been summarized by Linek and Vacek as well; these differ systematically from the heterogeneous reaction. Sawicki and Barron [198] related the difference in apparent activation energies for the two reaction methods to different rate controlling steps in the reaction sequence. They concluded that the rate of the heterogeneous reaction is affected by a diffusion-limited regeneration of the catalyst.

2.4 Closure

In Section 2.2.3, studies into the individual elements of system design were reviewed to explain their effects on power consumption/energy dissipation rate and bulk flow patterns. In Section 2.2.4, the sensitivity of the interfacial area and mass transfer coefficient to the these environmental conditions was assessed. But the linking of the two fields unfortunately is not straightforward.

[18]In the homogeneous reaction, sulphite solution reacts with water in which oxygen has already been dissolved.

The objective of the experimental design is to identify and describe those physical variables which distribute the liquid flow, energy and dispersed gas bubbles in a manner which yields the maximum volumetric rate of oxygen transfer, or the maximum ratio of oxygen transfer to power consumption.

Equation 2.36,

$$N_V = c_6\sqrt{\frac{Z'2g}{\pi^2 D^2}}.$$

defines the interesting condition of the critical tip speed where vortex aeration becomes theoretically possible. Yet this result went unnoticed by subsequent researchers.

DeGraaf [40] seized upon the underlying principles to propose a design criterion for gas pumping agitators. He defined the potential energy of a gas bubble of volume V_B at depth Z below the hydrostatic surface,

$$E_P = gZ(\rho_D - \rho_G)V_B, \tag{2.68}$$

where ρ_D and ρ_G are the densities of the dispersion, and the kinetic energy of a volume of the dispersion moving with the tip speed of the impeller,

$$E_K = \tfrac{1}{2}\rho_D V_D(\pi ND)^2. \tag{2.69}$$

An ideal impeller will transform the kinetic energy of a unit volume of slurry at depth Z into the potential energy of a unit volume of bubbles at the same depth; thence

$$\tfrac{1}{2}\rho_D V_D(\pi ND)^2 \equiv gZ(\rho_D - \rho_G)V_B. \tag{2.70}$$

With $V_D = V_B$ and, for most cases, $(\rho_D - \rho_G) \simeq \rho_D$, Equation 2.70 reduces to

$$(\pi ND)^2 = 2gZ, \text{ or} \tag{2.71}$$

$$N_V = \sqrt{\frac{2gZ}{\pi^2 D^2}}. \tag{2.72}$$

The right-hand side of Equation 2.72 may be made independent of impeller geometry by expressing the impeller tip speed as $N_V \pi D$. Then the critical tip speed of the impeller, v_C, may be defined as

$$v_C = \sqrt{2gZ}. \tag{2.73}$$

This means that impeller *immersion depth* should be the sole determinant of the tip speed at which an impeller begins to pump gas.

He was able to confirm experimentally, in principle, this fundamental relationship. Departure from ideality—*i.e.* values of v_C^2/gZ other than 2—was noted, due to effects within the mixing vessel such as viscosity, flooding of the impeller, direction of impeller discharge, and wall and baffle effects. Each of these acts to prevent perfect transformation of energy at the impeller tip; thus, departure from the ideal case of $v_C^2/gZ = 2$ becomes a tangible measure of the efficiency of the mixing system.

If the effects of those variables which cause departure from ideality can be systematically investigated, it should be possible to specify and scale up to new systems based on the ideal, designing so as to optimize the departures. The reliance on generalized, scale-dependent correlations can then be reduced, if not eliminated, through the use of this more fundamental approach.

Chapter 3

Experimental

3.1 Physical Apparatus

3.1.1 Mixing Vessel

The mixing vessel is shown in Figure 3.1. It was constructed of $\frac{1}{4}$" clear acrylic plexiglass with bonded seams down the side of the cylinder, between the cylinder and its reinforced extension, and between the cylinder and the near-hemispherical "dish" bottom.

A line denoting the operating volume of 200 litres was scribed on the outside at a point just below the extension, with 27 litres in the dish and 173 litres in the cylinder. The vessel was designed as a one-tenth scale replica of the 2000 litre Cominco mixing model at Trail, B.C. used by DeGraaf [40]. There were three purposes to this design:

1. To generate data in a 200 litre vessel, intermediate to those of DeGraaf at the twenty and 2000 litre scales, providing results at three orders of magnitude to assess the sensitivity to scale;

2. To study mixing where the interaction between the impeller and the tank is minimized, approaching the case of an impeller in the ocean;

3. To study mixing in the industrial configuration. While a horizontal arrangement was originally contemplated, it could not be pursued because of the importance of purpose 2. Baffles were then inserted to induce flow conditions characteristic of those found in the industrial vessels.

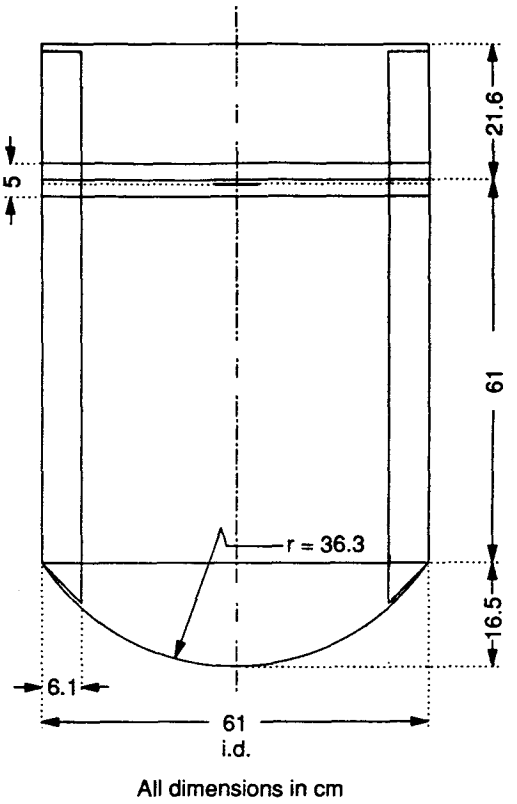

Figure 3.1: Dimensions of the mixing vessel.

The baffles were made of lucite, with width 6.1 cm or $T/10$. They extended up into the freeboard to permit complete baffling of the vortex, and had angled bottom ends to rest against the curvature of the dish.

3.1.2 Impellers

Two types of impellers were examined:

(i) four-bladed axial flow (upward pitch)

(ii) six-bladed radial disc.

Two families of radial disc ("Rushton") impellers were tested:

(i) with varying over-all diameter D

(ii) with varying disc diameter D_d (at constant D).

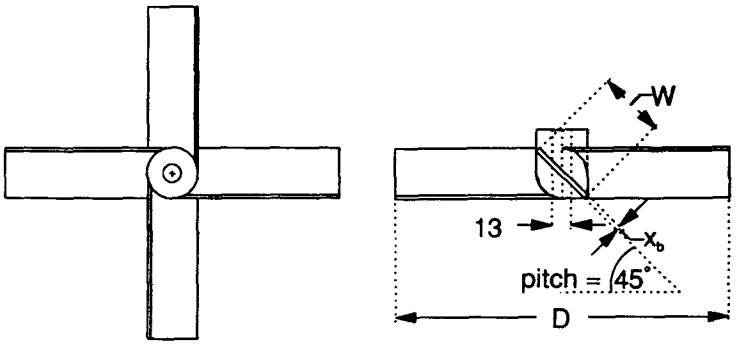

Axial Impeller — Upward Pitch		
D	W	x_b
229	46	3.2

Dimensions in mm

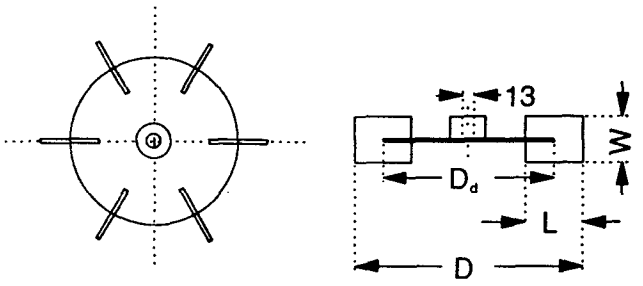

Radial Disc Impellers				
D	L	W	D_d	D_d/D
183	46	37	137	0.75
229	57	46	152	0.67
229	57	46	171	0.75
229	57	46	194	0.85
279	70	56	210	0.75

Figure 3.2: Types and dimensions of the impellers.

The dimensions of these impellers are displayed in Figure 3.2. They were attached to the agitator shaft by set screws, and two impellers could be easily attached to and adjusted on the shaft. The shaft and impeller(s) were coated with Glyptal paint to prevent corrosion.

3.1.3 Assembly

The initial assembly is shown in Figure 3.3. The vessel rested in a sand-filled box and had two additional particle-board brackets to maintain vertical alignment and absorb shock. The vessel could not move (turn) due to the packing of sand, and the box itself was restrained by the handi-angle brackets which formed the assembly frame.

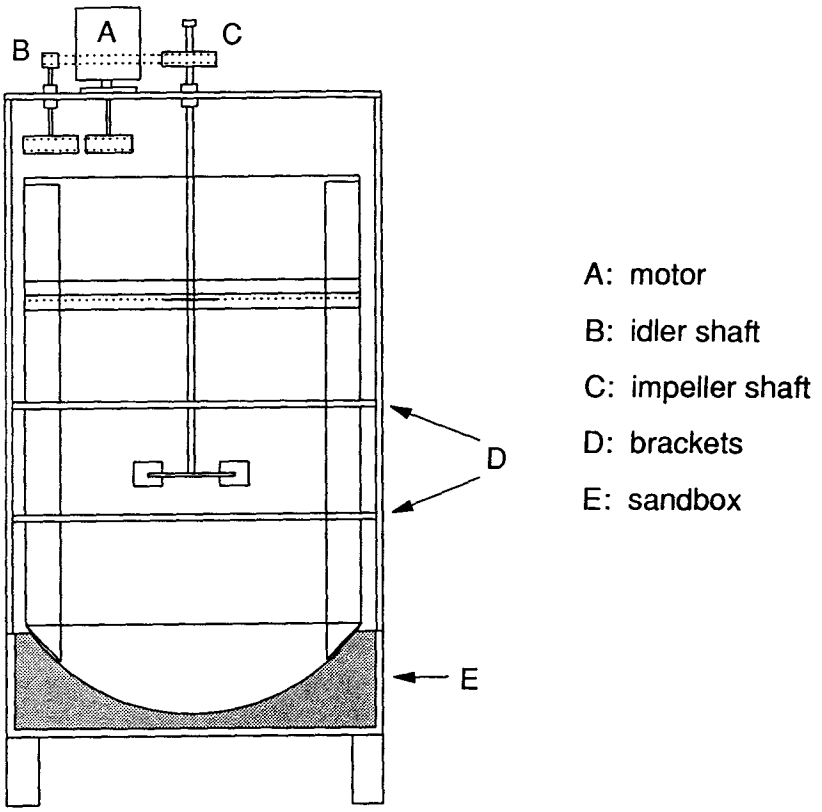

Figure 3.3: Initial assembly with vessel fixed in sandbox.

The agitator shaft was held and aligned by two shaft bearing assemblies. These were mounted on angle brackets which permitted centering of the shaft along the cylindrical axis of the vessel. Similarly an idler shaft was mounted to one side, which could be moved to allow snug adjustment of the v-belt between the idler and agitator shaft pulleys.

A one-horsepower 1725 rpm motor was mounted on a free-floating bearing, and the bearing was inserted in a steel plate. In turn, the plate was fastened to angle bracket "runners" which permitted $x - y$ movement of the motor to provide snug adjustment of the v-belt between the motor and idler shaft pulleys.

When the need for more accurate determination of power consumption values was assessed, the assembly was changed (Figure 3.4). The vessel was placed in a circular

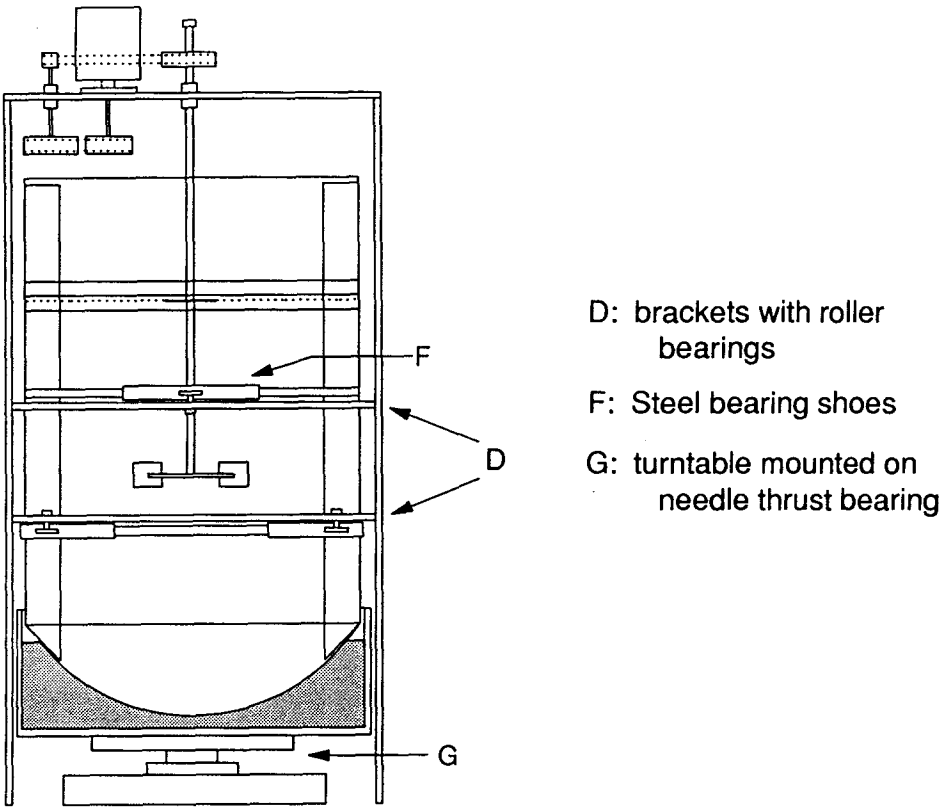

Figure 3.4: Assembly with freely-rotating vessel.

sandbox, which in turn was mounted on a turntable with a needle thrust bearing, which permitted free rotation of the vessel about its cylindrical axis. Two plywood brackets were placed at one-third intervals up the vessel, and three roller bearings were mounted in each at 120° offsets. The bearings were aligned to just touch curved steel bearing shoes which were strapped around the vessel. The contact of bearing on steel provided the necessary vertical alignment as well as unhindered rotation.

The steel shoes gave a smooth surface of constant radius of curvature on which the bearings could impinge (the vessel cylinder was fabricated from a sheet of plexiglass and was not a perfect circle itself). As well, the steel contact surface could absorb undue shock that might have arisen in the system and thus prevented cracking of the plexiglass.

3.2 Measurement Technique

3.2.1 Oxygen Consumption

3.2.1.1 Reaction Chemistry

The reaction describing the consumption of oxygen in sulphite solution was given in Reaction 2.52:

$$SO_3^{2-} + \tfrac{1}{2}O_2 \rightarrow SO_4^{2-}. \tag{3.1}$$

As the reaction proceeds in the vessel the sulphite ions will be depleted (by reaction with oxygen). The concentration of sulphite ion in a sample taken at any time can be determined by titration with iodine solution:

$$SO_3^{2-} + I_2 + OH^- \rightarrow SO_4^{2-} + 2I^- + H^+ \tag{3.2}$$

The strength of the iodine solution can be determined by titrating against thiosulphate solution of known strength:

$$2S_2O_3^{2-} + I_2 \rightarrow S_4O_6^{2-} + 2I^- \tag{3.3}$$

If the quantity of iodine solution required to titrate against the sulphite in each vessel solution sample is recorded and plotted against the elapsed time at which each vessel sample is taken, the slope of the curve will represent the depletion rate of sulphite ion. By Reaction 3.1 this is stoichiometrically related to the oxygen supplied and thus the oxygen consumption rate for the particular system (temperature, pressure) can be established by:

$$\frac{d[O_2]}{dt} = \tfrac{1}{2}\frac{d[I_2]}{dt} \tag{3.4}$$

Figure 3.5 shows the form of a typical iodine titration curve.

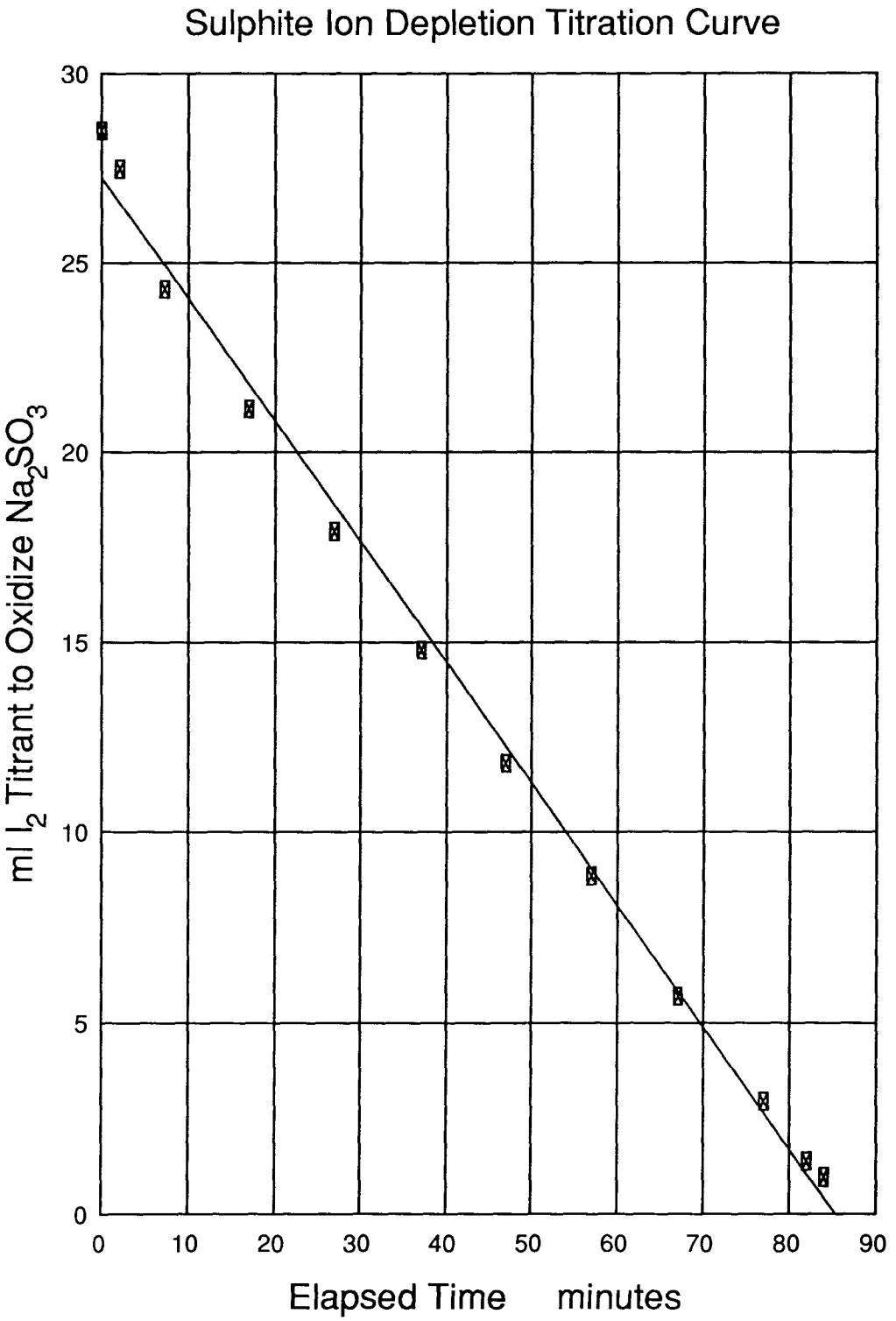

Figure 3.5: Typical iodine-sulphite ion titration (rate) curve.

3.2.1.2 Reagents, Preparation and Procedure

Anhydrous sodium sulphite was weighed out in 500.0 gram samples. A six litre erlenmeyer flask was filled almost fully with warm tap water. The crystals were funnelled into the flask, which was sealed with a rubber stopper and stirred with a magnetic stirring bar for about ten minutes to achieve complete dissolution.

Reaction 3.1 is catalysed by the cobaltic ion. A 9.540 gram sample of $CoSO_4 \cdot 7H_2O$ was dissolved in a little tap water with 3.0 mℓ of sulphuric acid. The flask was opened to add the cobalt solution, then resealed and stirred for about ten seconds to mix completely.

The dish of the vessel was filled with ambient tap water. A siphon hose drained the flask contents by gravity into the pool of water with minimal exposure to the air. After the flask was emptied the flow of tap water to the vessel was resumed. The hose end was weighted to maintain submerged delivery, to prevent air from being entrained by the jetting of a stream of water above the liquid surface. The turbulence of the immersed water stream provided sufficient blending of the entire vessel contents. Scavenging of dissolved oxygen in the tap water was assumed to be complete in the approximately ten minutes it took to fill the vessel to the 200 litre mark.

3.2.1.3 Sample Taking

Two sets of fourteen-60 mℓ plastic sample bottles were available for sample acquisition. Each was purged with nitrogen and left inverted prior to experimentation.

The sampling apparatus consisted of two rods of length one metre. One had a wire basket at its end to hold a sample bottle; the other had a flask stopper fixed to its end. When a sample was to be taken, an inverted bottle was placed in the basket and the stopper inserted upward. The two rods were then returned upright and immersed into the vessel to place the stoppered bottle against the vessel wall at a point 30 cm below

the (static) liquid surface. The stopper was then removed and solution allowed to fill the bottle while the nitrogen bubbled out. The bottle was then withdrawn from the vessel, removed from the basket and capped.

When preparation prior to an experiment was complete, a sample of the unagitated solution was withdrawn, assigned a time $t = 0$ and titrated immediately. The agitator motor was then started and elapsed time commenced from this point. Samples of solution were then withdrawn so as to provide twelve to fourteen data points spanning the duration of sulphite ion oxidation.

The samples were titrated at the earliest opportunity, usually while the experiment proceeded. This provided an estimate of the duration of the test and allowed an optimum sampling frequency. The end-point of the experiment could then be ascertained by the last few titration values and/or a subtle colour change in the bulk solution (from pale canary or rust to clear).

3.2.1.4 Sample Titration

The standard titrant for sulphite ion determination was an iodine solution, approximately 0.0125M I_2. It was prepared by dissolving a quantity of iodine (about 6.3 grams) in a small amount of distilled water and about 40 grams of potassium iodide. When all the solid iodine had dissolved, the solution was diluted with distilled water in a two litre volumetric flask.

A 10 mℓ aliquot of sodium thiosulphate was used to standardize the molarity of the titrant. A quantity of $Na_2S_2O_3 \cdot 5H_2O$ was weighed accurately and dissolved in distilled water to produce a solution of known molarity (close to 0.1000M $Na_2S_2O_3$).

Iodine solutions need attention on two accounts. The first is due to incomplete dissolution of I_2 solids during solution make-up. If there is some iodine which did not dissolve in the first small mixture with KI, then complete dissolution is very slow in a diluted

(0.0125M) solution. Thus, the molarity may increase slightly with time; a two litre flask of iodine solution would last approximately ten experiments.

The second account is deterioration of iodine solution by direct exposure to sunlight [215]. In this instance, the molarity may decrease slightly with time.

Every care was taken to ensure complete initial dissolution (by visual inspection) and storage in a dark cupboard when not in use. As a safeguard, the $Na_2S_2O_3$ solution used in the initial standardization was retained to perform a recheck when the flask of iodine was nearly exhausted. The discrepancy was less than about 0.2 per cent and was apportioned linearly by time (*viz.* days) to the experiments performed.

The indicator used for iodine-sodium sulphite titrations was a simple starch suspension. It was prepared by mixing a little solid starch, dissolved water and acetic acid. The bottle was shaken prior to the withdrawal of one or two drops for the titration.

3.2.2 Power Consumption

The principle of power measurement is derived from Newton's Third Law: to every force acting there is always a force equal in magnitude and opposite in direction. Practically, the force supplied by the motor to the agitator shaft is equivalent to the force of the agitator impeller acting on the mixing tank. More specifically, the force supplied by the motor, less slippage losses at the motor pulley, idler pulley and (agitator) shaft pulley and their connecting belts, is equivalent to the force applied to the mixing tank contents.

Power is the measurement of a force, acting over a distance, over an interval of time (*i.e.* the time rate at which work is done). For a constant moment M with direction parallel to the axis of rotation:

$$\text{power} = \frac{dU}{dt} = \frac{d}{dt}(\mathrm{M}d\theta) = \mathrm{M}\frac{d\theta}{dt} = \mathrm{M}\omega. \tag{3.5}$$

Equation 3.5 is then applied to the motor and vessel.

3.2.2.1 Power at the Motor

Thus at the motor (Figure 3.6), M is the product of:

$$\left(\begin{array}{c}\text{the reading on the spring balance}\\ \text{attached to the motor arm}\end{array}\right) \times \left(\begin{array}{c}\text{gravitational}\\ \text{constant}\end{array}\right) \equiv \text{F, and}$$

$$\left(\begin{array}{c}\text{the distance from the axis of rotation to}\\ \text{the point of attachment on the motor arm}\end{array}\right) \equiv \text{lever arm.}$$

Then, ω is the product of:

(rpm/60 as measured at the motor shaft), in rev/sec, and

2π rad/rev.

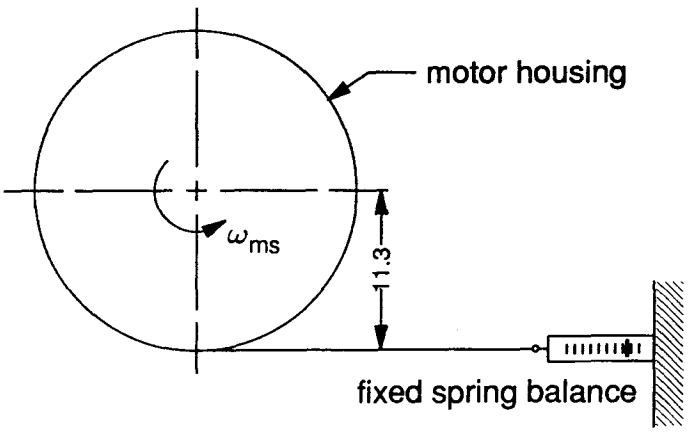

Figure 3.6: Lever arm dimension (cm) of motor: plan view.

3.2.2.2 Power at the Tank

The torque at the tank was calculated similarly (Figure 3.7). The spring balance was attached to the turntable, and the lever arm was the distance from the axis of rotation to the point of attachment. The rotational speed at the impeller shaft gave ω.

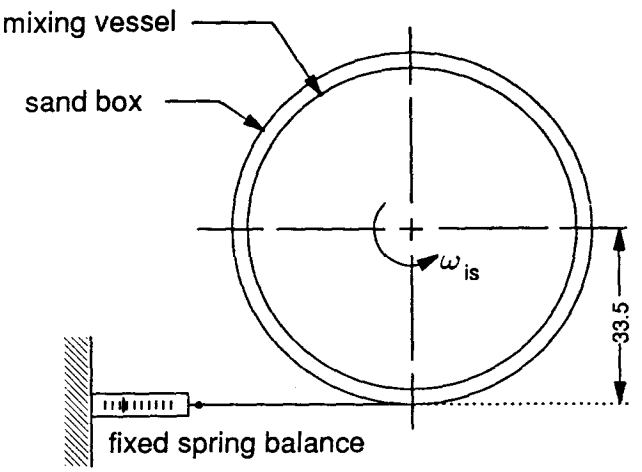

Figure 3.7: Lever arm dimension (cm) of mixing vessel: plan view.

3.2.2.3 Instruments and Procedure

The rpm of the shafts was measured using a hand-held tachometer. Typically this was done for ten consecutive measurements, with the cumulative reading divided by ten and recorded. Such measurements were taken between one and four times per sampling interval. The over-all rpm was the time-average of all recordings.

Small pulleys were fastened to the shaft ends to provide sufficient contact area for the bevelled rubber end fitting of the tachometer. In some instances the idler pulley rpm was also measured to provide an estimate of the location and magnitude of belt-pulley slippage.

Ohaus spring balances of ranges 0.10, 0.50, two, five and ten kg were used to measure the load of the motor and tank turntable. Nylon line was used for the connections. Balance readings were recorded for both the motor and turntable between one and four times per sampling interval. The over-all balance reading was the time-average of all recorded values.

Chapter 4

Results

4.1 Overview and Data Treatment

Three hundred and fifty five experiments were completed. Data were tabulated to evaluate for each of the impellers:

- The adherence to the critical tip speed equation (Equation 2.71);
- The effect on oxygen transfer rate, power consumption and oxygen transfer efficiency (the quotient of these two terms) of: (a) baffles; and (b) impeller diameter, as a function of immersion depth and impeller tip speed.

As well, investigations were made into:

- Impeller type: axial flow *vs.* radial flow;
- Effect of impeller disc size; and
- Dual impeller systems, without baffles.

The titrations to measure sulphite depletion provided curves from which rates of oxygen absorption could be estimated. Results are sometimes reported in the literature as (kg $O_2/m^3 \cdot min$), but this restricts their utility only to the temperature at which they were obtained. The solubility and diffusivity of oxygen vary with temperature and, as is shown in Appendices A and B, these effects can be significant even over small temperature ranges.

From the general equation for the rate of oxygen absorption,

$$R = k_L^o \cdot a \cdot (C^I - C^b) \tag{4.1}$$

in *moles/volume·time*, the oxygen solubility term[1] can be divided from the measured value of R. Oxygen diffusivity is linked to the mass transfer coefficient by $k_L^o \propto \mathcal{D}_{O_2}^n$ and thus cannot be factored out entirely. However, it can be normalized[2] from the observed temperature T to a reference, e.g. $\mathcal{D}_{O_2}$ at 20°C. Assuming the volumetric surface area a does not vary substantially with temperature, the oxygen transfer rate can be expressed as the mass transfer parameter K_G^{20} ,

$$K_G^{20} = k_L^o \cdot a \left(\frac{\mathcal{D}_{O_2}^{20}}{\mathcal{D}_{O_2}} \right)^n , \tag{4.2}$$

in units min^{-1}. This facilitates the comparison of data, and greatly assists in modelling endeavours as described in Section 1.2.2. For this work, n was assumed[3] equal to 0.5.

4.1.1 Reproducibility

Table 4.1 summarizes data from an initial series of experiments (D = 23 cm, Z = 10 cm, unbaffled) which give an indication of the experimental error. The large error in the power measurement arises because in these runs the value of P is the small difference between two similar numbers—the power at the motor during the experiment and when running empty. The error decreases as the P_{net} becomes larger.

Another view of reproducibility is given in Figure 4.1. In this instance only three pairs of experiments were made, but on different dates and with greater variability in water temperature.

---

[1]Estimation of oxygen solubilities is given in Appendix A.
[2]Normalization factors are given in Appendix B.
[3]Experimental justification appears in Section 6.1 and Figure 6.1.

Table 4.1: Comparison of Repeat Run Results

Run #	T_{avg} °C	v m/sec	$R \times 100$ $\frac{kgO_2}{m^3 \cdot min}$	K_G^{20} (p/sr) min^{-1}	K_G^{20} (film) min^{-1}	P W	$\frac{K_G^{20}(p/sr)}{P}$ $(kWhr)^{-1}$
7	9.2	1.78	0.0734	0.0761	0.090	4.7	972
6	9.3	1.79	0.0799	0.0829	0.097	5.2	962
± Per Cent Deviation from the mean				4.3	3.7	10	0.5
10	9.8	2.54	0.321	0.334	0.389	14.7	1367
8	9.9	2.54	0.289	0.300	0.350	13.5	1337
9	9.8	2.55	0.303	0.314	0.367	11.9	1585
11	9.9	2.55	0.284	0.295	0.344	14.7	1209
± Per Cent Deviation from the mean				7.4	7.3	13	15
13	20.4	2.99	0.492	0.535	0.532	27.1	1187
12	11.0	3.00	0.520	0.543	0.622	20.1	1623
14	18.3	3.03	0.487	0.525	0.538	25.5	1233
± Per Cent Deviation from the mean				1.8	10.3	17	20

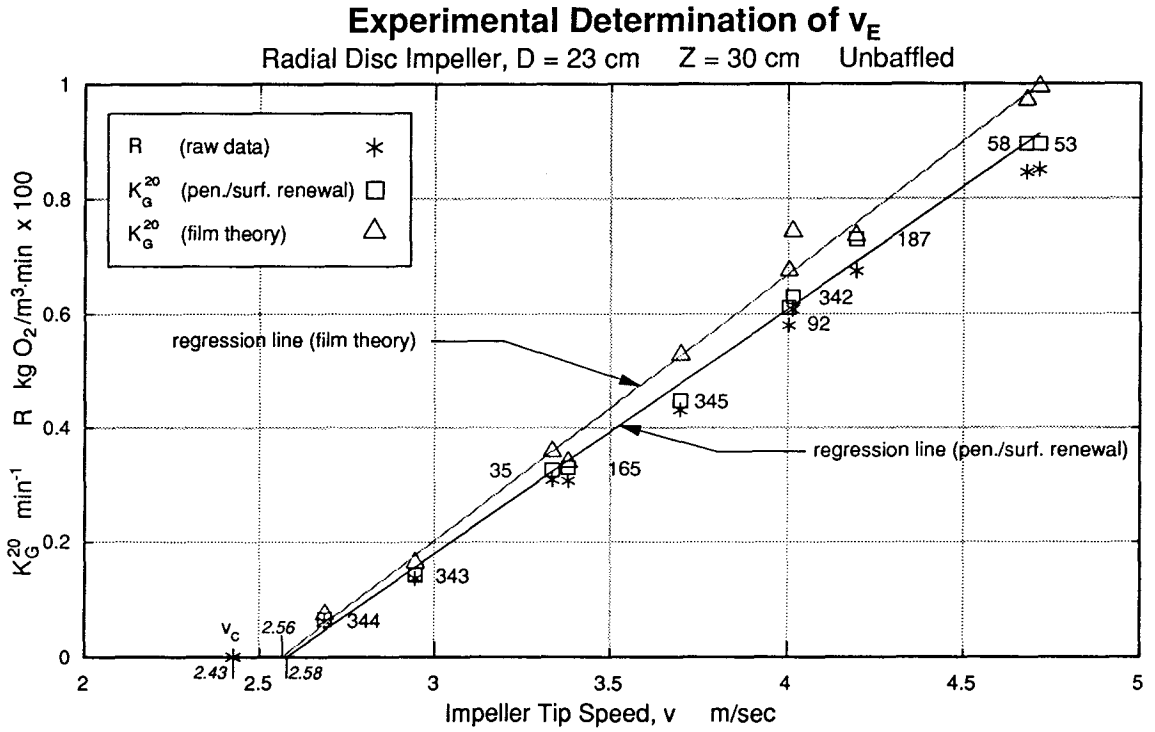

Figure 4.1: Reproducibility over Different Time Intervals

These data are also presented in Table 4.2 and show that the error in the value of P falls as the magnitude of P increases. As was seen for runs 12-14 in Table 4.1, the deviation in K_G^{20} is greater when corrected for diffusivity by the film theory, which supports the selection of the penetration/surface renewal theory correction factors.

Table 4.2: Reproducibilty Data over Different Time Intervals

Run #	date y-m-d	T_{avg} °C	v m/sec	$R \times 100$ $\frac{kgO_2}{m^3 \cdot min}$	K_G^{20} (p/sr) min^{-1}	K_G^{20} (film) min^{-1}	P W	$\frac{K_G^{20}(p/sr)}{P}$ $(kWhr)^{-1}$
35	88-04-21	13.5	3.34	0.309	0.326	0.359	44.9	436
165	88-08-12	17.9	3.38	0.307	0.330	0.340	39.9	496
± Per Cent Deviation from the mean					0.6	2.7	5.9	6.9
92	88-06-10	13.3	4.00	0.580	0.611	0.675	55.4	662
342	89-03-08	9.0	4.01	0.607	0.629	0.744	58.4	752
± Per Cent Deviation from the mean					1.4	4.9	2.6	6.8
53	88-05-04	12.9	4.71	0.851	0.895	0.995	74.5	721
58	88-05-07	14.5	4.68	0.846	0.896	0.972	70.9	759
± Per Cent Deviation from the mean					0.1	1.2	2.4	2.6

Radial Disc Impeller, D = 23 cm, Z = 30 cm, Unbaffled

4.1.1.1 Power Consumption Measurements

When the vessel was mounted in the fixed sandbox (Figure 3.3), power consumption was calculated by first subtracting the power requirement of the impeller running in air from the power measured at the motor during the experiment. From this was subtracted a quantity based on the ratio of the impeller shaft speed which should have been delivered by the motor (*i.e.* the impeller speed running in air, but deflated for the decrease in motor rpm output as it is works under a load) and the impeller shaft speed measured during the experiment. This was attributed to losses in the drive system between the motor and impeller shafts which includes belts, pulleys, the idler shaft and shaft bearings. This quantity typically was less than 1 watt, although in one case when the impeller shaft rpm was 369 empty and 297 during the experiment, it computed to 98 watts.

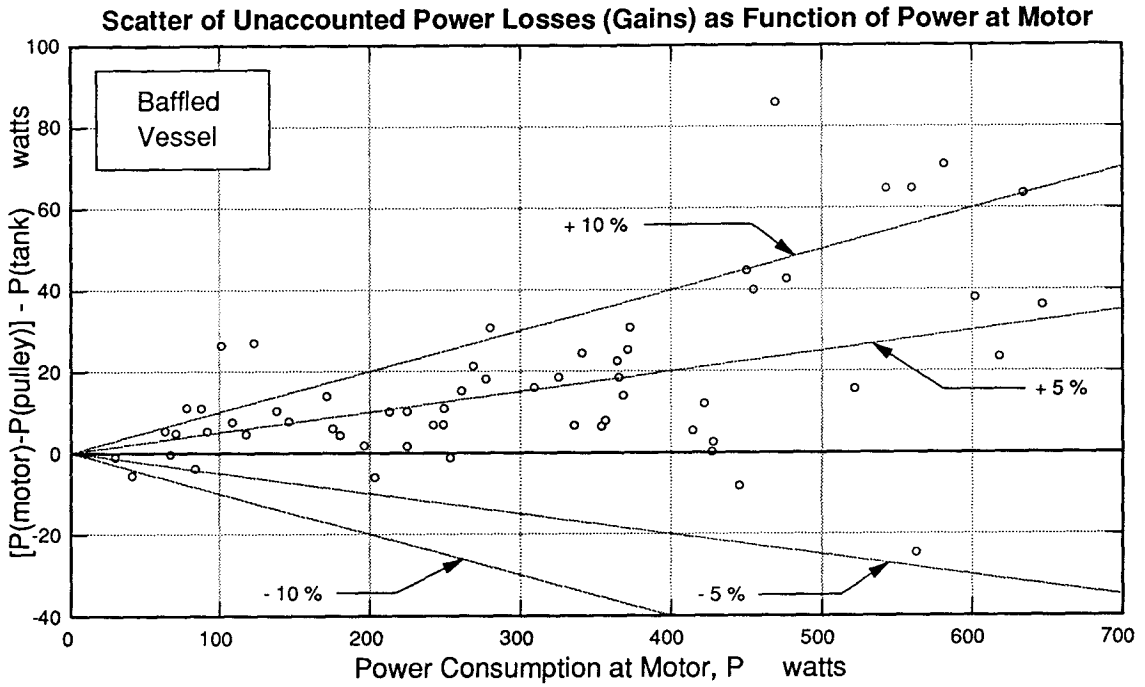

Figure 4.2: Distribution of Unaccounted Power Losses in the Baffled Vessel

When the sandbox was allowed to rotate freely, power at the tank was measured as described in Chapter 3, but motor power measurements were continued as before to establish a data base to compare the two methods of measurement. The results are shown in Figures 4.2 and 4.3 with the unaccounted losses (the difference between [net motor power minus the 'pulley losses'] and the power measured at the tank) plotted against the net motor power minus pulley losses. In the baffled vessel the scatter can be reasonably accounted for by an error band of + 10/- 5 per cent; the five data points above 60 W were measured using a suboptimal spring balance at the motor. In the unbaffled vessel the data can be described by an error band of $\pm$ 22 per cent. Noteworthy is the much smaller abscissa scale, with the largest P(motor) being only 103 W. The absolute value of the unaccounted power is not as large as in many of the baffled vessel experiments, but of course is plotted relative to the much smaller abscissa. Figure 4.3 illustrates the difficulty in obtaining reliable power measurements when using the difference between the motor power during the experiment and when running empty. When both numbers are small

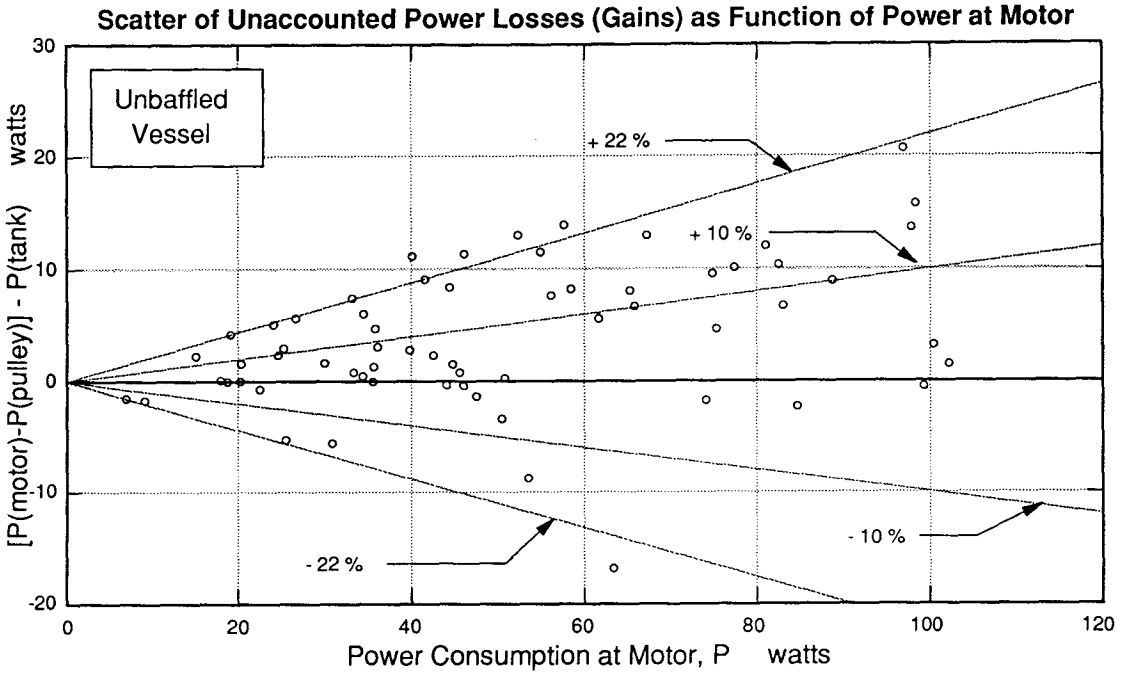

Figure 4.3: Distribution of Unaccounted Power Losses in the Unbaffled Vessel

and of comparable magnitude, the sum of the errors associated with each measurement can be a large percentage of the small difference between them.

4.2 The Critical Tip Speed v_C

Since by the theory of the critical tip speed given in Equation 2.73, Section 2.4

$$v_C = \sqrt{2gZ}\,,$$

a line with slope $(2g)^{0.5}$ on the plot of v *vs.* $Z^{0.5}$ will define the theoretical minimum tip speed v_C required for an impeller to pump gas at a given immersion depth Z. Thus the alignment of experimental data on this plot will determine the validity of the theory, and characterize the nature of gas pumping of each impeller.

Data for the four impellers were first plotted as K_G^{20} *vs.* v; the linear portion of each curve was extended to the abscissa to determine the experimental critical tip speed v_E.

4.2.1 Unbaffled Vessel

Values of v_E are given in Table 4.3. The number n of data points used and the coefficient of determination R^2 are a measure of the reliability of each v_E. While often only three data were present in the linear region, the values of R^2 for these usually exceeded 0.99, which indicates the condition of linear behaviour was identified experimentally.

Table 4.3: v_E Data in the Unbaffled Vessel

Immersion Depth Z, cm	v_C m/sec	Radial Disc, D = 18 cm v_E m/sec	data, n	correlation R^2	Radial Disc, D = 23 cm v_E m/sec	data, n	correlation R^2
10	1.40	1.75	4	0.941	1.61	10	0.973
15	1.72	1.94	3	0.998	2.11	7	0.983
20	1.98	2.16	3	0.980	2.18	4	0.996
25	2.21	2.44	3	1.000	2.28	4	0.999
30	2.43	2.46	5	0.973	2.58	10	0.995
35	2.62	2.45	4	0.962	2.87	3	0.998
40	2.80	2.94	3	0.998	3.02	5	0.994
45	2.97	3.09	3	0.999	2.96	4	0.997
50	3.13	3.14	3	0.989	3.26	4	0.974
Z	v_C	Radial Disc, D = 28 cm			Axial - Upward, D = 23 cm		
10	1.40	2.01	4	0.992	2.41	3	1.000
15	1.72	2.46	3	0.999	...	...	...
20	1.98	2.76	3	0.999	2.64	3	0.999
25	2.21	2.92	3	0.998	...	...	...
30	2.43	2.98	3	1.000	2.78	3	0.999
35	2.62	3.18	3	0.990	...	...	...
40	2.80	3.31	3	0.998	3.16	4	0.996
45	2.97	3.35	3	0.994	...	...	...
50	3.13	3.39	3	0.995	3.62	3	0.994

These results are plotted in Figure 4.4. While the regression line for the 18 cm impeller shows some curvature, this is due mainly to difficulty in defining the true linear portion in some of the K_G^{20} *vs.* v plots.

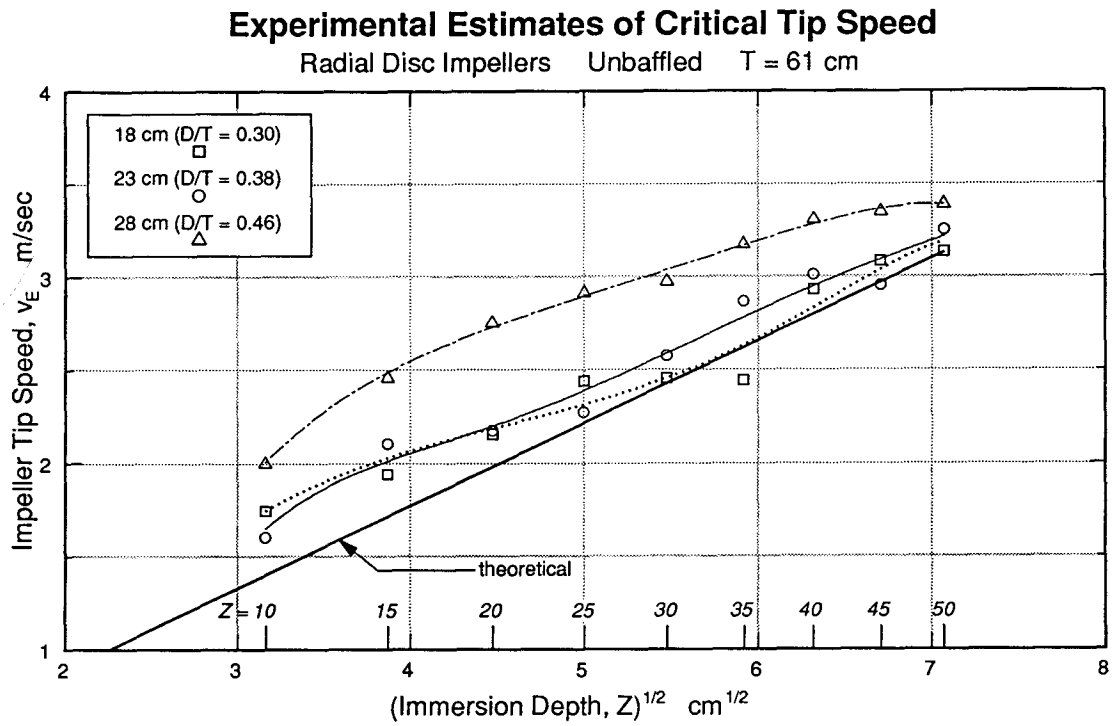

Figure 4.4: Experimental and Theoretical Critical Tip Speeds—Unbaffled Vessel

Generally, the data follow the theoretical line very closely. Although the they do appear to converge slightly to the theoretical line at the deeper immersions, values of v_E rise with $Z^{0.5}$ at close to the same slope as predicted by the theory. *Linear* regression against the theoretical line gives relative slopes (and R^2) of 0.82 (0.950), 0.90 (0.966) and 0.77 (0.951) for the 18, 23 and 28 cm diameter impellers respectively.

The departure from ideality may be assessed by the offset from the theoretical line; this offset, or 'energy penalty', increases as the impeller diameter increases in relation to the vessel diameter. That is, in a right-cylindrical unbaffled tank, a greater tip speed is required by a larger impeller to *begin* to pump gas. The regression slopes suggest that for all three impellers this offset—the magnitude of extra tip speed required to initiate gas pumping—tends to decline gradually with $Z^{0.5}$.

4.2.2 Baffled Vessel

Values of v_E are given in Table 4.4. The 18 and 23 cm diameter impellers were able to sustain a vortex at $Z = 10$ cm in spite of the baffles. The vortex was not always stable, and Figure 4.5 for the 23 cm impeller suggests a hysteresis over intermediate ranges of tip speed. For instance, run #355 began with a stable flow pattern but a vortex broke through to the impeller at 7:29 into the run. At a faster tip speed, run #248 began with a vortex but reverted to the typical flow after 30 seconds.

Table 4.4: v_E Data in the Baffled Vessel

Immersion Depth Z, cm	v_C m/sec	Radial Disc, $D = 18$ cm v_E m/sec	data, n	correlation R^2	Radial Disc, $D = 23$ cm v_E m/sec	data, n	correlation R^2
10	1.40	2.61	3	1.000	2.10	4	0.998
10 cm vortex		1.96*	3	0.999	1.53	4	0.977
20	1.98	2.64	3	0.999	2.21	3	1.000
30	2.43	2.84	5	1.000	2.32	4	0.994
40	2.80	3.09	3	0.991	2.54	3	0.997
50	3.13	3.12	3	0.984	2.81	3	0.891
Z	v_C	Radial Disc, $D = 28$ cm					
10	1.40	1.86	4	0.996			
20	1.98	1.94	4	0.995			
30	2.43	1.86	5	0.990			
40	2.80	2.13	5	0.991			
50	3.13	2.31	3	0.954			

For $D = 18$ cm and $Z = 10$ cm only two rate data points were obtained with typical flow; the third run developed a vortex before sampling could establish the oxygen transfer rate R. The R result for the same v at $Z = 20$ cm was used as the third data point. Since K_G^{20} at $Z = 10$ would be greater or equal to that at $Z = 20$, this substitute data point will inflate the v_E estimate. However, R^2 of the three points (0.999) suggests this is not a poor substitute. This point is indicated by the dotted regression curve in Figure 4.6.

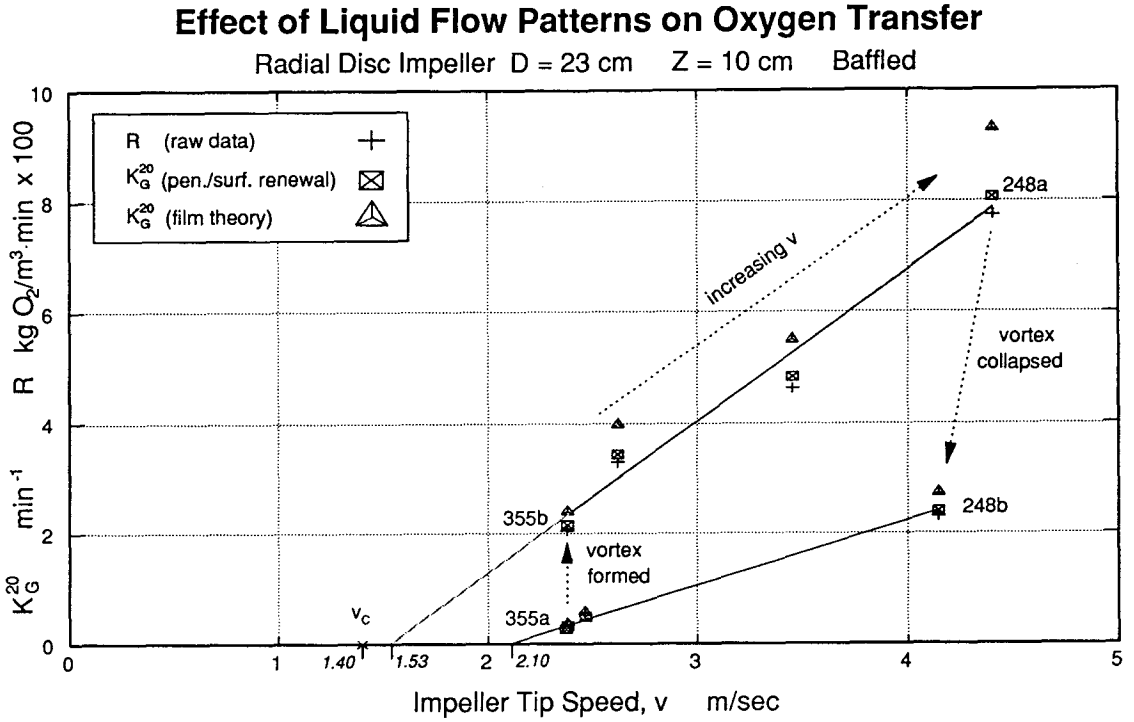

Figure 4.5: Vortex Hysteresis in Baffled Vessel ($D = 23$ cm)

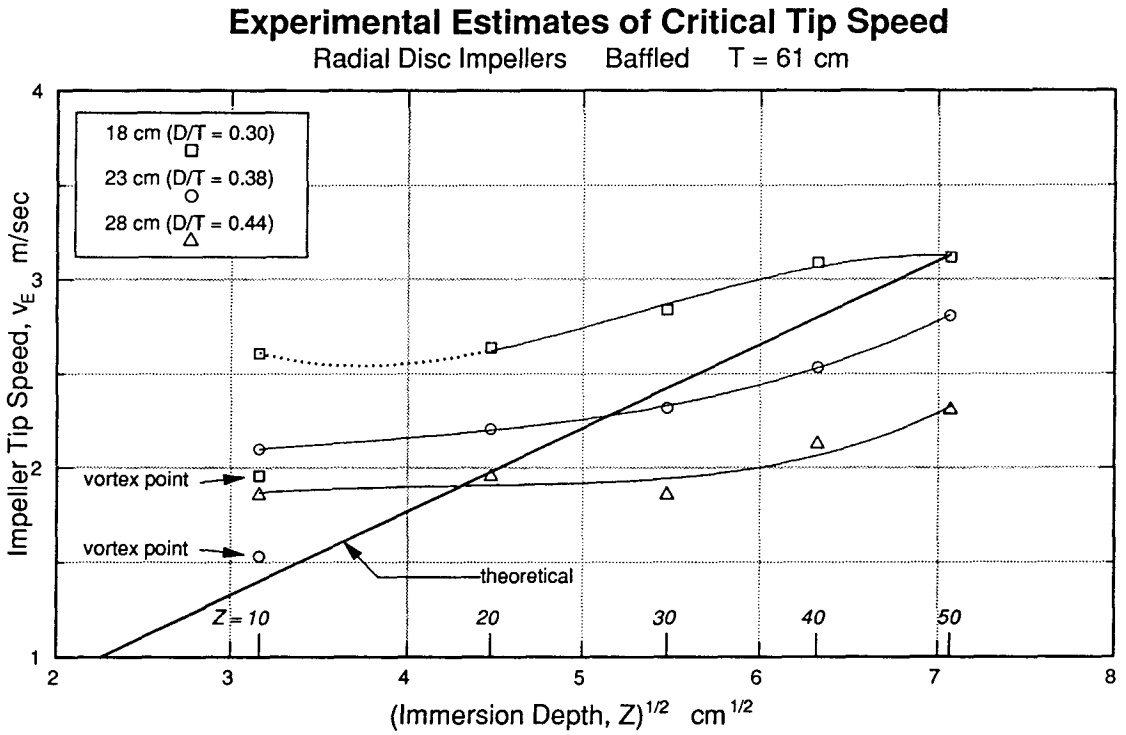

Figure 4.6: Experimental and Theoretical Critical Tip Speeds—Baffled Vessel

When four $T/10$ baffles are present, the critical tip speed behaviour is very different. Figure 4.6 illustrates how v_E increases only very slowly until the immersion increases beyond about mid-vertical height. Data at $Z = 50$ cm were difficult to obtain (large power requirement, slow transfer rate) and displayed poor linearity, making the estimation there of v_E difficult.

The remarkable feature in the baffled vessel is the crossing *over* the theoretical line for at least the two larger impellers. The data align into a family of curves where the vertical offset is opposite to that in the unbaffled vessel: the larger diameter impeller now begins to pump gas at a lower value of v.

The ability of the impellers to pump gas below the theoretical tip speed at deep immersion indicates the aeration mechanism in these instances cannot be described solely by the impeller tip energy balance. More power is required to turn an impeller in a vessel when baffles are used, due to their opposition to flow of the discharged liquid. There must be a contribution to gas draw-down caused by the energy associated with these liquid discharge streams.

4.2.3 Upward Pumping Axial Impeller

The upward pumping axial impeller ($D = 23$ cm) used for the dual impeller experiments was studied in the unbaffled vessel. Since in this case it produces a vortex but at the same time generates axial flow, its flow should show characteristics of both unbaffled and baffled radial flow impellers. It is compared with the radial disc impeller ($D = 23$ cm) in the unbaffled and baffled vessel in Figure 4.7. The v_E for the axial impeller is larger than either of the radial disc impeller applications. A surprising feature is the nearly parallel offset from the curve for the *baffled* 23 cm radial disc impeller. In fact it is nearly identical to the curve for the baffled 18 cm radial disc impeller shown in Figure 4.6.

The axial impeller was studied only twice by itself in the baffled vessel. For the sake

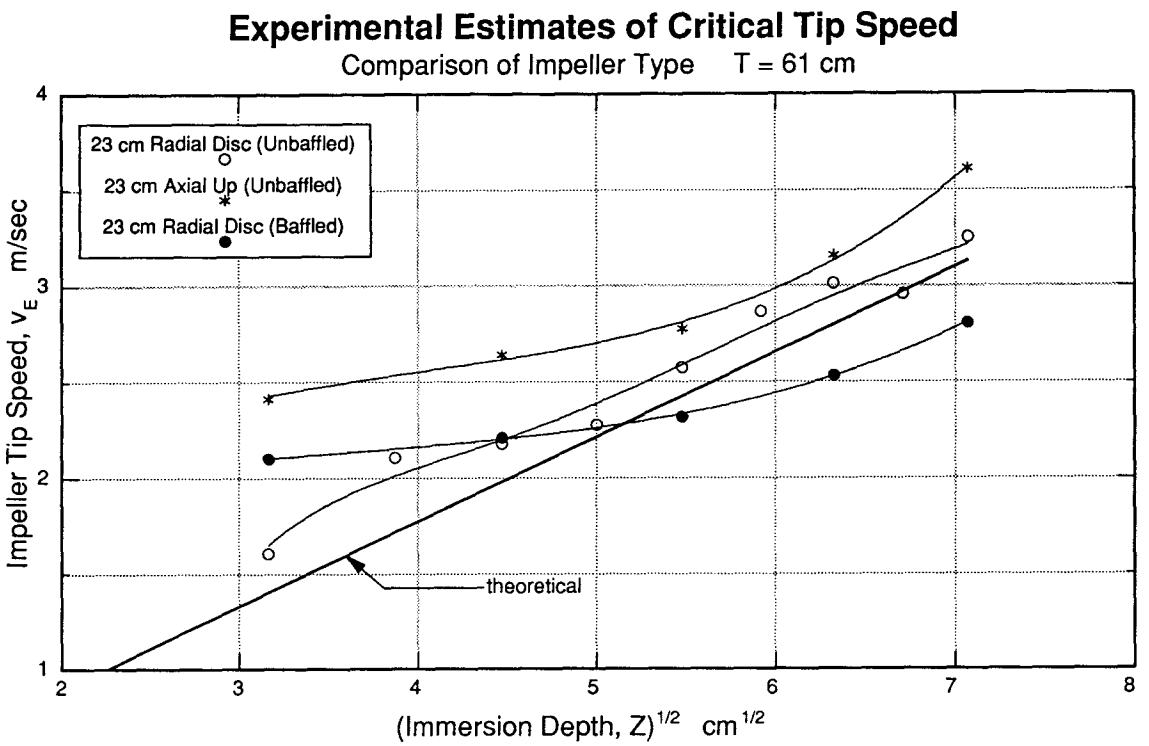

Figure 4.7: Comparison of v_E and v_C for (Upward) Axial and Radial Disc Impellers

of comparison in Table 4.5, results for the baffled radial disc impeller were interpolated from data at $Z = 10$ and 20 and $Z = 40$ and 50 cm.

Table 4.5: Comparison of Axial and Radial Disc Impellers in Baffled Vessel

Impeller Type	Immersion Depth, Z cm	tip speed v m/sec	K_G^{20} min^{-1}	P watts	R.O.T.E. kW hr^{-1}
Radial	15	3.48	1.586	327	291
Axial	15	3.48	1.626	77.0	1270
Radial	45	3.49	0.404	380	63.8
Axial	45	3.49	0.030	88.1	20.4

At the shallow immersion the axial impeller may give a comparable oxygen transfer rate and certainly is more efficient, but of prime importance is the fact the data used for the radial disc at $Z = 10$ cm correspond to the condition *without* the vortex. Also it is uncertain if the froth layer developed by the axial impeller at $Z = 15$ cm would give a

transfer rate at 10 cm similar to the vortex condition of the radial disc impeller. It is apparent, though, that at deeper immersion the axial impeller is poorer both in rate and efficiency, and that its transfer rate is much more sensitive to immersion depth.

4.3 Effect of Baffles on the Rate and Efficiency of Oxygen Transfer

Baffles were used to increase the physical interference of the mixing environment. When absent, the effect is minimized and the vessel approaches the ideal case of an impeller rotating in an ocean. When present at the so-called 'fully-baffled condition' ($B = T/10$), the effect is accentuated and departures from ideality can then be assessed.

Figures 4.8 to 4.10 compare the effect of baffles on K_G^{20}, the power consumption P, and the relative oxygen transfer efficiency[4] defined as

$$\text{R.O.T.E.} = \frac{K_G^{20}}{P}, \quad (\text{kW hr})^{-1} \tag{4.3}$$

at five immersion depths for the three impeller diameters. It is important to note the ordinates in each pair of graphs are not always identical, and that two ordinates are sometimes employed on the same graph. This was done to keep the effect of immersion depth from being obscured by too narrow a band of scaling.

4.3.1 Effect of Baffles on the Rate of Oxygen Transfer K_G^{20}

Graphs (a) and (b) in Figures 4.8 to 4.10 show the *general* trend that K_G^{20} is enhanced by the introduction of baffles. This enhancement increases as impeller diameter increases, and is more pronounced at the shallow immersions.

[4]To obtain oxygen transfer efficiency values in the units of $kg\ O_2/m^3{\cdot}kWhr$ (adopting the penetration/surface renewal theory), the value of R.O.T.E. should be multiplied by the value of $(C^I - C^b)$ in kg/m^3, where C^I is the solubility of oxygen at the ambient partial pressure in the gas bubbles, and C^b is the mean dissolved concentration of oxygen in the bulk vessel liquid (negligibly small in the system studied). Since C^I is roughly 0.01 $kg\ O_2/m^3$ in the temperature range considered here, transfer efficiencies in $kg\ O_2/m^3{\cdot}kWhr$ can be approximated by dividing R.O.T.E. by 100.

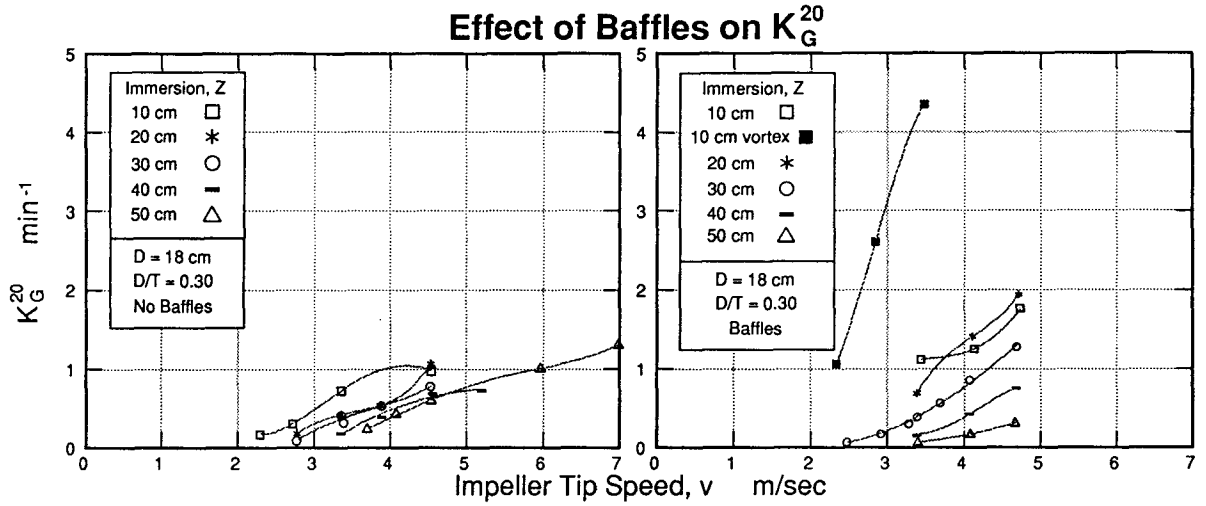

(a) K_G^{20} Without Baffles (b) K_G^{20} With Baffles

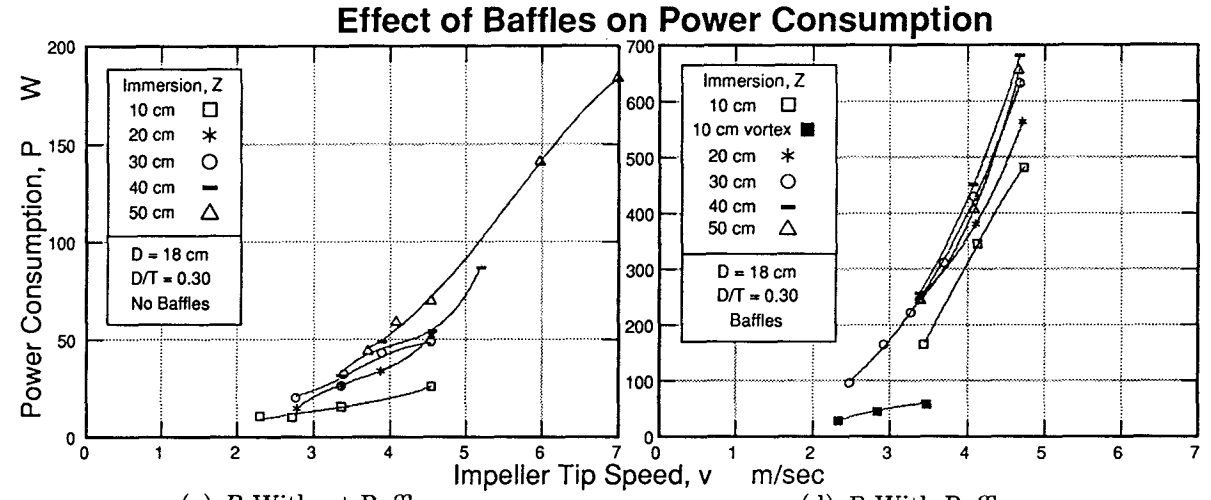

(c) P Without Baffles (d) P With Baffles

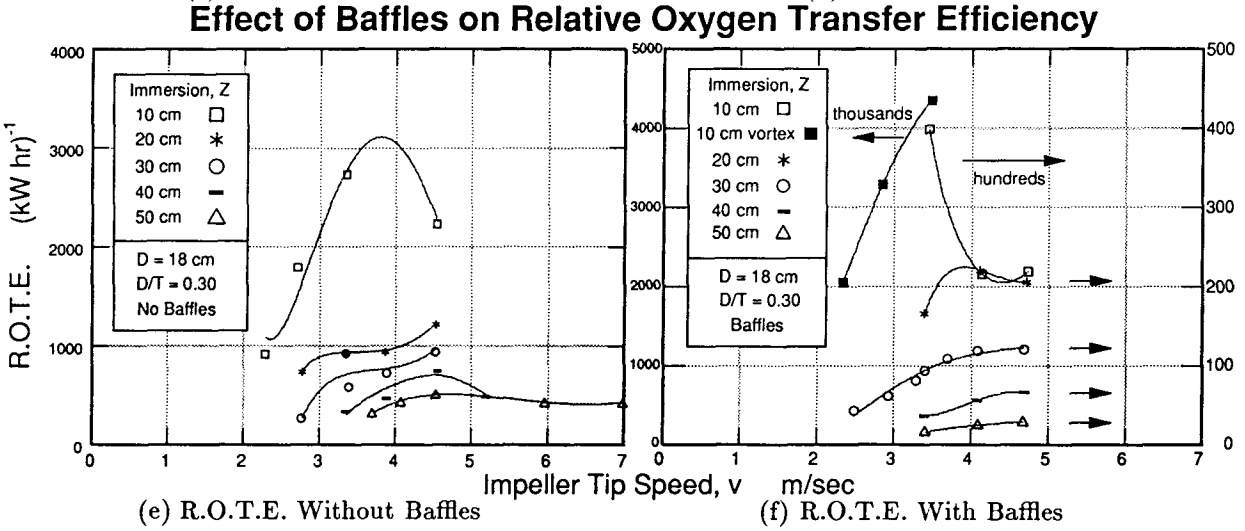

(e) R.O.T.E. Without Baffles (f) R.O.T.E. With Baffles

Figure 4.8: Effect of Baffles on Performance of $D = 18$ cm Radial Disc Impeller

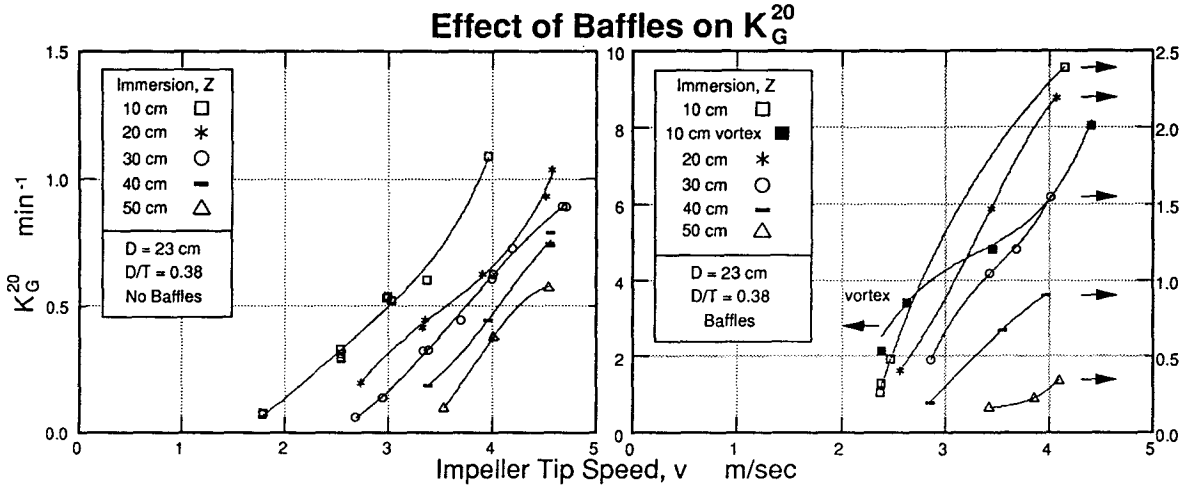

(a) K_G^{20} Without Baffles (b) K_G^{20} With Baffles

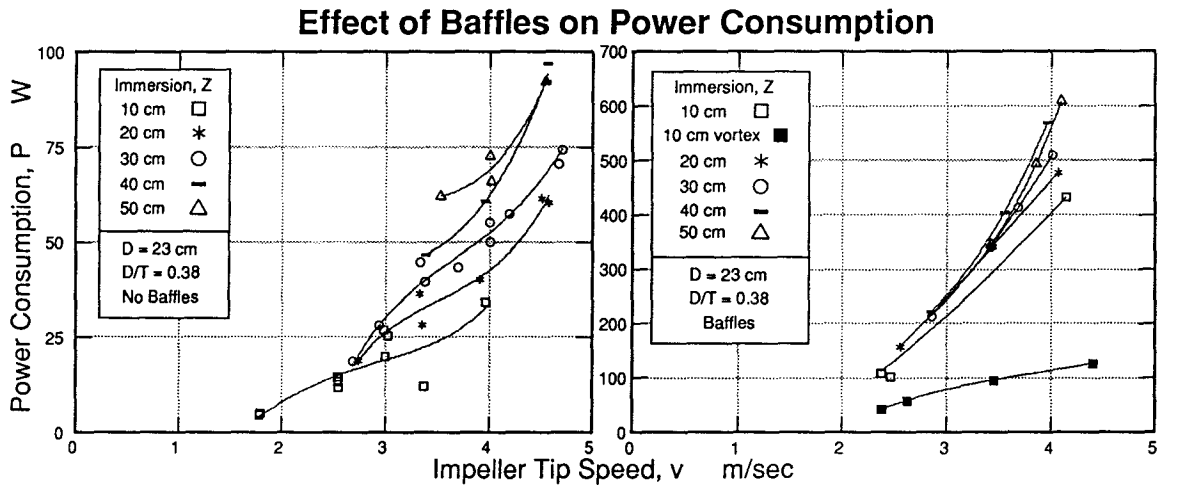

(c) P Without Baffles (d) P With Baffles

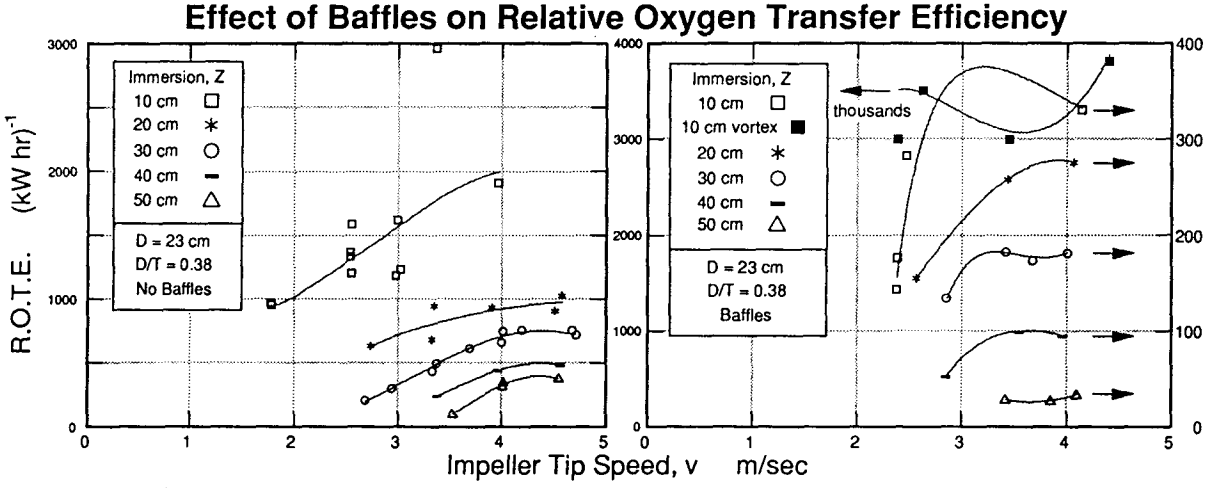

(e) R.O.T.E. Without Baffles (f) R.O.T.E. With Baffles

Figure 4.9: Effect of Baffles on Performance of D = 23 cm Radial Disc Impeller

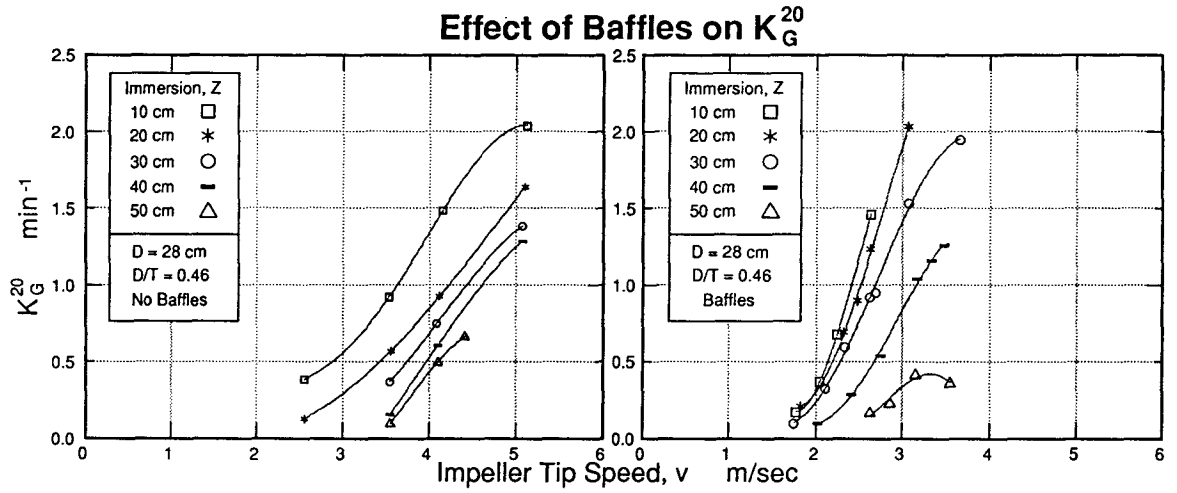

(a) K_G^{20} Without Baffles (b) K_G^{20} With Baffles

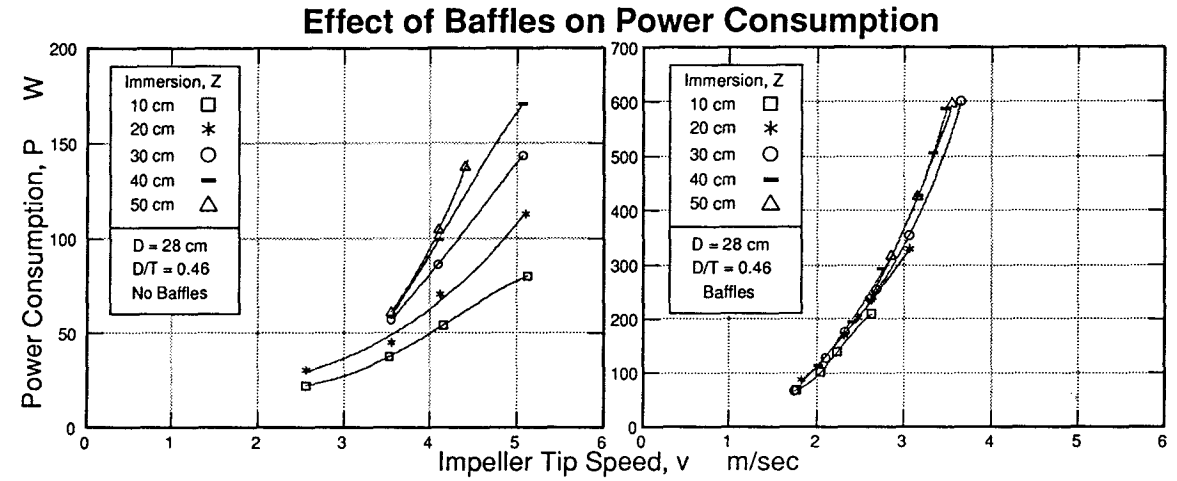

(c) P Without Baffles (d) P With Baffles

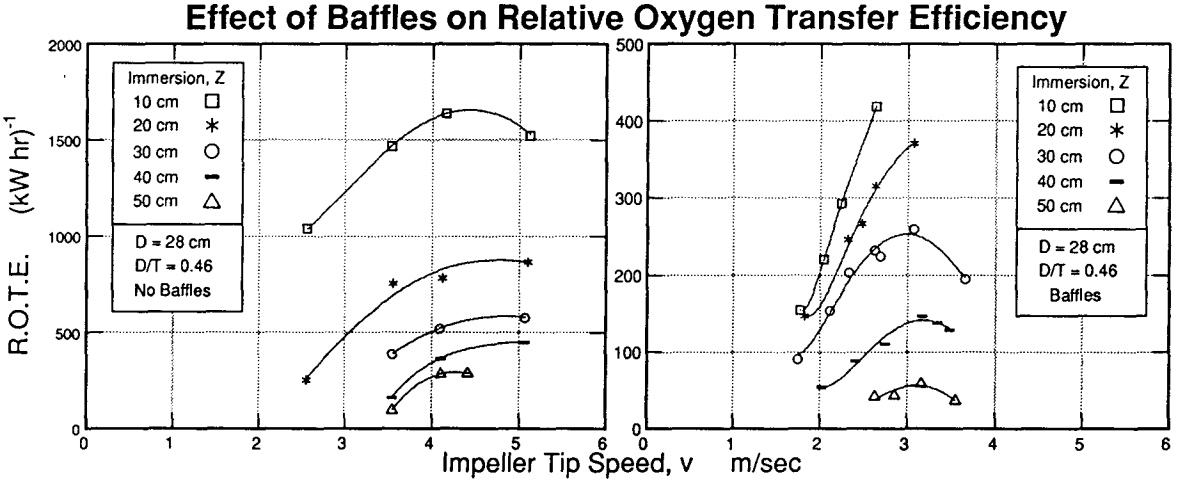

(e) R.O.T.E. Without Baffles (f) R.O.T.E. With Baffles

Figure 4.10: Effect of Baffles on Performance of $D = 28$ cm Radial Disc Impeller

But there is an important exception to this trend. For this vessel shape, for a given impeller there appears to be a critical immersion depth Z_C above which baffles improve K_G^{20} but below which they cause a reduction. (Alternatively, this may be defined for a given immersion depth as a critical impeller diameter.) This is better illustrated in Figure 4.11, where the data have been interpolated to two impeller tip speeds and plotted as a function of the immersion depth[5].

In Figure 4.11(a:b) where $D = 18$ cm, K_G^{20} is *lower* with baffles until Z is brought to about 35 cm. With an increase in D to 23 cm (Figure 4.11(c:d)), the improvement in K_G^{20} caused by baffles is now seen to occur at or near $Z = 50$ cm. With $D = 28$ cm (Figure 4.11(e:f)), the improvement appears to occur at some point below $Z = 50$ cm. Thus for a given tip speed, improvement in K_G^{20} by the addition of baffles will be enhanced by an increased impeller diameter (K_G^{20} will be increased at a deeper Z) or a more shallow immersion depth (K_G^{20} will be increased at a smaller D).

The existence of a stable vortex in the presence of baffles was mentioned in Section 4.2.2, and Figures 4.8(a:b) and 4.9(a:b) illustrate their profound increase in K_G^{20}. Over the tip speed range where they are stable, baffled vortices gave transfer rates about four times greater than the standard baffled condition and about six times greater than the unbaffled vessel. Clearly, a geometry which can sustain a vortex and concurrently exploit the increased mixing provided by baffles offers much promise for improvements in oxygen transfer.

[5]Dotted lines have been included for the sake of reference. In Figure 4.11(a:b) it indicates the extrapolation of vortex behaviour for the 18 cm impeller although the vortex was no longer stable at tip speeds above about $v = 3.44$ m/sec. In Figure 4.11(c:d) the 'typical' flow pattern was stable only outside of the tip speed range shown. In Figure 4.11(e:f), the impeller was not run at $v = 3.5$ or 3.8 m/sec at all immersion depths; thus the extrapolation from lower tip speeds has been included.

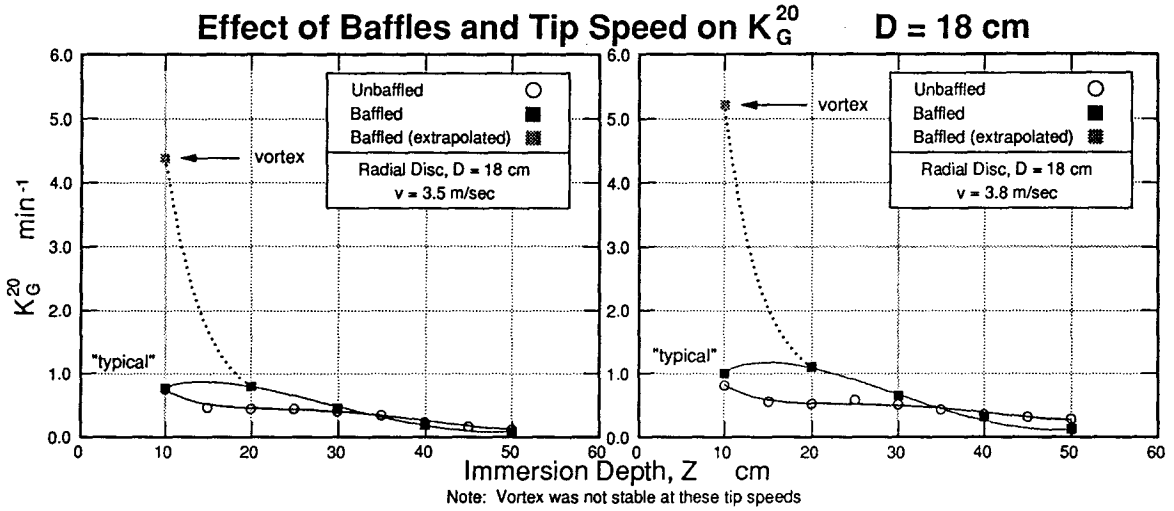

(a) K_G^{20} at $D = 18$ cm, $v = 3.5$ m/sec (b) K_G^{20} at $D = 18$ cm, $v = 3.8$ m/sec

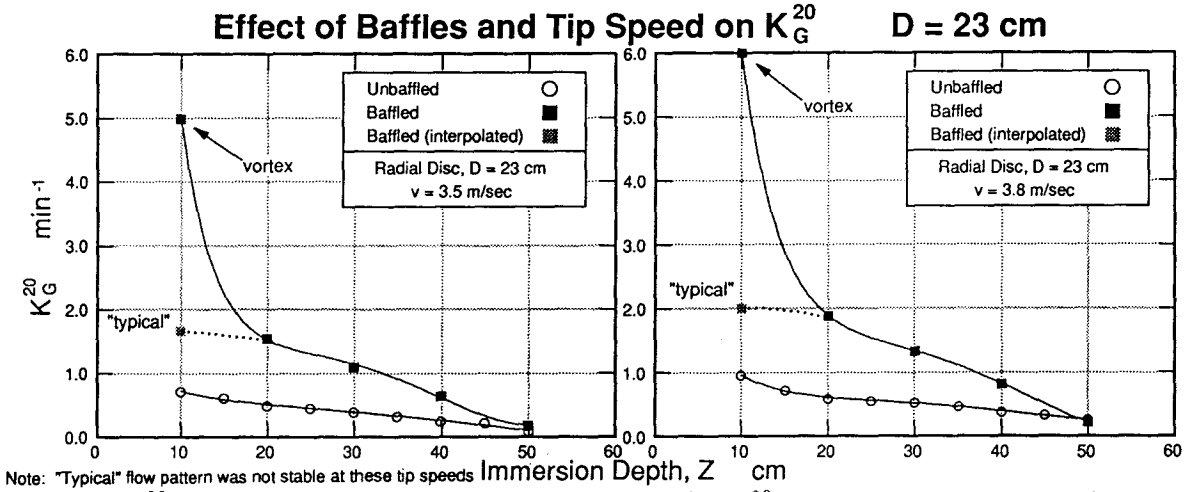

(c) K_G^{20} at $D = 23$ cm, $v = 3.5$ m/sec (d) K_G^{20} at $D = 23$ cm, $v = 3.8$ m/sec

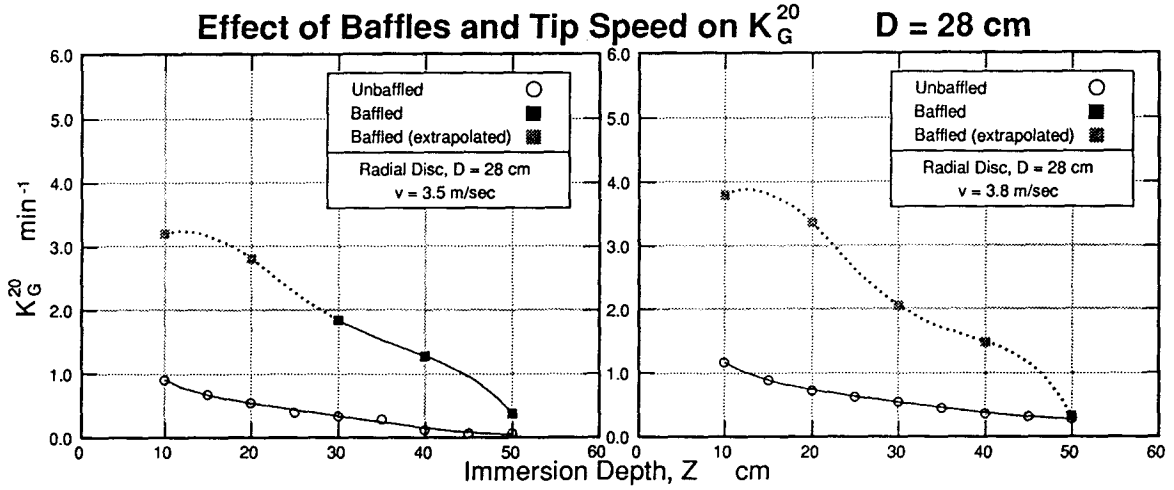

(e) K_G^{20} at $D = 28$ cm, $v = 3.5$ m/sec (f) K_G^{20} at $D = 28$ cm, $v = 3.8$ m/sec

Figure 4.11: Effect of Baffles on K_G^{20} for a Given D, Z

4.3.2 Effect of Baffles on Power Consumption

Graphs (c) and (d) in Figures 4.8 to 4.10 show the substantial increase in power consumption when baffles are inserted into the mixing vessel. At tip speeds between 3 and 5 m/sec the power consumed is increased by a factor of between six and ten. The flow patterns are made much more complex by the baffles, and the magnitude of the difference in P suggests the conversion of radial flow to axial flow is large, and that the impeller must be rotating against some of its discharge flow which has been returned by the baffles.

The increase in power consumption as immersion depth increases shows some uniformity in Figure 4.10(d) for $D = 28$ cm in the unbaffled vessel. A similar trend is apparent at $v = 4$ m/sec in Figure 4.9(c) although there is more scatter of the data.

In the baffled vessel there is an apparent inversion for the power consumption at $Z = 50$ by the two smallest impellers at higher tip speeds: it lies between that consumed at $Z = 30$ and 40 (Figures 4.8(d) and 4.9(d)). This may be a reflection of less severe baffling occurring in the impeller region as the impeller approaches the dish bottom. Experiments in a flat-bottomed vessel would confirm if this interpretation is correct.

When the stable vortex was sustained in spite of the baffles (denoted by the shaded boxes in Figures 4.8(b) and 4.9(b)) the power consumption relative to the typical baffled flow was reduced by about 60 per cent. But relative to unbaffled flow it still was approximately three to four times as great. This indicates that less than 'full baffling' is provided when both vortex and surface aeration are operative.

4.3.3 Effect of Baffles on Relative Oxygen Transfer Efficiency

Graphs (e) and (f) in Figures 4.8 to 4.10 illustrate that the improvements in K_G^{20} caused by baffles are more than matched by the corresponding increase in power consumption.

It is difficult to put an exact value on the per cent reduction relative to the unbaffled

condition, due to the different slopes of the curves. In broad terms, for the smaller two impeller diameters the efficiency with baffles is reduced by about 70 to 80 per cent, *i.e.* the unbaffled vessel is about three to four times more energy efficient. This is not valid for the largest impeller (Figure 4.10(e:f)), which with baffles is able to pump gas at tip speeds lower than without baffles (and even below v_C). Hence at low tip speeds it is more efficient by default, but is surpassed by the unbaffled impeller at about $v = 3.5$ m/sec.

While energy efficiency with or without baffles increases with tip speed but with diminishing returns, Figure 4.10(f) gives a good illustration that a break-point exists beyond which the increase in P outstrips the increase in K_G^{20}. There are indications this may occur for the other impellers but is especially pronounced in this example where impeller-baffle interaction would be at its greatest.

When the vortex was present in the baffled vessel, as mentioned the oxygen transfer rate was increased by a factor of six and four, while power consumption increased by a factor of four and declined by three-fifths relative to the unbaffled and typical baffled cases respectively. Since it is superior not only in terms of relative efficiency but also in oxygen transfer rate, it is the most attractive means of oxygen transfer.

4.4 Comparison of Axial Flow (Upward Pitch) and Radial Flow Impellers

As noted in Section 4.2.3, the upward pumping axial impeller was studied at one diameter $D = 23$ cm in the unbaffled vessel. This allows a basic comparison of its performance with the radial flow impeller of the same diameter, displayed in Figure 4.12.

4.4.1 Effect of Impeller Type on the Rate of Oxygen Transfer K_G^{20}

In the absence of baffles both the radial disc and upward pumping axial impellers pump gas from a vortex. Figures 4.12(a) and (b) illustrate chiefly their abilities at creating the

gas vortex. The axial impeller is uniformly inferior at the lower immersion depths, and expectedly so since it discharges its flow both radially and axially. The axial component contributes little to the creation of the forced liquid vortex. At $Z = 10$ its transfer rate is much increased due to the ease with which the shallow pool of liquid above the impeller plane can be made into a vortex. At the highest tip speed this liquid pool was converted into a froth; at high tip speed but increasing immersion the froth subsided, and the vortex was uneven and slopped against the vessel walls. Only at $Z = 10$ cm was K_G^{20} for the axial impeller comparable to the radial disc impeller.

4.4.2 Effect of Impeller Type on Power Consumption

Figures 4.12(c) and (d) show the power consumed by the axial impeller is reduced to just over one-half that consumed by the radial disc impeller. While this comparison is true for a given tip speed, the oxygen transfer results in Figures 4.12(a) and (b) suggest this is because vortex development is not as great with the axial impeller: less energy is required to sustain a forced liquid vortex of smaller diameter.

4.4.3 Effect of Impeller Type on Relative Oxygen Transfer Efficiency

Figures 4.12(e) and (f) show efficiencies for the axial impeller equal or marginally inferior to the radial disc impeller for $Z = 20$ through 50 cm. While this can be attributed to the axial component of discharge from the impeller, the expected efficiencies should be much lower on this account.

Comparison of the results at $Z = 10$ cm indicates that the vortex, splashing and froth generated by the axial impeller at high tip speeds is more efficient than the stable vortex of the radial disc impeller. The dubious data point for the latter impeller is the result of an unusually low value for net power consumption.

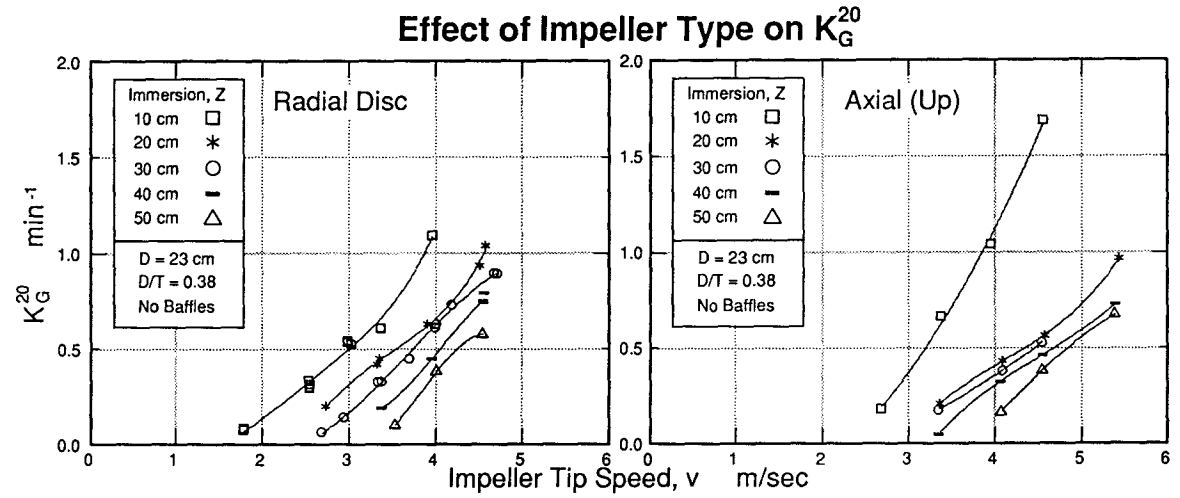

(a) K_G^{20} Radial Disc (b) K_G^{20} Upward Axial

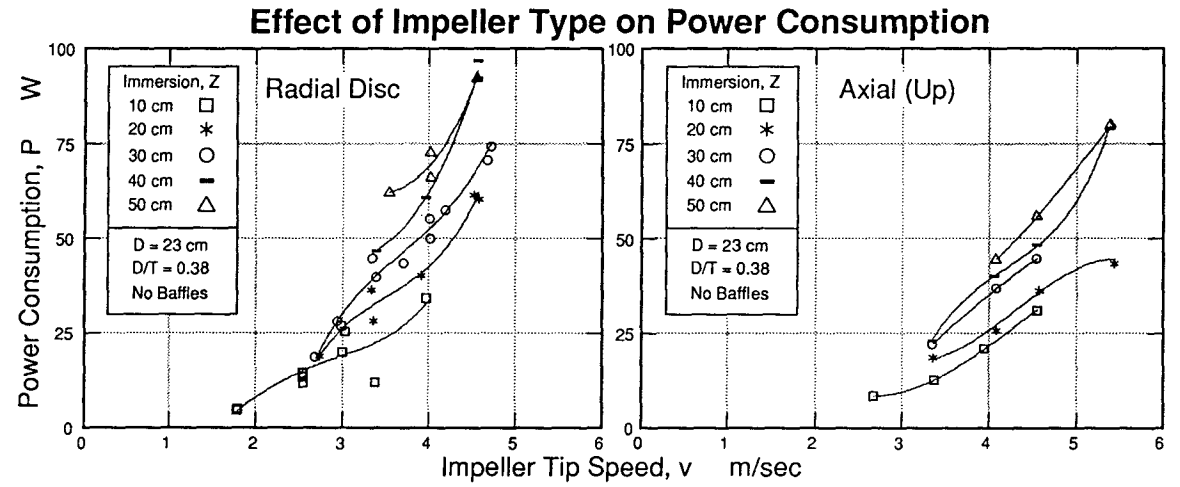

(c) P Radial Disc (d) P Upward Axial

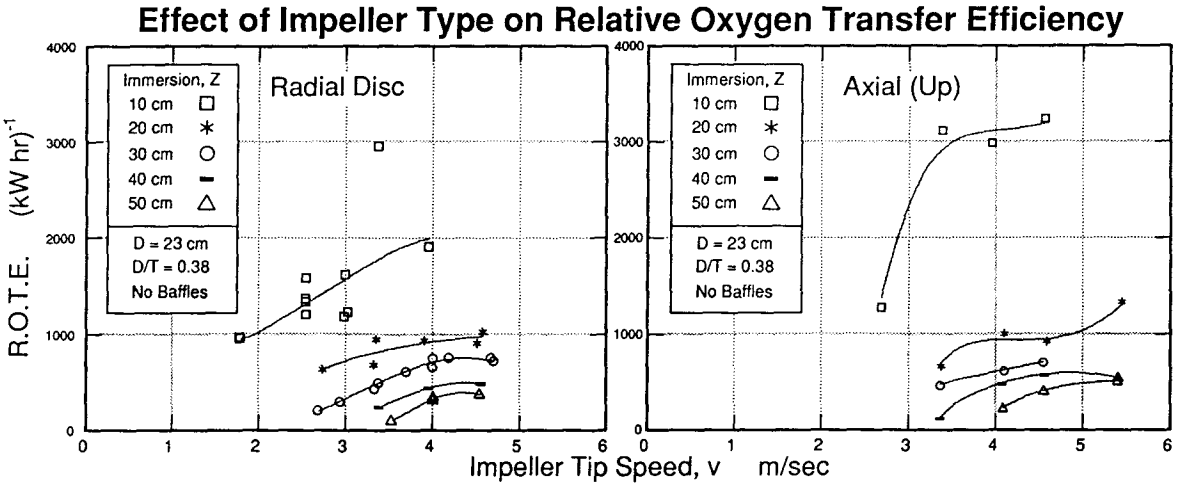

(e) R.O.T.E. Radial Disc (f) R.O.T.E. Axial

Figure 4.12: Effect of Impeller Type on Performance in Unbaffled Vessel

4.5 Impeller Disc Diameter

A brief series of experiments was performed with a series of radial disc impellers with $D = 23$ cm and identical blade dimensions but ratios of disc diameter to impeller diameter of 0.67, 0.75 and 0.85. The results are presented as bar graphs in Figures 4.13 and 4.14.

For the three impeller tip speeds at $Z = 15$ cm, two at $Z = 30$ cm and one at $Z = 45$ cm, the K_G^{20} results are consistently within about 0.04 units of each other. No conclusive pattern emerges to indicate superiority of one disc size over another, although the results for $D_d/D = 0.67$ appear to be the least favourable.

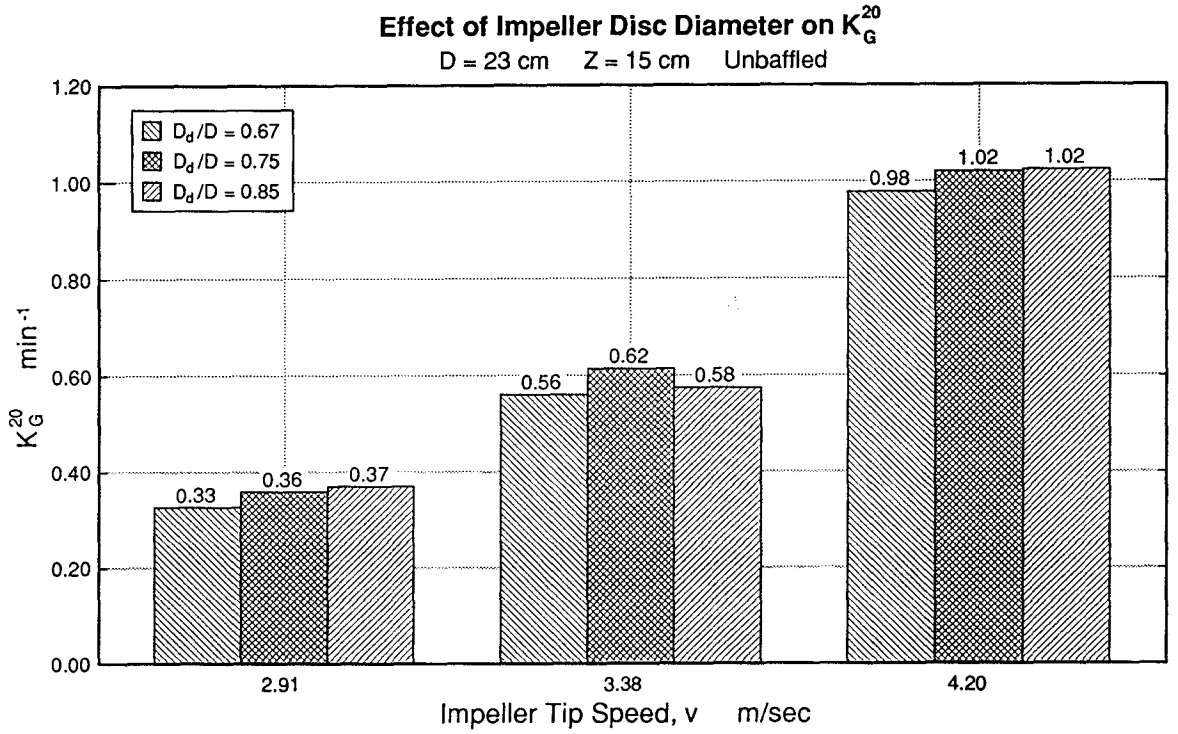

Figure 4.13: Effect of Impeller Disc Diameter on K_G^{20} at $Z = 15$ cm ($D = 23$ cm)

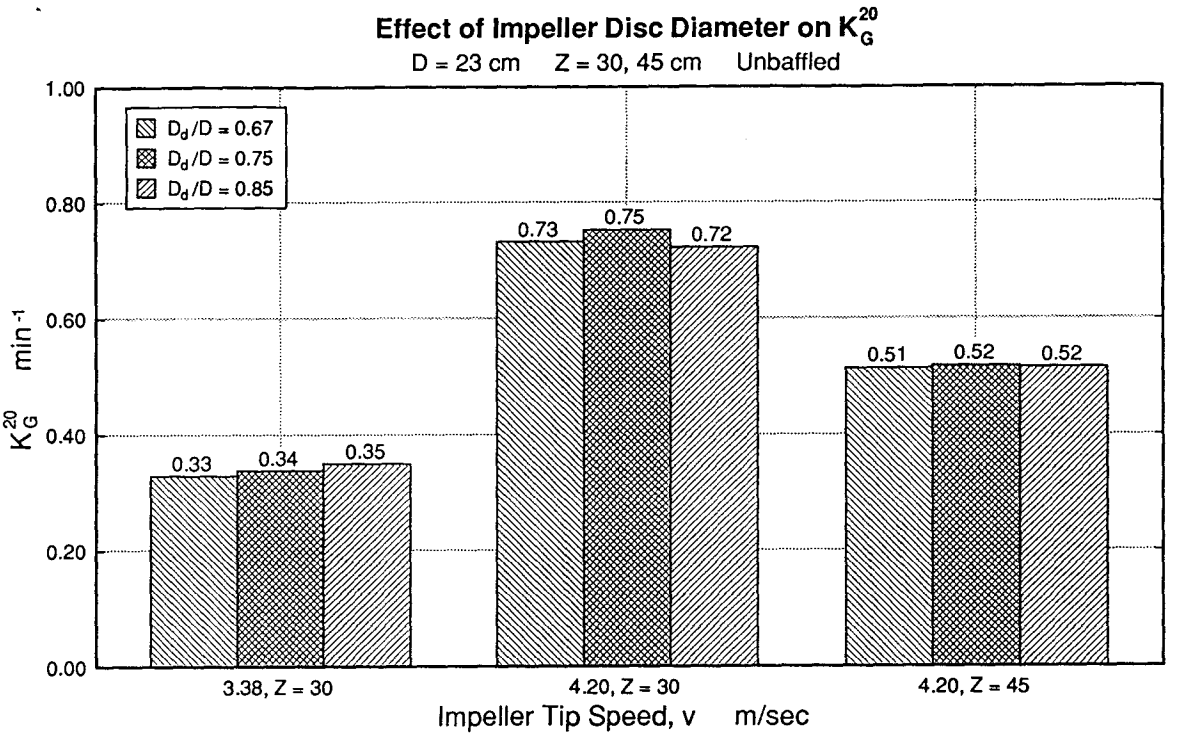

Figure 4.14: Effect of Impeller Disc Diameter on K_G^{20} at $Z = 30$, 45 cm ($D = 23$ cm)

4.6 Dual Impeller Configurations

Six dual impeller configurations were investigated in the unbaffled vessel as an extension of the work of DeGraaf, approximating the standard configuration employed in the zinc pressure leach autoclave used by Cominco (upward pumping axial above/four blade radial below). The six blade radial disc was selected in place of the four blade radial since DeGraaf determined it gave superior performance in his gas-liquid mass transfer experiments [40, p. 47]. The D/T ratio was maintained by using the 28 cm diameter impellers.

4.6.1 Adherence to the Critical Tip Speed Equation

The first analysis compared the v_C values for each impeller location with the v_E for each configuration calculated from three experiments, and is given in Table 4.6.

Table 4.6: Initial Results of Dual Impeller Configurations Investigated

Designation	Upper	Lower	$v_{C(\text{UPPER})}$	$v_{C(\text{LOWER})}$	v_E	R^2
For $Z_U = 15$ cm, $Z_L = 45$ cm:						
A15/R45	Axial	Radial	1.72	2.97	3.13	1.000
R15/A45	Radial	Axial	1.72	2.97	2.64	0.972
R15/R45	Radial	Radial	1.72	2.97	3.09	0.995
For $Z_U = 25$ cm, $Z_L = 35$ cm:						
A25/R35	Axial	Radial	2.21	2.62	2.76	0.998
R25/A35	Radial	Axial	2.21	2.62	2.71	0.999
R25/R35	Radial	Radial	2.21	2.62	2.55	0.969

The v_E for four configurations was similar to but larger than v_C for the lower of the two impeller positions. The two cases where v_E was intermediate to the two v_C values are marked by poor linearity. For R25/R35 there was slopping of the vortex caused by interference between the flow patterns of the two closely spaced impellers; the result for R15/A45 is caused by a large K_G^{20} at low tip speed which cannot be easily explained.

Generally, v_E is best matched by $v_{C(\text{LOWER})}$. Restated, the *onset* of gas pumping by dual impellers in an unbaffled vessel may be characterized by v_E of the lower impeller.

4.6.2 Performance of Dual Impeller Configurations

The six configurations were evaluated for oxygen transfer rate, power consumption and relative oxygen transfer efficiency. The results appear in Figures 4.15 to 4.17 as bar graphs. Impeller tip speeds very close to 3.36, 4.12 and 4.61 m/sec were used for each configuration, and linear interpolation (or extrapolation) was used where required to adjust the data to these tip speeds.

Oxygen Transfer Rate of Dual Impeller Configurations

The major conclusion from Figure 4.15 is that better oxygen transfer is provided when

the lower impeller is at the more shallow position. This indicates it is the lower of the two impellers which defines the shape of the vortex from which both pump gas.

It would be expected that the pair with a lower axial impeller would give the poorest result amongst the R/R, R/A and A/R combinations, since it would create the weakest vortex. In fact this is seen for the 25/35 setting, but at 15/45 the R/A pair gives the best result, not the poorest. The axial impeller by itself pumps poorly from its vortex at $Z = 45$ cm so it cannot be said that the gas pumping performance *per se* can be characterized by the lower impeller (although the v_E performance can). This must mean that the radial disc impeller at $Z_U = 15$ cm is contributing the bulk of the pumping from the vortex.

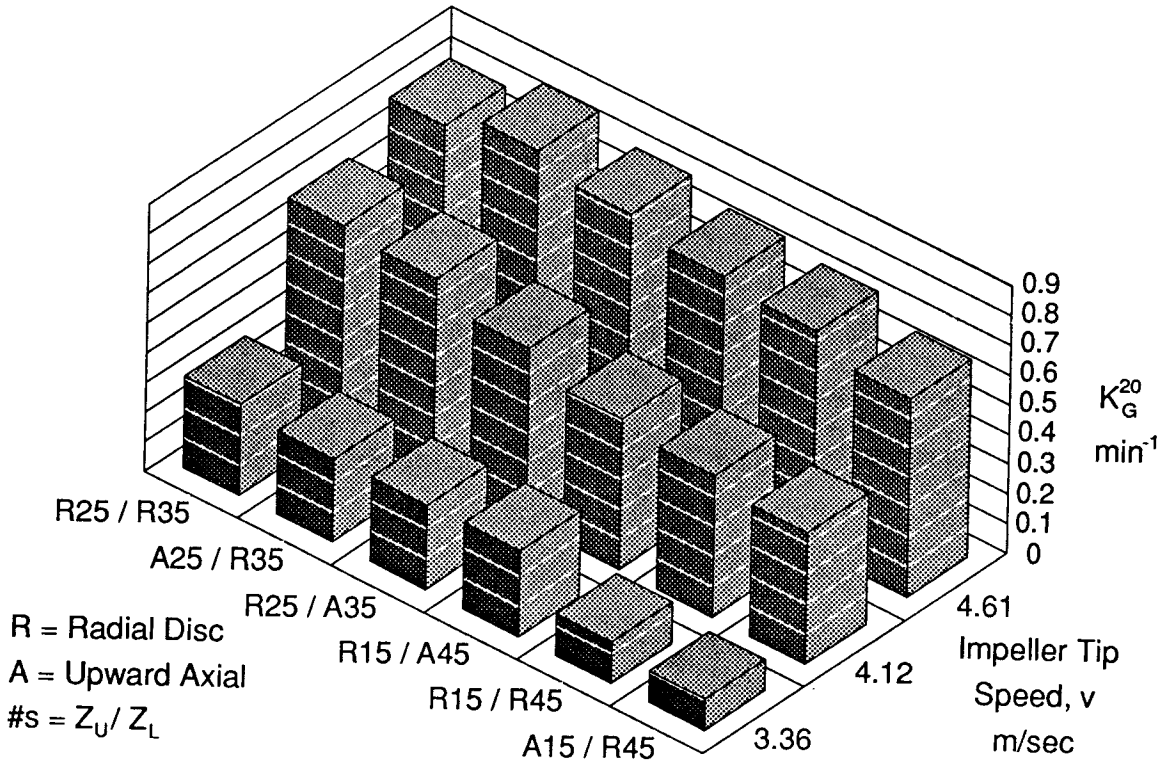

Figure 4.15: Oxygen Transfer by Dual Impellers in Unbaffled Vessel

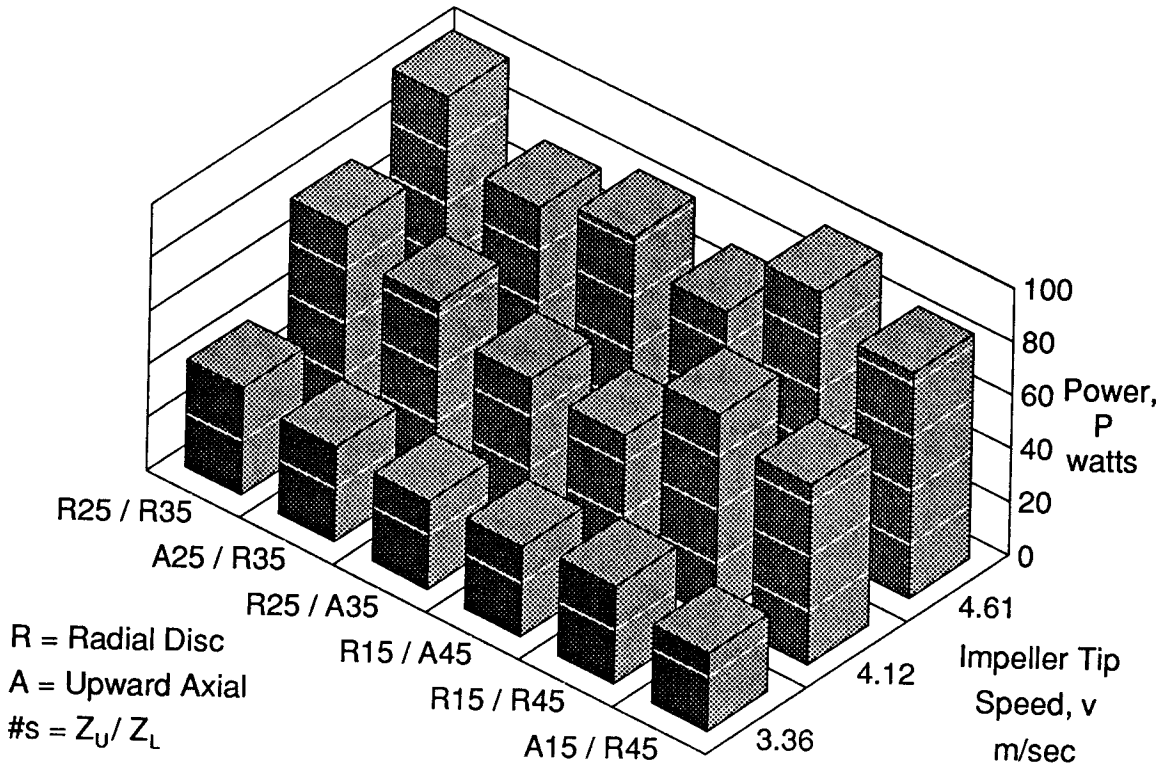

Figure 4.16: Power Consumption by Dual Impellers in Unbaffled Vessel

The slopping caused by flow interactions in the R25/R35 pair caused its result at $v = 4.61$ m/sec not to exceed A25/R35. Until this point the R25/R35 pair gave the largest rates of oxygen transfer. It is expected that at even greater tip speeds the slopping would continue to be a problem, and that A25/R35 would yield the best results.

Power Consumption of Dual Impeller Configurations

From the power consumption data in Figure 4.16, very generally it can be concluded that for a given Z_U/Z_L, the least power was drawn by the R/A pairs, A/R were intermediate and R/R drew the most power. As well, for a given R/A, A/R or R/R pair, power consumption was very similar whether the inter-impeller spacing was 10 cm or 30 cm.

The value of P for A25/R35 at $v = 4.61$ m/sec appears to be lower than the trend suggests. It had the greatest disparity between power measured at the motor (96.9 W)

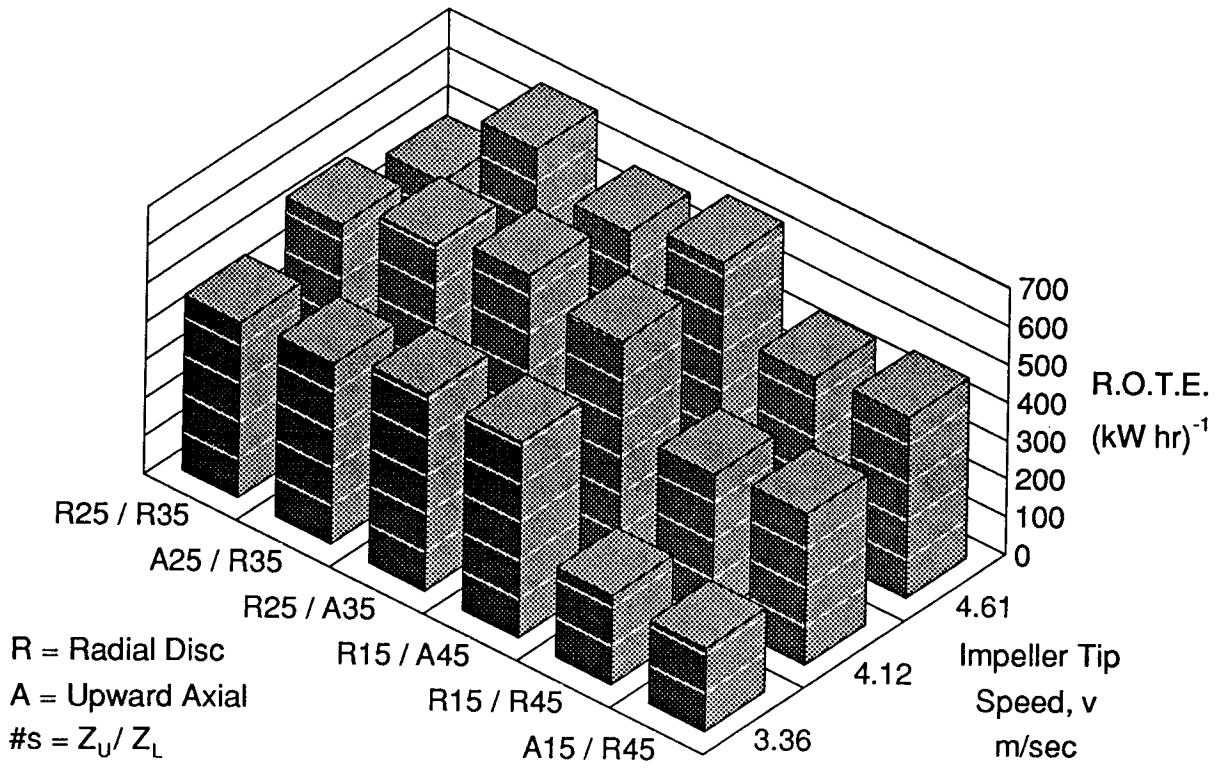

Figure 4.17: R.O.T.E. by Dual Impellers in Unbaffled Vessel

and at the tank (76.2 W).

Relative Oxygen Transfer Efficiency of Dual Impeller Configurations

Oxygen transfer efficiency is plotted in Figure 4.17. The R/R pairs were the least efficient at the two immersion settings. The R/A pairs generally were the best, especially if P for A25/R35 was underestimated.

4.6.3 Comparison of Dual and Single Impeller Performance

It is important to evaluate the oxygen transfer characteristics of dual impeller systems for systems such as the zinc pressure leach where two impellers are required for three-phase mixing. But the usefulness of dual impellers only for gas-liquid mixing also needs to be addressed. Figures 4.18 to 4.22 compare the K_G^{20}, P and R.O.T.E. performance for

the impeller pairs to the performance of the constituent single impellers, and evaluates the 'additivity' principle suggested for dual impellers in baffled vessels [161]. Data bars denoted within apostrophes, e.g. 'R25+R35', are the mathematical or weighted sums of K_G^{20}, P and R.O.T.E. Data for the axial impeller at $Z = 25$, 35 and 45 cm were extracted[6] from regression curves computed for the data for $Z = 20$, 30, 40 and 50 cm.

Performance of the R25/R35 Dual Impeller Configuration

Easily the most striking feature of Figure 4.18(a) is that there is little improvement in K_G^{20} by adding the second impeller. The R25/R35 pair is poorer than either single impeller at $v = 4.61$ m/sec but offers some improvement over R35 at the lower tip speeds.

On the other hand, power consumption for the pair increases with tip speed more rapidly than for either of the single impellers, and is greater than either beyond the lowest tip speed. Clearly, power consumption of the pair is not additive, although it is greater than the power consumed by the lower impeller.

As expected, relative oxygen transfer efficiency is lower than for R25 and declines at high tip speed because of the rapid increase in P mentioned above. Again, there appears to be some improvement over R35 at the lowest tip speed, and the efficiency of the pair is close to the weighted sum of the two individual impellers.

Performance of the R15/R45 Dual Impeller Configuration

The R15/R45 pair in Figure 4.19 show a slight improvement in oxygen transfer *vs.* R45 if a second radial disc impeller is added at $Z_U = 15$ cm. The power consumption is affected very little and oxygen transfer efficiency is improved. However, it would be far simpler to use the single R15 impeller, which would give a superior K_G^{20}, P and efficiency.

---

[6]Since the performance of the axial impeller at $Z = 10$ cm is dissimilar from $Z = 20$ cm and below, and it is unclear if the change is gradual or occurs at a sharp break, regression estimates for K_G^{20} and R.O.T.E. at $Z = 15$ cm would be subject to uncertainties of about $\pm$ 100 per cent and thus have not been employed.

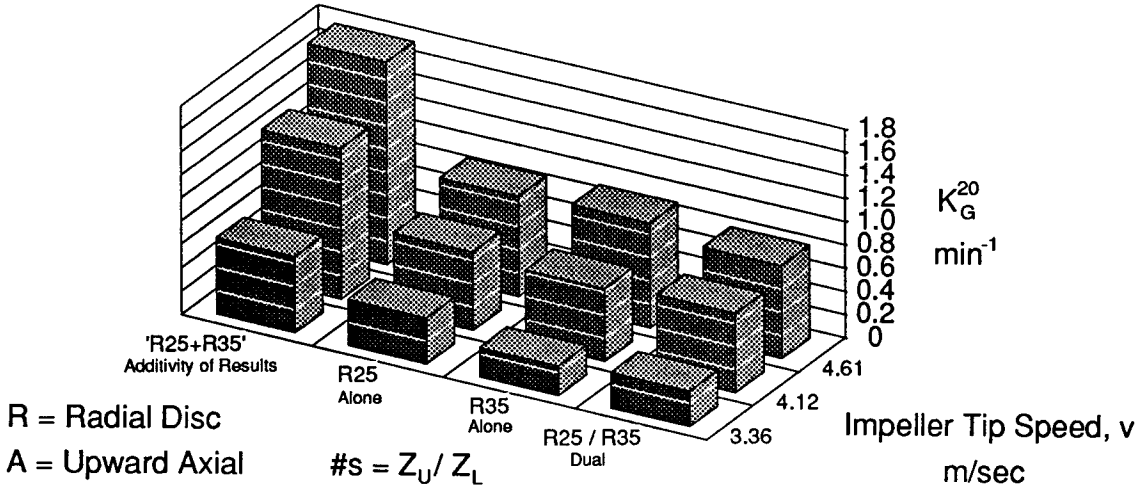

(a) Oxygen Transfer Rate K_G^{20}

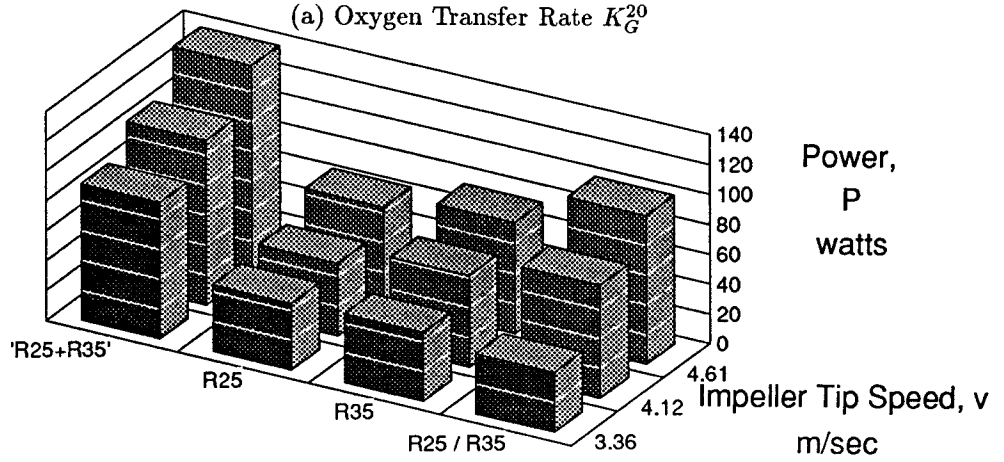

(b) Power Consumption P

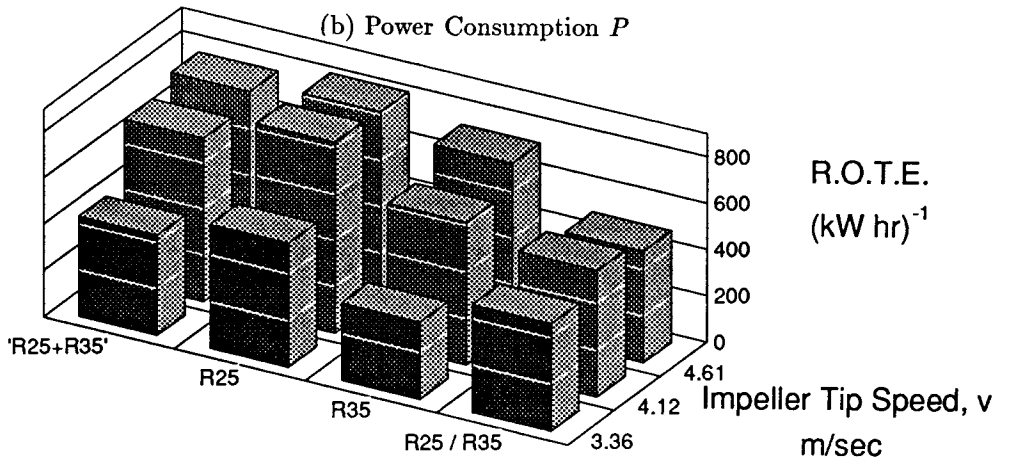

(c) Relative Oxygen Transfer Efficiency

Figure 4.18: Comparison of Single and Dual R25/R35 Impellers in Unbaffled Vessel

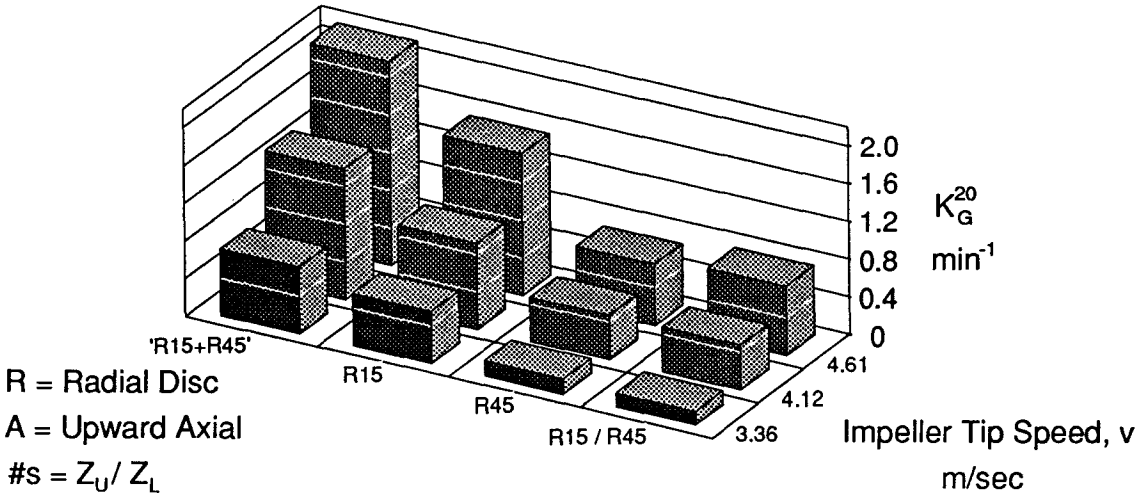

(a) Oxygen Transfer Rate K_G^{20}

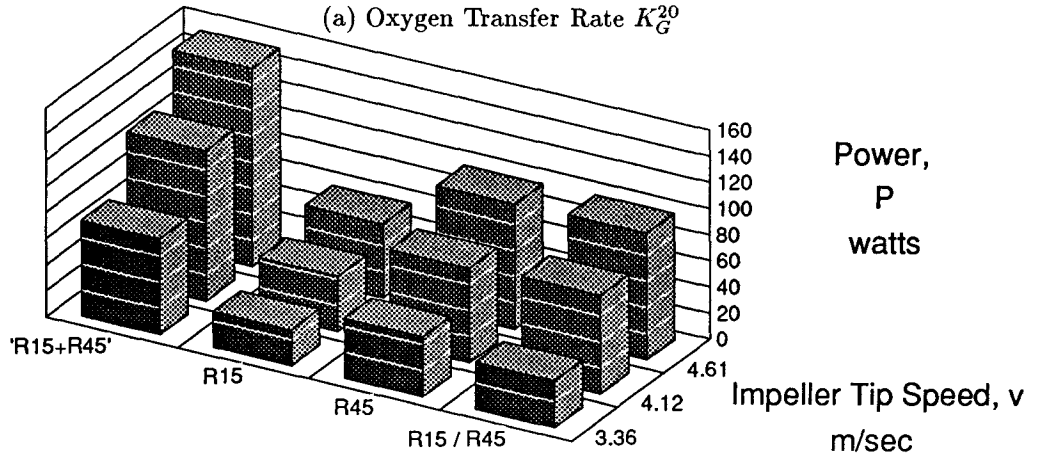

(b) Power Consumption P

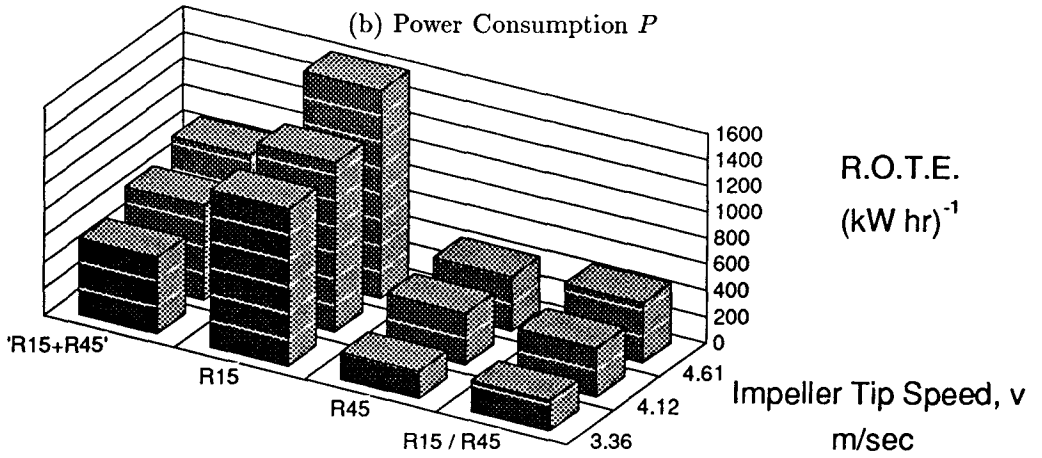

(c) Relative Oxygen Transfer Efficiency

Figure 4.19: Comparison of Single and Dual R15/R45 Impellers in Unbaffled Vessel

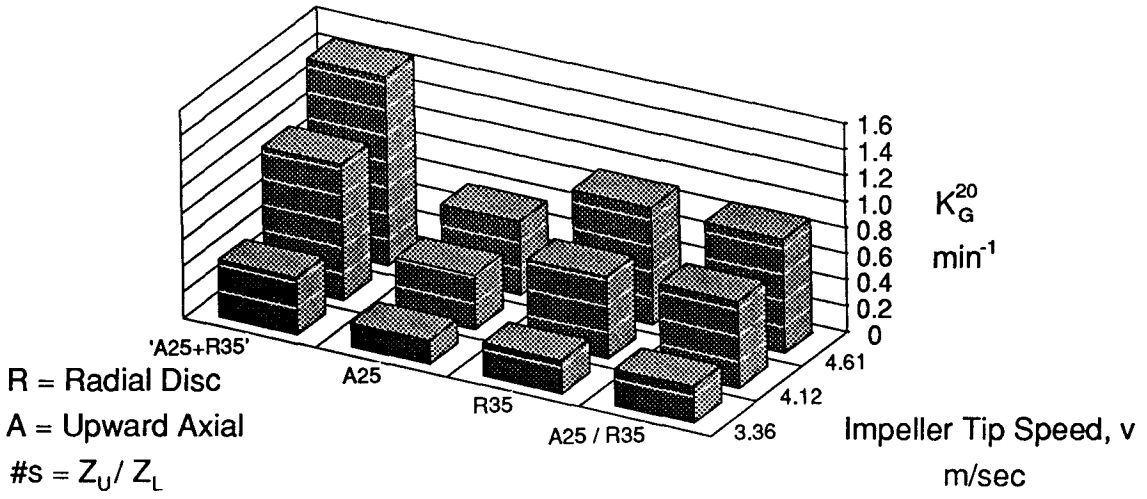

(a) Oxygen Transfer Rate K_G^{20}

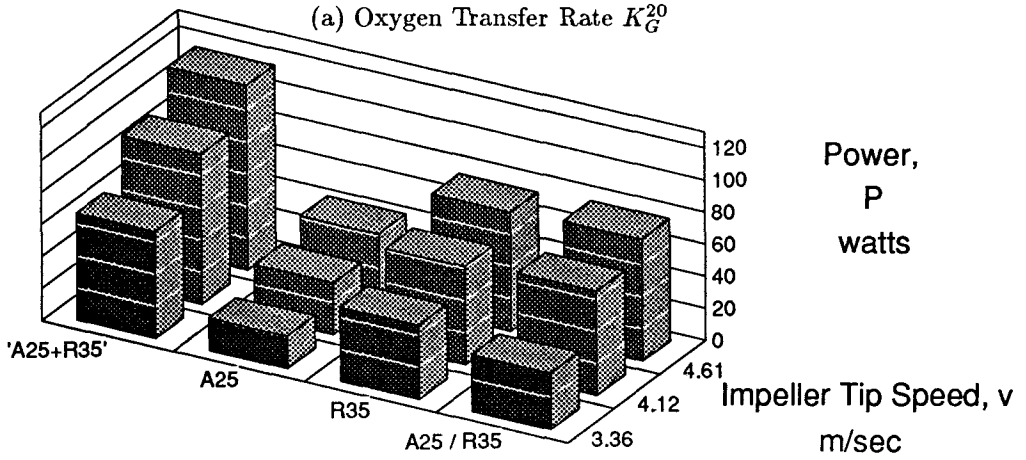

(b) Power Consumption P

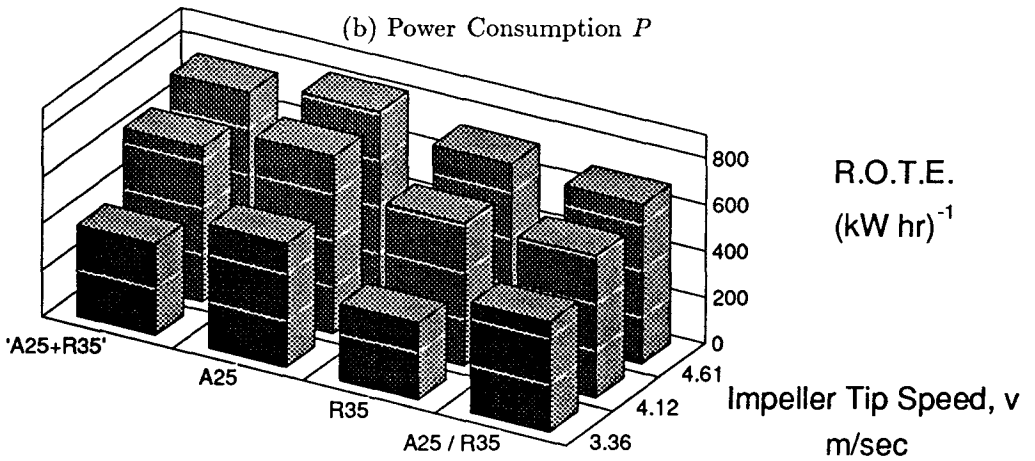

(c) Relative Oxygen Transfer Efficiency

Figure 4.20: Comparison of Single and Dual A25/R35 Impellers in Unbaffled Vessel

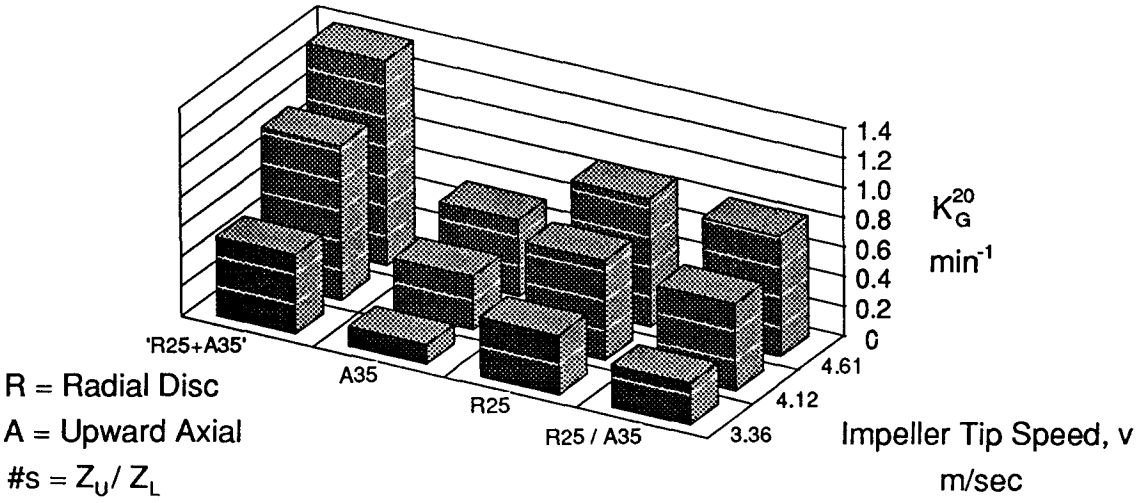

(a) Oxygen Transfer Rate K_G^{20}

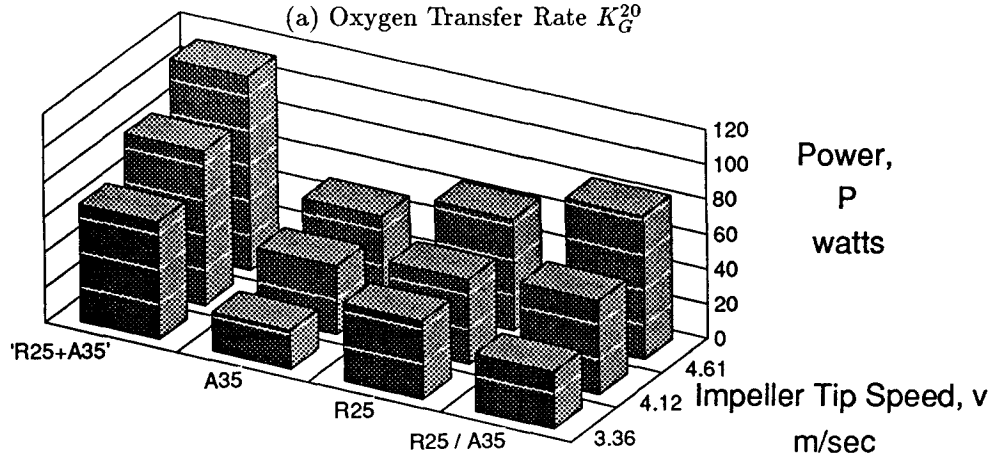

(b) Power Consumption P

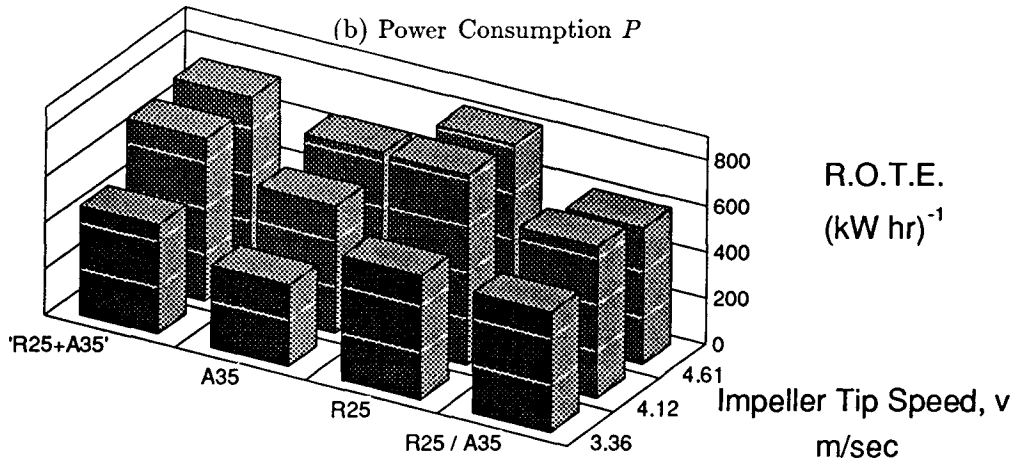

(c) Relative Oxygen Transfer Efficiency

Figure 4.21: Comparison of Single and Dual R25/A35 Impellers in Unbaffled Vessel

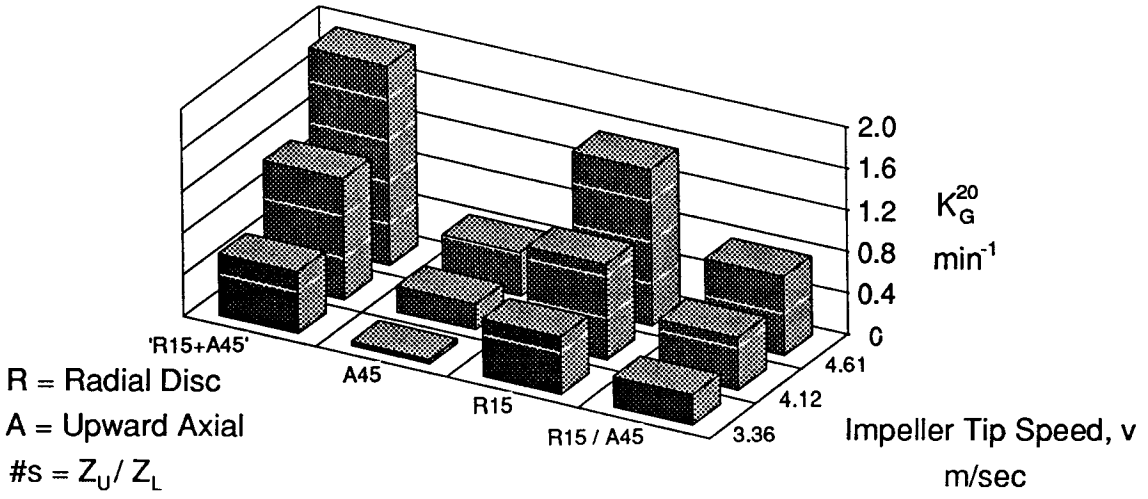

(a) Oxygen Transfer Rate K_G^{20}

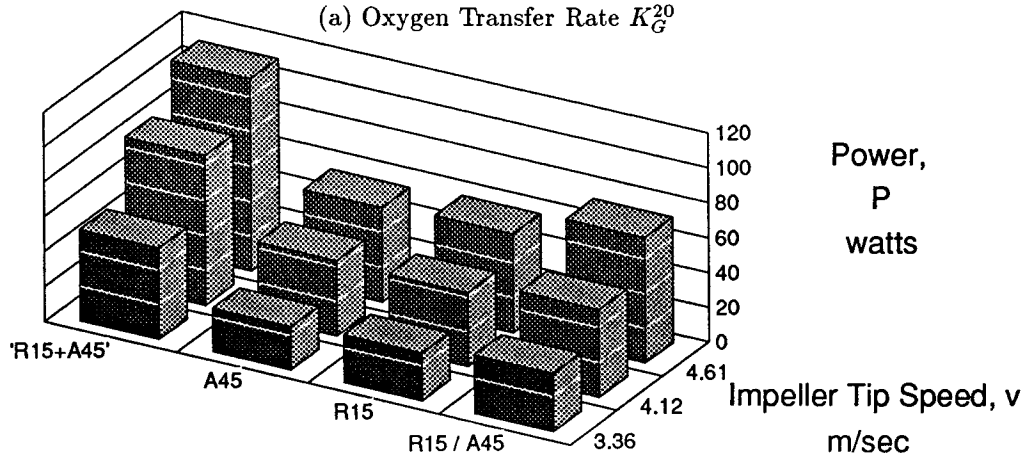

(b) Power Consumption P

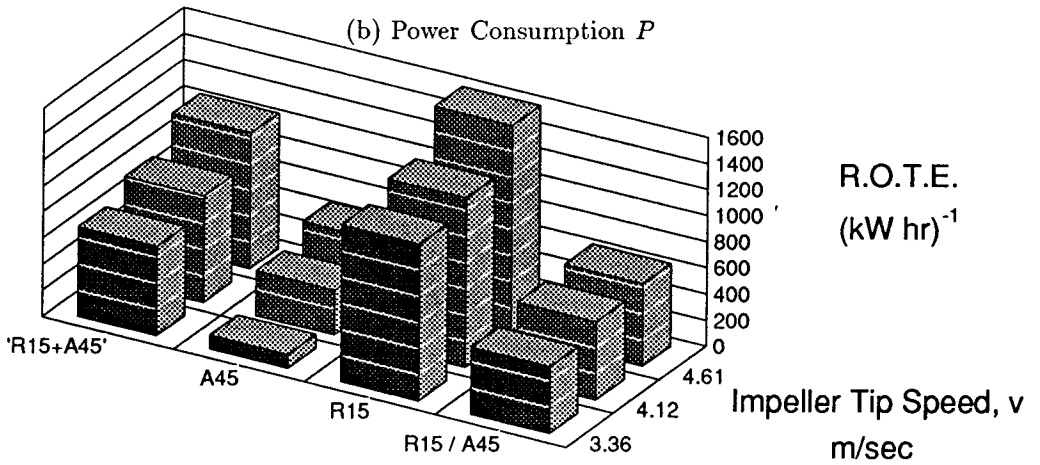

(c) Relative Oxygen Transfer Efficiency

Figure 4.22: Comparison of Single and Dual R15/A45 Impellers in Unbaffled Vessel

Performance of the A25/R35 Dual Impeller Configuration

As with the R25/R35 pair, the A25/R35 pair in Figure 4.20 shows evidence of slight improvement in K_G^{20} over the lone lower radial disc impeller at the lower tip speeds. The A25 impeller pumps much less gas alone than does the R25 mentioned above, so in this case the impeller pair actually offers improvement, albeit small, in K_G^{20} over either of the two individual impellers.

Power consumption appears to be erratic when compared to the R35 impeller. This may be due to flow interactions between the two impellers which are beneficial at lower tip speeds but detrimental as v increases. For this reason the efficiency of the pair at the lowest tip speed is superior to R35, but declines as v increases.

Performance of the R25/A35 Dual Impeller Configuration

The R25/A35 pair in Figure 4.21 gives K_G^{20} results intermediate to the two single impellers. Again, power consumption is lower than the single radial impeller at the lowest tip speed, but increases more quickly with v.

Performance of the R15/A45 Dual Impeller Configuration

The R15/A45 pair in Figure 4.22 does not show a lower power consumption at the lowest tip speed; it is possible the impeller spacing is so large that no beneficial flow interaction can develop.

4.6.4 Use of Dual Impellers for Gas Pumping in Two-Phase Systems

Only a slight increase in K_G^{20} and relative oxygen transfer efficiency is given by the R25/R35 and A25/R35 pairs at low tip speeds. This is hardly strong justification for the use of a dual impeller system for gas-liquid mass transfer by gas pumping in an unbaffled cylindrical vessel. Use of the lower radial impeller of the pair provides superior K_G^{20} and efficiency performance in all but these two cases and is far simpler to operate

and maintain.

The addition of baffling would change the gas pumping mechanism either partly or entirely to surface aeration, and thus would change the roles of the impellers as they have been defined for the unbaffled vessel. This scenario must be investigated before the applicability of dual impellers for gas pumping in two-phase gas-liquid systems can be fully analyzed.

Chapter 5

Discussion

5.1 Critical Tip Speed Theory and Nature of Flow Patterns

Allowing for the difficulty in generating many data points from the experimental regime where K_G^{20} increases linearly with impeller tip speed, the values of v_E presented in Figure 4.4 must be considered as confirming the principle of the critical tip speed theory under conditions of radial flow in a right-cylindrical vessel in the absence of baffles. Although correlations have been published which suggest its existence [79,83,82,84], this result demonstrates that the value of v_C is directly linked to the depth of immersion of the impeller.

Before the equation can be used to great advantage, the departures from ideal energy conversion will need to be firmly characterized.

5.1.1 Unbaffled Vessels

Confirmation of the v_C equation should be expected in unbaffled cylindrical vessels, because the equations defining the critical tip speed (Equation 2.73)

$$v_C = \sqrt{2gZ},$$

and the onset of vortex aeration (Equation 2.36)

$$N_V = c_6\sqrt{\frac{Z'2g}{\pi^2 D^2}},$$

are identical when the vortex height Z' is defined as the distance from the impeller to the static interface, and when $c_6 \equiv 1$, which would be true for ideal energy conversion.

5.1.1.1 Vortex Aeration Mechanism

The gas pumping mechanism under this condition was observed closely. Gas pumping does not commence until the inner edges of the impeller blades are able to slice through the gas-liquid interface of the conical vortex. Gas is induced into the liquid in a kind of reverse analogy to a cyclone cloud: the funnel is stationary and the surroundings are rotating. The pumped gas clings to the back of the impeller blades before being dispersed from the trailing edges of the cavities. The cavity form in plan view could not be ascertained at the impeller speeds employed, but blade coverage was seen to begin along the top and angle down to the outer edge. Discharge occurs initially from a point about one-quarter of the blade height (width) from the top. As gas coverage of the blade increases, discharge is possible from the middle half of the outer blade edge.

5.1.1.2 Effect of Impeller Diameter

The position of the gas vortex relative to the impeller substantiates the slight mis-match but general equality of the vortex and critical tip speed equations, and assists in determining the departures from ideality which cause the tip speed offsets shown in Figure 4.4. This is illustrated schematically in Figure 5.1. As the impeller speed increases, the nose of the parabolic gas vortex approaches the impeller plane. At the speed N_V (or v_V) where the nose just reaches the impeller disc (Figure 5.1(a)), Equation 2.36 is satisfied (although the definition of vortex height Z' is still arbitrary). Since the blades of a Rushton-type turbine do not extend to the hub, they are not able to intersect the gas cone and thus cannot yet pump gas. An *extra increment of impeller speed* is necessary to draw the vortex even deeper into the liquid, such that the nose now lies some distance beneath the impeller disc (Figure 5.1(b)). The deeper gas vortex presents a wider diameter to the impellers, and finally the upper inside corners of the impeller blades are able to chop at

the gas and pump it into the liquid. Thus v_E is attained.

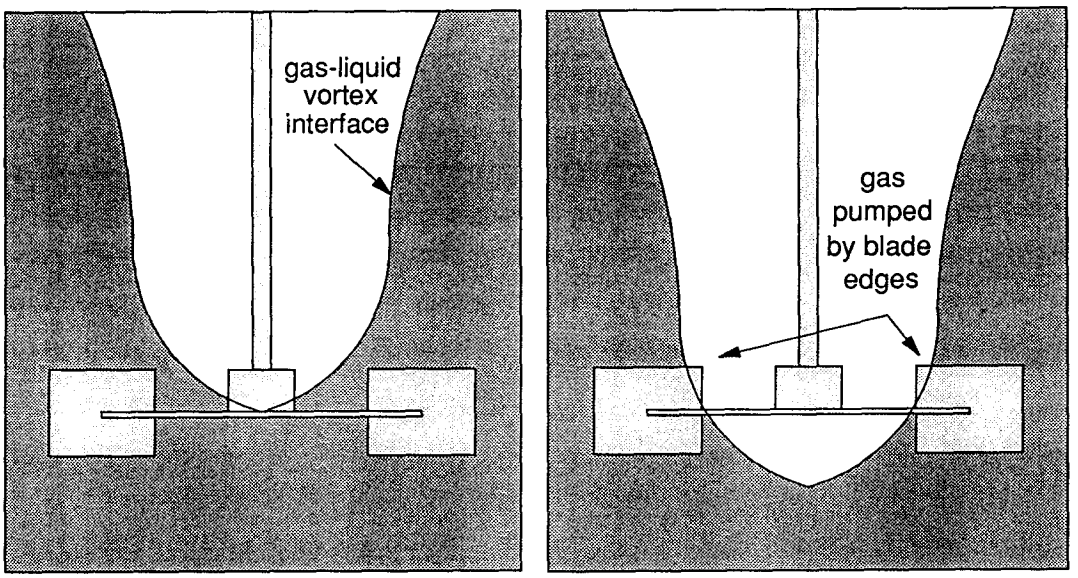

Figure 5.1: Gas Pumping Relative to Gas Vortex Position

The greater offset of v_E from the theoretical v_C displayed by impellers with larger D (Figure 4.4) should be due in large part to the greater distance from the axis of rotation of their inside blade edges. A standard Rushton turbine has an inner blade edge-to-inner blade edge distance of $D/2$. Thus, the blades of the 18 cm impeller will first encounter gas when the gas vortex diameter (at the plane of the blade tops) is 9.1 cm. But the 28 cm impeller will require a gas vortex diameter of 14.0 cm before it begins to pump gas[1].

This is not a complete explanation since an impeller with larger D should sweep out and sustain a forced liquid vortex of greater diameter as well, *i.e.* the gas vortex should also have a greater diameter. The existence of the different offsets, however, indicates

[1]The plane of the blade tops for the 28 cm impeller is only about 1 cm closer to the static interface than for the 18 cm impeller fixed at the same Z.

the wider vortex cone does not entirely compensate for the larger blade-to-blade gap, *i.e.* the two do not vary proportionately with D.

The gas in the nose of the vortex trapped beneath the impeller disc appears as a 'cup'. The cup base was very rounded when Z was small, but was more like a square 'U' when Z was large.

Table 5.1: Impeller 'Cup' Depth at Different Z

Immersion Depth, Z cm	Radial Disc, D = 18 cm		Radial Disc, D = 28 cm	
	tip speed, m/sec	Cup base cm	tip speed, m/sec	Cup base cm
10	2.30	19	2.55	21
50	4.41	64	4.54	65

This is an artifact of the parabolic surface of the gas vortex, which changes with immersion depth. This observation can be used to explain the gradual convergence of the v_E curves to the theoretical line in Figure 4.4. At shallow immersion, the gas-liquid vortex interface has a shallow slope, which means the ability of the blades to reach the gas will be very sensitive to Z: *i.e.* $(\mathrm{d}D_{\mathrm{vortex}}/\mathrm{d}Z)$ is large. At the largest Z (50 cm), the slope was much larger, giving the gas vortex the appearance of a nearly uniform cylinder. In this case, $(\mathrm{d}D_{\mathrm{vortex}}/\mathrm{d}Z)$ is small and the impeller blades sense little difference in D_{vortex} between 40 and 50 cm.

This would predict a gradual diminution of the slope of the v_E *vs.* $Z^{0.5}$ curve as Z increases, which was particularly evident with the 28 cm impeller in Figure 4.4.

5.1.1.3 Validity of the Critical Tip Speed Theory in Unbaffled Vessels

The two major factors preventing strict adherence of v_E values to a $\sqrt{2gZ}$ relation thus are the extra increment of tip speed required to pump gas, as seen in the vertical offset

from the theoretical line, and a possible variation in slope with Z.

If the variation in slope of v_E is due to the slope (curvature) of the parabolic vortex interface, then this implies the theory is better at predicting critical tip speed as the gas vortex becomes cylindrical—at deeper immersions. The departure is observed for shallow vortices, and any phenomena such as splashing which may occur due to large energy dissipation in the small liquid volume in the immediate vicinity of the impeller, will detract from the ideal conversion of energy.

The non-ideality associated with the v_E offset can be simply summarized by recognizing that gas pumping from the vortex occurs at the *inner* blade edge, while the theory is defined by the *outer* blade edge. However, this is more a question of impeller geometry than the lack of fit of the theory. It would seem logical that gas pumping will commence sooner if the impeller diameter is held constant but the *blades* are extended inward toward the shaft hub.

Power consumption in liquid mixing has been defined ably by the outer blade diameter. Correlations for gas-liquid mixing, though not as universal, also made use of the outer diameter. In the little work reported where blade length was varied [152,143,144,69], no attempts were made to isolate it from changes in blade width. However, the effects of blades extended inward might not prove detrimental. First, gas discharge occurs at the outer blade tip so there should be no influence there. Power consumption might be expected to increase due to increased blade area, although the extra area should in theory serve to assist in creation of the liquid and gas vortices. Thus, a Rushton-type impeller with blades extending toward (or even reaching) the shaft hub may provide superior performance where vortex aeration is utilized, and should display even closer adherence to the critical tip speed theory.

5.1.2 Baffled Vessels

The theoretical energy balance at the impeller tip is not changed by the presence of baffling, *i.e.* v_C is identical in both cases. However, the power consumption of an impeller is increased substantially when baffling occurs. Extra power is required to discharge the gas-liquid dispersion against the opposition of the complex, asymmetrical flow patterns induced by the baffles. This extra increment of power can be up to ten times that required in the unbaffled, cylindrical vessel. It is thus large enough to obscure the theoretical energy conversion which may occur at the impeller tip, and makes v_E almost impossible to predict.

5.1.2.1 Surface Aeration Mechanism

The complex flow may prevent or supplement gas pumping, and could possibly produce both effects simultaneously. The schematic drawing in Figure 5.2 illustrates the flow.

(a) Plan View (b) Side View

Figure 5.2: Schematic Flow Patterns in a Baffled Vessel
From Rushton, Gallagher and Oldshue [156].

In plan view, the dispersion is seen to be discharged radially and a portion assumes tangential motion upon reaching the vessel wall. Its tangential path is impeded by the baffle, which redirects it back toward the impeller. It can be seen that a portion of this

stream will oppose the discharge stream from the impeller, which will greatly restrict the radius of the forced liquid vortex. This smaller liquid vortex in turn will induce a concentric gas vortex of much smaller diameter, *i.e.* with its nose much more shallow than in the unbaffled vessel at the same v and Z. As the degree of baffling increases, the gas vortex diameter will decrease to zero and vortex aeration will be eliminated. It is worth noting that under these conditions, both an increase in baffle width B and an increase in impeller diameter D will act to 'choke off' the gas vortex. Thus, the energy of radial discharge which in the unbaffled vessel is used to create a gas vortex, serves to prevent it in a baffled vessel.

At the same time, it can be seen that in each quadrant between two baffles a crude kind of cylindrical motion is being established. When combined with the axial flow up the walls and back down the shaft axis, cylindrical eddies are able to induce gas vortices into the dispersion. Greaves and Kobbacy [105] have proposed a qualitative model of these eddies as in Figure 5.3. They proposed the eddies A to be large and stable, with smaller eddies B and C forming with increasing impeller speed. They found B eddies rotated slowly about the shaft axis until they combined to form an actual gas vortex.

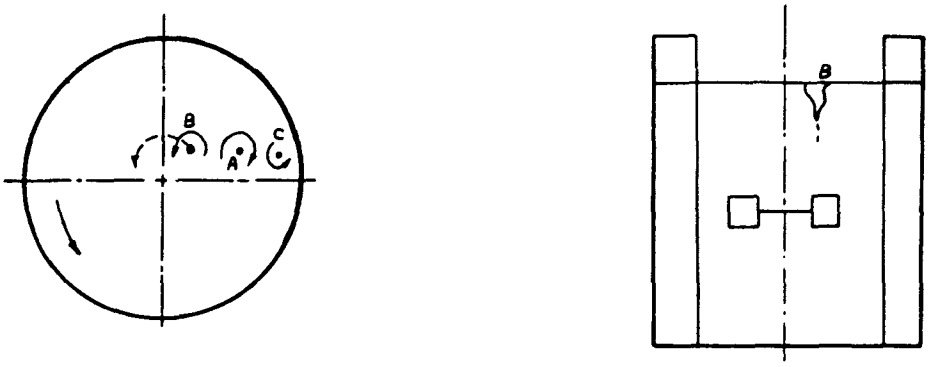

(a) Plan View (b) Side View

Figure 5.3: Eddy Behaviour and Surface Aeration in Baffled Vessels
From Greaves and Kobbacy [105].

The eddies observed in this work were of very small diameter, penetrated only a few centimetres into the dispersion, and survived only for a few seconds. However, there was a continual replenishment of them in any quadrant. It was not possible to distinguish between the B and C types suggested by Greaves and Kobbacy—the movement of eddies was chaotic, there was no apparent migratory pattern about the shaft axis, and the distribution of sizes and ages appeared fairly random within each quadrant. The A type probably describes what appeared as 'invisible' gas vortices, those of the smallest or indistinguishable diameters, but from which small gas bubbles were visibly drawn down.

5.1.2.2 Effect of Impeller Diameter

The shape of the family of v_E curves in Figure 4.6, particularly their shallow slopes at lesser immersion, reflects phenomena which at present cannot be described quantitatively. But qualitative considerations coupled with visual observation can provide plausible explanations for such features. Greaves and Kobbacy [105] had observed point gas hold-up near the surface was always larger than near the impeller, and suggested the ability of the circulating dispersion to carry gas down to the impeller was the limiting factor in surface aeration, rather than the strength of the eddies. This would mean bulk flow patterns are predominant over energy considerations.

According to this postulation, physical factors within the vessel which promote flow interaction about the impeller region will cause a lowering of v_E. Referring to the curves in Figure 4.6, this is in fact borne out. The reduction in v_E with increasing impeller diameter is quite clear. This provides support for the postulation, suggesting the increased impeller–baffle interaction plays a key role in enhancing recirculatory flow patterns.

If the nature of the flow patterns is accepted to be the critical phenomenon, then the gradual slope to the v_E curves implies that both the eddy capture of gas in the surface region as well as the flow patterns produced at a particular tip speed deteriorate only

very slowly as the impeller is lowered into the vessel. Finally at about mid-vertical height the effect becomes significant; this may be attributable to 'bottom' effects caused by flow from the vessel base sweeping up and interfering with the impeller, to 'top' effects caused by the increased volume of liquid above the impeller, or to surface eddies finally too weak to induce gas into the liquid.

For this qualitative model to be consistent one would expect flow pattern deterioration to occur at more shallow Z and more sharply for smaller impellers. This is indicated in Figure 4.6, particularly for $D = 23$ and 28 cm, although within the scatter of the data the support is not conclusive.

5.1.3 Comparison with Previous Work

Dependence of v_E on Z

Equation 2.31 in Section 2.2.2.3 gave the dimensional correlation derived by Greaves and Kobbacy [105] for the onset of surface aeration:

$$N_{SA1} = c_3 \left(\frac{H_L T}{D^3}\right)^{0.67} \cdot \left(1 - \frac{C}{H_L}\right)^{0.33} \cdot \left(\frac{\mathcal{P}}{\mathcal{P}_a}\right)^{-0.13}.$$

The term $\left(1 - \frac{C}{H_L}\right)$ can be seen to be (Z/H_L), similar to the per cent of maximum immersion. Linear regression for all three impellers gave lower values of R^2 against $Z^{0.33}$ than against $Z^{0.5}$, indicating no improvement in linear fit of the data of this work when using the emprical correlation of Greaves and Kobbacy.

Effect of D/T on v_E

The effect of impeller diameter on v_E in baffled vessels has been reported previously. Westerterp, in developing his correlation for the critical tip speed N_o [216,79] and Boerma and Lankester [86] each used at least five different D/T ratios in generating their N_o values. The data of Westerterp [216] and Boerma and Lankester were extracted from

the paper of the latter group [86, Figs. 2 and 3] and are plotted in Figure 5.4 against data from this work with a fortuitously similar v_C. What is interesting about the general

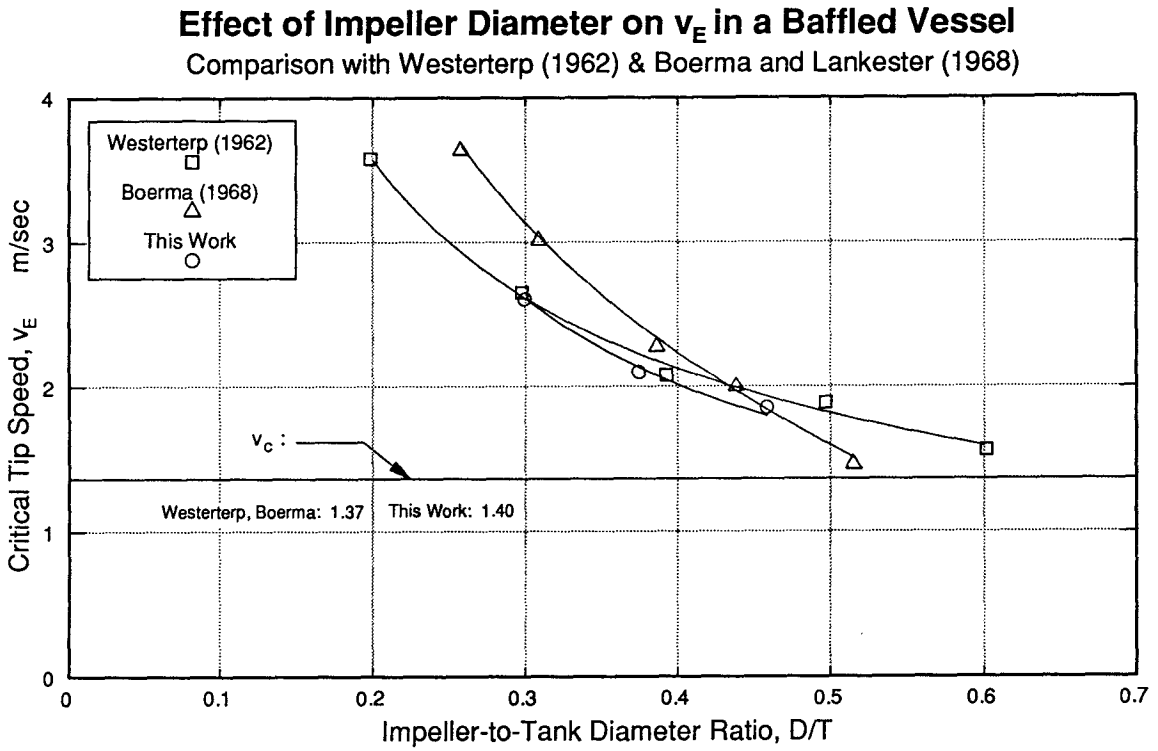

Figure 5.4: Effect of Impeller-to-Tank Diameter Ratio on v_E in a Baffled Vessel

agreement of this work relative to that done earlier is the difference in vessel size. The present work was done in a vessel of $T = 61.0$ cm, while Westerterp used $T = 19.1$ cm and Boerma and Lankester used $T = 19.4$ cm, giving a volume difference of 200 litres *vs.* about 6 litres.

DeGraaf claimed there was essentially no change in v_E with D [40, p. 62], but used only two six-blade radial disc impellers with D/T of 0.38 and 0.44, where the effect on v_E is seen to be less pronounced. Linear regression to determine v_E from data read from his graph (Figure 19, p. 106) gave v_E values of 2.50 and 2.12 for $D/T = 0.38$ and 0.44 respectively. This difference in v_E is similar to that found by Boerma and Lankester over the same D/T range. The v_C for the measurements of DeGraaf was 2.34 m/sec.

The strong dependence of v_E upon D especially as D diminishes again serves to indicate an important effect of the impeller on flow interactions within the vessel when surface aeration occurs.

Measure of Agreement with the Critical Tip Speed Theory

DeGraaf used the correlation coefficient R to describe the agreement between v_E and v_C [40, p. 61]. However, this is not a useful statistic since R (or R^2) describes only the *linearity* of the experimental data and says nothing of its positioning relative to the theoretical. This is illustrated in Figure 5.5 where his data have a fine R^2 of 0.999 but increase at a slope of 1.4 relative to the theoretical. Both the slope and intercept must be reported to make experimental results useful for design. A more appropriate alternative is graphical presentation, which permits even non-linear data to be interpreted relative to the prediction of the theory.

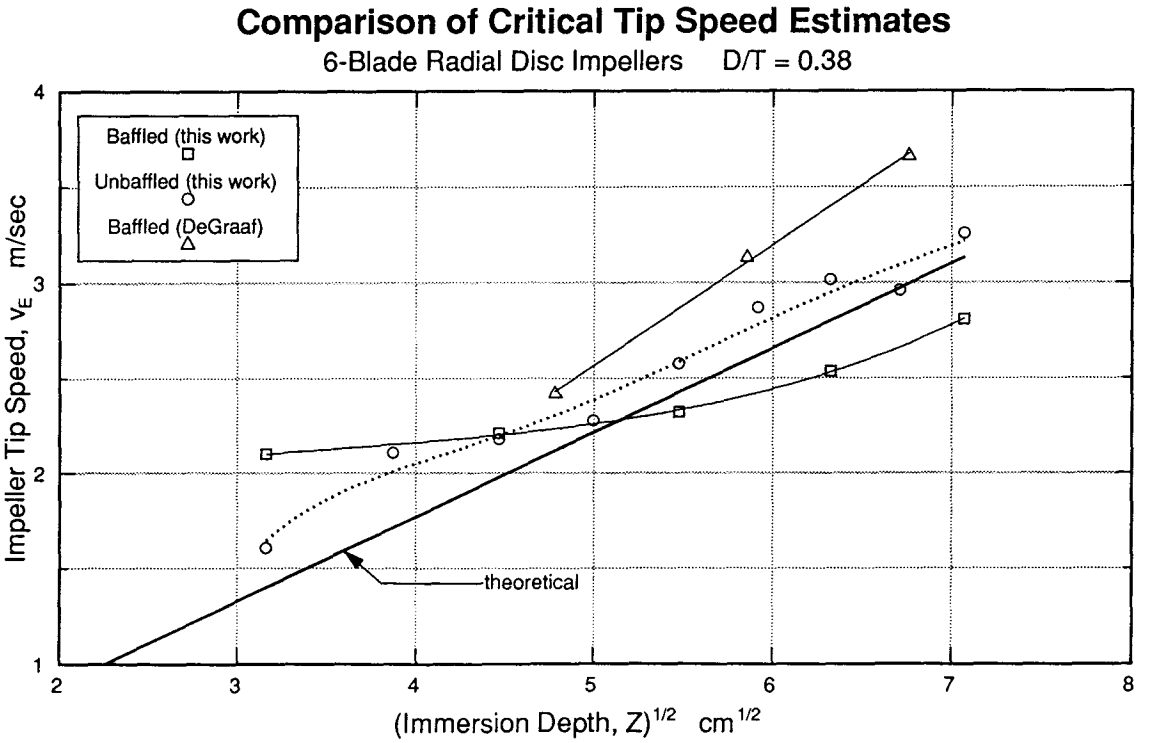

Figure 5.5: Comparison of Critical Tip Speed Estimates

5.1.3.1 Validity of the Critical Tip Speed Theory in Baffled Vessels

If surface aeration in a fully-baffled right-cylindrical vessel is indeed described by the ability of recirculatory flow to carry a more highly aerated surface layer down to the impeller region, then the phenomenon is not well described by considerations of the energy balance at the impeller tip.

5.1.4 Application of the Critical Tip Speed Theory for Design Purposes

The critical tip speed equation should be useful for designing mixing systems with radial disc impellers where baffling is mild or absent, and/or where the impeller diameter is not a large fraction of the tank diameter. Applications would include wastewater aeration basins, and fermentors which pump gas from the vessel freespace especially by vortex aeration.

Due to the complex interactions between the liquid flow patterns and the impeller caused by a large impeller diameter, axial impellers, significant baffling and/or an asymmetric vessel shape, the tip speed energy balance is insufficient to account for the gas pumping process in these cases. This would include systems such as the zinc pressure leach autoclave at present, or those where gas pumping is achieved mainly by surface aeration.

5.2 Effect of Baffles

5.2.1 Effect on Oxygen Transfer Rate K_G^{20}

The appearance of a critical impeller immersion depth Z_C for improvement in K_G^{20} caused by the addition of baffles, and its dependence on impeller diameter, can be interpreted by considering the effect of the baffle–impeller interaction. At the deepest immersion ($Z = 50$ cm), the flow interactions induced by the 18 cm impeller were more *destructive*

than *constructive* for oxygen transfer. Either as the impeller was raised or made larger, the balance between constructive and destructive influences was made to favour enhanced oxygen transfer.

Destructive influences would be maximized at the deepest immersions, where bottom effects would be at their greatest and the liquid volume above the impeller is maximized. Increasing the impeller diameter would increase the size of the discharge stream and assist in bringing captured gas bubbles down to the impeller region (of course at much greater power consumption). Alternatively, raising the impeller from the base would draw it away from the interference of flow patterns at the bottom, and decrease the distance it must pump gas bubbles.

Figures 4.4 and 4.6 for the critical tip speed estimates show how the dependence of v_E on impeller diameter reverses when baffles are used. The data in Tables 4.3 and 4.4 indicate the cross-over immersion point for $D = 18$ cm occurs at about $Z = 50$ cm, and for $D = 23$ cm at about $Z = 20$ cm. In the presence of baffles, the 28 cm diameter impeller begins to pump gas at a lower tip speed at any immersion. Thus for an unbaffled vessel where the process result makes it desirable to place the impeller deeper into the tank, but where the impeller tip speed cannot be adjusted to be greater than v_C at the new immersion, the addition of baffling would be an alternative to the fabrication of a larger impeller or a change in the motor or motor drive.

5.2.2 Effect on Power Consumption

Assuming the flow patterns drawn schematically in Figure 5.2 are correct, it is apparent a large portion of the dispersion which is discharged radially by the impeller is directed axially by the baffle at the baffle-wall intersection. That which travels upward must return back to the bulk, generally by cascading back upon the small forced liquid vortex which the impeller maintains. As well there is a portion which maintains tangential flow

in the impeller plane and opposes the direction of motion of the impeller discharge. Each of these flow patterns is essentially absent in an unbaffled vessel, and each demands an increase in the power consumed by the impeller.

5.2.3 Effect on Relative Oxygen Transfer Efficiency

At the point of contact between a tangential flow element and the baffle, the daughter elements may be considered to have opposing effects on gas-liquid mass transfer. That portion which is converted to axial upward flow is beneficial in that it sustains the surface eddies and contributes to the recirculatory flow patterns which bring the gas bubbles to the impeller. That which flows axially and downward does not contribute to gas bubble capture, but does carry the gas already brought to the impeller region. The tangential portion which remains in the impeller plane neither captures nor distributes gas bubbles, and ultimately it constricts the forced liquid vortex and opposes impeller discharge. This component of flow cannot be eliminated, but surely a compromise must exist between the beneficial effects of the axial flow generated and the negativing effects of tangential flow.

DeGraaf [40] examined half-baffles (extending from the base to half liquid height) at the 20 and 2000 ℓ scales. In the smaller tank, which was a flat-bottomed right-cylindrical vessel, he found the oxygen transfer rate R (in kg $O_2/m^3 \cdot min$) decreased with the reduction in baffle height, although P also decreased and the relative mass transfer efficiency (in kg $O_2/kW \cdot min$) still increased. For these experiments, however, only one Z was studied, D/T was only 0.19 and the impeller was imprecisely fabricated.

In the larger vessel, which was a scale model of the zinc pressure leach autoclave, R was increased and power consumption was either similar or decreased when half baffles were used. The relative mass transfer efficiency also increased. The improvement in R decreased as Z was increased. This would be expected since the vortex would become

less stable and the volume of opposing tangential flow would increase as the impeller plane was moved to immersions at which the baffles were present.

Only a four-blade upward-pumping axial impeller was employed in these 2000 ℓ experiments, and the differences in both R and P which would be delivered by a Rushton-type impeller would be interesting to examine in greater detail.

While the 'fully-baffled' condition of four baffles of width $B = T/10$ (or $T/12$) mounted radially 90° apart has been adopted industrially and is obediently duplicated in laboratory research, it must be recalled that it was developed to provide an environment for *liquid* mixing. No confirmation has appeared in the literature to suggest it is the appropriate amount of baffling for gas-liquid contacting or transfer applications. The experiments which yielded a vortex in the baffled vessel suggest rapid and energy efficient gas-liquid mass transfer environments exist where the *degree of baffling* permits surface aeration and vortex aeration to occur simultaneously.

Consideration of the *degree* of baffling as a variable has not been explored in the literature and, one assumes, to any great degree industrially. The rate and efficiency of oxygen transfer measured for the baffled–vortex condition lay claim that the prevailing biases of liquid mixing theory must be reconsidered.

5.3 Interaction Between Impeller Diameter and Baffles

The increase in K_G^{20} with impeller diameter is very slight in the absence of baffles, but substantial with their addition. This is best illustrated in Figure 4.11, where for a constant v and Z the gap between the K_G^{20} curves for the baffled and unbaffled cases widens substantially as D increases. Only at the most shallow immersions is there sensitivity to impeller diameter in the unbaffled vessel.

The result in the unbaffled vessel is to be expected. This vessel represents an environment with minimized physical interference to the mixing process. It can be thought to characterize the action of an impeller in the ocean, which ideally encounters no wall, baffle or bottom effects. Comparing the values of K_G^{20} at each diameter in Figure 4.11, it is seen that only a slight change occurs with v except for the largest impeller, *i.e.* where impeller-wall effects will finally become significant. Thus the right-cylindrical unbaffled vessel used is insensitive to impeller diameter over a broad range of D/T extending at least up to 0.38.

The sensitivity to D in the unbaffled vessel at shallow immersion is thought to be caused by the degree of splashing which occurred. This is a surface effect and not true vortex aeration.

Baffles improve the mixing within the vessel by changing the flow patterns of the liquid discharged by the impeller. The degree of these changes should be acutely sensitive to the relative proximity of impeller and baffles, and indeed this was recorded.

Recall that a vortex could be sustained in the baffled vessel but only for the smaller impellers (D small) and at the most shallow immersions (Z small), which provide the least amount of constriction of the vortex. An analog to a decrease in impeller diameter would then be a decrease in baffle width B. There appears to be an impeller-to-tank diameter ratio D/T of about 0.46 at which the impeller-wall effects in the unbaffled vessel contribute to oxygen transfer. That is, the unbaffled vessel begins to develop a level of flow complexity similar to a small degree of baffling. It should then follow that there exists a baffle width ratio B/T below which the flow complexity in the baffled vessel begins to resemble that in the unbaffled vessel. If the interactions between impeller and baffles can be adjusted by changing the B/T and D/T ratios, it should be possible to engineer the energy efficient surface-vortex aeration system by this method.

5.4 Comparison of Axial Flow (Upward Pitch) and Radial Flow Impellers

The v_E values in Figure 4.7 for the axial impeller appear to follow the form of radial disc impellers in baffled vessels, which themselves use axial flow in their gas pumping mechanism. However this must be considered a coincidence because the unbaffled axial impeller does not pump gas from surface eddies but rather from a gas vortex as does the unbaffled radial disc impeller. The vertical offset for v_E between the unbaffled axial and radial flow impellers demonstrates the axial is less efficient at creating a vortex from which to pump.

Because a component of the discharge from the axial impeller is in an axial direction, the conversion of energy toward the creation of a forced liquid vortex is smaller than for a radial flow impeller, and this is evinced in Figure 4.7 in the vertical offset for v_E between the two unbaffled impellers.

Since for a given tip speed the axial impeller dedicates less energy to vortex creation, its gas vortex is narrower and hence it cannot pump as much gas as the radial impeller (Figure 4.12(a:b)). Its blades certainly extend to the shaft hub, but because of their upward pitch it is difficult for a gas cavity to form and cling to the back of the blades. As with radial disc impellers, bubbles were discharged from the outer edge of the blades.

For the same given tip speed, the axial impeller produces the smaller vortex but also draws less power. In a sense this can be considered to be a reduced effective gas pumping tip speed relative to the radial disc impeller. That is, at the same Z the radial disc impeller will produce a vortex of equal size at a lower tip speed since it dedicates more energy to vortex formation. The energy required by the axial impeller will be the sum of that required to create the vortex, to produce axial flow, and to compensate for the axial flow patterns which diminish the vortex. The latter two terms are variable and depend upon the amount of axial flow generated by the impeller. In this way the v_E offset can

be used to estimate the degree of axial flow produced, and should be different for blades of different pitch angle α.

When it produced a froth at the shallow immersion and high tip speed, the axial impeller also was able to exploit the axial characteristic of its flow. Bubbles were observed being drawn from the surface froth in cascading sheets, and dispersed below the impeller plane by the axial flow patterns which are somewhat similar to those from a radial impeller in the vessel. Observation of the bubbles which reached the base indicated they were very similar to those produced and dispersed by shallow radial disc impellers in the baffled vessel. They were very small in size (less than 0.5 mm by visual identification) and remained as a very slowly ascending mist-like dispersion even eight minutes after the impeller had been stopped at the end of the experiment.

It is left to speculation if a *downward* pumping axial impeller would be more efficient either at drawing bubbles from the froth or dispersing them to the rest of the vessel.

5.5 Impeller Disc Diameter

For gas-liquid mixing systems where gas is sparged at a point beneath the (lower) impeller, the impeller disc size may be an important factor due to the physical barrier it presents to bubbles, which may otherwise rise vertically through the impeller region and escape the shearing and distributing action of the impeller. For gas pumping agitators the effect is less predictable, since gas is brought down to the impeller and contacts the impeller blades at a point above the disc. In either instance, there is no report in the literature of the effect of impeller disc diameter.

The results in Figures 4.13 and 4.14 suggest that the smallest disc diameter may produce slightly inferior rates of oxygen transfer. However, because of the small range of the K_G^{20} data for all three impellers it is difficult to draw a firm conclusion. A more

thorough investigation with many repeat runs would be required to verify if this is indeed a systematic result or is only within the bounds of experimental reproducibility.

As mentioned, the gas vortex (in the unbaffled vessel) extended beneath the impeller disc to form a 'cup', and in instances as depicted in Figure 5.1 it was possible for the disc to completely separate the cup from the remainder of the gas vortex. Thus, the disc does not completely prevent the migration of the vortex nose to a point below the impeller plane. It is possible, however, that the disc exerts an influence on the shear and flow patterns in the impeller region, and that the shear and inducement of radial flow increases with impeller disc diameter. Such an investigation was beyond the scope of the present work, but a cursory examination could be performed fairly simply by using a flat blade turbine impeller (without disc), a standard radial disc impeller ($D_d/D = 0.67$ or 0.75) and a modified vaned disc impeller with the disc extending though the middle of the blades to the shaft hub ($D_d/D = 1.00$). The contribution of the disc to radial flow, and the importance of radial flow to oxygen transfer could be assessed using these extreme cases.

5.6 Dual Impeller Systems in the Unbaffled Vessel

In an unbaffled vessel, the lower of the two impellers works to establish the vortex from which both impellers will pump gas. When an upward axial impeller is placed in the lower position, the radial disc impeller contributes most of the gas pumping, *i.e.* the gas pumping performance of the pair more closely resembles that of the radial disc impeller even though it is in the upper position.

It follows that improvement in K_G^{20} will be realized by reducing the immersion depth of the characteristic impeller, and that at least up to a near mid-height immersion, distribution of bubbles into the lower part of the vessel is not significantly impaired.

The shape of the gas vortex is almost identical to that produced by the lower impeller. With a radial disc impeller below, the upper impeller contributes very little to the creation of the vortex, but it would be simplistic to suggest it merely 'rides for free' and therefore should always be a radial disc impeller because the upward pumping axial impeller does not pump gas *via* its blades as effectively. It can be seen in Figure 4.15 that the A25/R35 pair produces nearly the same K_G^{20} at lower tip speeds and larger K_G^{20} at greater tip speeds, probably due to the more stable flow interaction when impeller separation S is only 10 cm. Although the blades are only partly covered by liquid, the flow patterns they induce still are important to the operation of the *system*.

Thus it would be expected that a downward pumping axial impeller in the A25/R35 setting would not give so large a K_G^{20}, and that when S is increased or v is decreased the flow interaction will become less important such that the radial disc impeller might again be the superior choice in the upper position.

The poor K_G^{20} performance of the A15/R45 pair can be explained by considering the diameter of the gas vortex at $Z = 15$ cm. Again invoking the analogy of the funnel cloud, close to the freespace interface the vortex will be much wider at $Z = 15$ than at $Z = 25$ cm, and coupled with the poor geometry of a pitched blade for cavity formation, very little gas pumping should be expected by A15. But in light of the remarkable K_G^{20} results for a single axial impeller at $Z = 10$ cm, it would be interesting to observe if it could induce frothing or splashing at this more shallow immersion in spite of the still wider gas vortex through which it would be rotating.

Alternatively, an axial impeller of wider diameter may be selected for the upper position to improve gas pumping. In fact, since the vortex—and consequently the power—characteristics of the impeller pair appear to be determined by the lower impeller, it may be prudent to increase the diameter of the upper impeller regardless of its flow type, in order to maximize capture of gas from the vortex. Again, flow interaction could be a

limitation as S is reduced.

5.6.1 Use of Dual Impellers for Gas Pumping in Two-Phase (Gas-Liquid) Systems

In the series of figures in Section 4.6 it was demonstrated that only two dual impeller configurations gave K_G^{20} and relative oxygen transfer efficiencies even slightly improved over those provided by the single lower radial disc impeller. The effect of dual impeller systems with baffling was not investigated but is expected to yield unrelated results since the gas-pumping mechanism will revert mostly to surface aeration, with the degree of vortex aeration dependent upon the proximity of the upper impeller to the freespace interface.

The role of the impellers in the unbaffled vessel to create the gas vortex and pump from it will not apply, but factors such as impeller spacing and the interference of flow patterns should be much more prominent. The direction of axial impeller flow could prove to be influential in determining the ability of the liquid flow to carry captured gas bubbles to the impellers.

Different impeller diameters were not investigated in the unbaffled vessel. As mentioned, an increase in D at the upper impeller may increase the gas pumping from the vortex. An increase in D at the lower impeller likely would yield results similar to gas pumping by a single impeller in an unbaffled vessel: v_E should increase but the gain in K_G^{20} with v should also increase. In the baffled vessel the same impeller-baffle interactions also should be expected to figure in the oxygen transfer rate and power consumption.

Chapter 6

General Observations

6.1 Film Theory *vs.* Penetration/Surface Renewal Theories

For the sake of completeness the oxygen transfer rate data R for each experiment were normalized using factors for both the film theory method ($n = 1.0$) and the penetration/surface renewal (P/SR) theory method ($n = 0.5$). For reasons 2 and 3 enumerated in Appendix B, namely that 0.5 is considered the best estimate of n for $\mathcal{D}$ and that it provides the more conservative estimate of K_G^{20}, use of the P/SR normalization factors is preferable in the absence of experimental data.

A triad of experiments was performed to examine the effect of water temperature on the process result. Hot tap water supplemented the supply from the cold tap to obtain the warmer temperatures. The results appear in Figure 6.1. Though this was not an exhaustive evaluation, the wide difference in temperatures for runs #12 and #13 are an acid test of the ability of the theories to harmonize the staggered K_G values obtained by initially dividing R by the estimate of oxygen solubility (cluster 2). The P/SR normalization factors for $n = 0.5$ are seen to bring these two extreme runs into concordance (cluster 3), while the film theory factors fail by a substantial margin (cluster 4).

The data in Table 4.2 for repeat runs done after long intervals, where seasonal effects led to different tap water temperatures, also demonstrate the better concordance given by the P/SR factors.

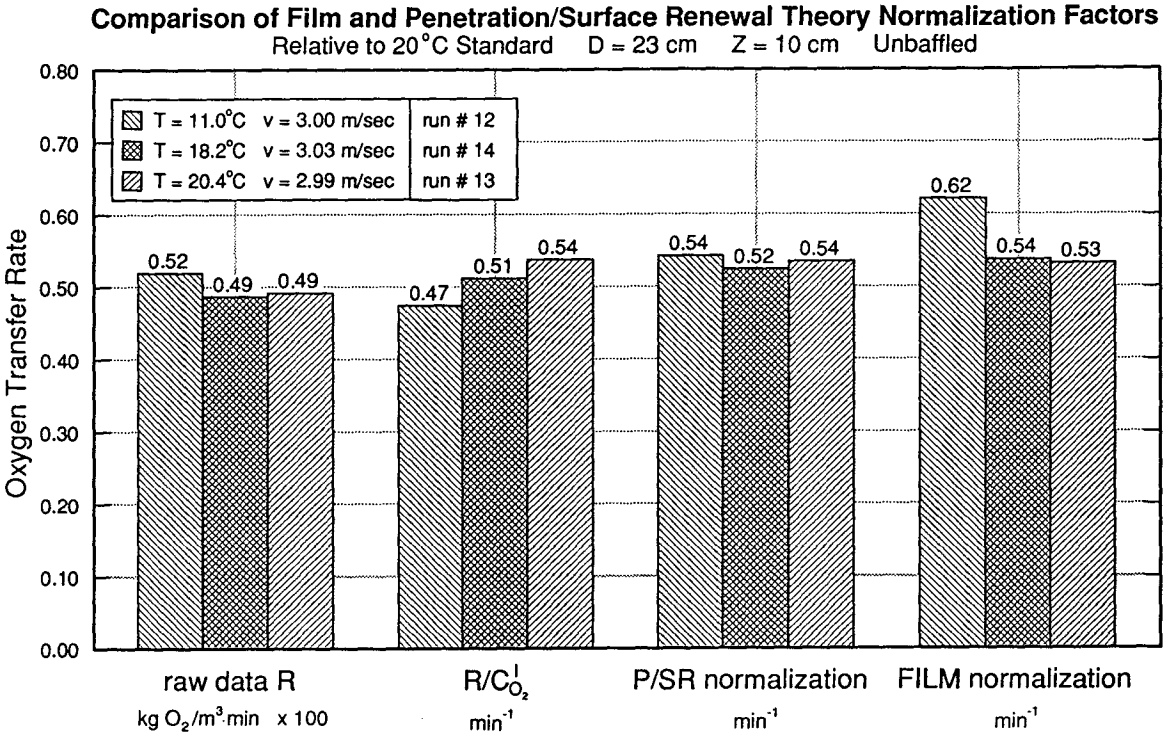

Figure 6.1: Comparison of Diffusivity Normalization Factors

The use of film or P/SR factors makes only a minute difference in the determination of v_E. Since the film factors are the square of the P/SR factors they simply inflate or deflate the K_G values by a proportional amount. The difference in v_E was rarely greater than 0.04 m/sec.

6.2 Oxygen Solubility Estimations

Predictions of oxygen solubilities in water by the correlation of Linek and Vacek [199] are seen in Figure A.1 of Appendix A to stray somewhat from a set of published values [217] at about 16°C. An alternative method of estimation would be to consider 0.02M Na_2SO_3 to be practically identical to water and to use the data for water. But use of the correlation, which was based on the available published experimental data, affords the ability to make estimates for those experimental runs where the Na_2SO_3 concentration

was changed from 0.02M, which cannot be estimated by other means. Finally, considering the maximum error induced by the correlation is in the order of 2 per cent, its universal application was considered to be the most suitable compromise.

The temperature of the solution was not constant during the experiment and rose due to the energy dissipation by the impeller and to equilibration with the ambient temperature in the laboratory. As such both the diffusivity and solubility estimates are called into question. For the longer experiments the solution and ambient temperatures were recorded every hour, but an integrated time average of diffusivity and solubility would require the acquisition and treatment of an unwieldy amount of data. The marginal increase in accuracy, relative to the average of the initial and final temperatures, would not seem to warrant the extra work.

Where the change in temperature is of concern is on the measured rate of sulphite depletion. Typical temperature increases ranged between 1.5 and 2.0 C°, with a maximum of 8.7 C° over 444 minutes (run #239, baffled) and another of 6.6 C° over 125 minutes (run #250, baffled). Thus as the solution temperature increases, the driving force (C^I taken as oxygen solubility) decreases while the mass transfer coefficient (taken as $(\mathcal{D}_{O_2}^{20})^{0.5}$) increases.

For temperatures from 8 to 25°C, the solubilities given by the Linek-Vacek correlation (Equation A.3, Appendix A) decline from 11.6 to 8.4 mg/ℓ while values of $(\mathcal{D}_{O_2}^{20})^{0.5}$ from the Wilke-Chang relation (Equation B.4, Appendix B) increase from 3.83 to 4.92×10^{-3} cm/sec$^{-0.5}$. The product then decreases from 4.44 to 4.12×10^{-5} (mg/cm^2·sec$^{-0.5}$) over this temperature range, a difference of 7.2 per cent. So for even the most extreme case of temperature variation, the influence on the instantaneous rate of sulphite oxidation would only be about a 4 per cent decline between the initial and final measurement, based on solubility and diffusivity considerations only.

6.3 Oxygen Depletion in the Gas Bubble

The estimation of oxygen solubility (Appendix A) was made assuming the liquid was saturated with oxygen at a concentration of $\mathcal{P}^g$; for this work atmospheric air was used so $\mathcal{P}^g$ is taken to be 0.209 atm. However, as absorption from the bubble into the sulphite solution occurs the bubble becomes depleted in oxygen and $\mathcal{P}_{O_2}$ decreases. The longer the residence time of the bubble before it reaches the freespace interface, the greater will be the depletion and the decrease in the driving force. Thus, the method of estimation (Appendix A) causes the average effective oxygen solubility to be overestimated, which understates the computed value of K_G.

Coalescence also determines the 'average' oxygen concentration of the bubbles. But since not all bubbles share the same residence time, the distribution of oxygen concentration amongst bubbles is a more exact, but tedious, specification.

Bubble composition has been measured by a variety of means. Reith and Beek [109] withdrew a stream of single bubbles from the dispersion through a thin glass pipe under vacuum, and contacted the stream with a pyrogallol-KOH solution to absorb the oxygen. The difference in bubble length before and after contacting was used to determine the oxygen content. Their data were obtained with sparged oxygen in a baffled vessel and are plotted in histograms of bubble oxygen content. This makes data extraction difficult but a depletion of about 20 per cent can be estimated for a sparge rate of $v_s = 3.0$ m/sec and impeller tip speed of 2.4 m/sec ($v_C = 1.37$ m/sec).

DeGraaf placed inverted beakers in the 2000 ℓ vessel to capture rising depleted bubbles and found a 37 per cent reduction in volume per cent of oxygen, *i.e.* a 42 per cent depletion of oxygen [40, p. 125].

Since the residence time distributions and coalescence phenomena will be influenced by the flow patterns, *i.e.* by (D, D/T, Z, v, impeller type), the magnitude of depletion

will be expected to vary with each unique set of variable set-points. The average oxygen concentration should be constant during a given experiment, so if a relationship between per cent depletion and transfer rate R can be established, it will greatly reduce the effort required to determine oxygen depletion for the purpose of solubility estimation. The degree of depletion must be quantified in the future to ensure the accuracy of K_G^{20} computations.

From another viewpoint, knowledge of oxygen depletion from the bubble is the critical component in evaluating the efficiency of *oxygen utilization* in an oxygen absorption system. This characteristic is related but certainly not identical to measurements of oxygen transfer rate or the energy efficiency of oxygen transfer. For a process such as the zinc pressure leach which utilizes oxygen as a reagent, economies are available if the per cent utilization is increased. For example, when oxygen makes a single pass through the slurry from the sparger to the compartment headspace and is then purged and vented, it is not as efficiently utilized as when it is recycled within the autoclave by gas pumping impellers. Vortex and surface aeration would extend the recirculation time within the autoclave.

The extent to which this is achieved by a given impeller system could be estimated using an ambient air/sulphite solution system in a model of the autoclave; of course this requires development of a reliable technique for bubble analysis and the over-all mass balance. This represents the refined extension of the present work: the true optimization of oxygen transfer for the pressure leaching system.

6.4 Residual Oxygen in Sulphite Solution

The second term defining the oxygen driving force is C^b, the concentration of oxygen in the bulk liquid. If this is non-zero or changes with time, it will decrease or change the

driving force for oxygen transfer.

The reaction of oxygen with sulphite ion is irreversible, and C^b historically has been assumed equal to zero. In his experimental method DeGraaf [40, p. 43] filled the vessel with water and then added the Na_2SO_3 crystals. Mixing was provided and gas pumping prevented by the repeated starting and stopping of the agitator. This was continued until the reading on the dissolved oxygen meter fell below 0.3 mg/ℓ. Thus it can be assumed that if C^b is finite and non-zero it is at most 0.3 mg/ℓ. At an oxygen solubility of 8.5 mg/ℓ (24°C) the maximum reduction in oxygen driving force would be 3.5 per cent.

The sulphite samples in this work were titrated at the earliest convenience, generally within five minutes of acquisition. In the event there was a residual C^b which reacted slowly but at a known rate, the times at which the samples were titrated (relative to the start of the experiment) were recorded on the data sheets.

In run #96, the regression line for ten samples gave an iodine titration slope of -0.7603 with intercept 30.66 and R^2 of 0.999. The sample taken at t = 12 min was titrated with 21.51 mℓ of I_2 solution. The regression line predicts a value of 21.54 mℓ.

A duplicate sample was taken at t = 12:30 and set aside until t = 144 min, *i.e.* an incubation time of 131:30. The regression line predicts a value of 21.16 mℓ; 21.08 mℓ of titrant was actually required. If the offset of - 0.03 mℓ is assumed to be typical during this period of the run (although the samples at t = 9 and t = 16 min each required *more* titrant than predicted by the regression line), the difference of 0.05 mℓ I_2 could be attributed to the reaction of residual oxygen with the unreacted sulphite in the sample bottle. While this is almost certainly covered by the error in the burette measurements, nonetheless it computes to an error of 0.24 per cent. Recast, 0.05 mℓ of 0.0125M I_2 solution is equivalent by stoichiometry to 3.1×10^{-7} moles of O_2; in the 60 mℓ sample bottle this equates to an initial residual oxygen concentration of 0.2 mg/ℓ.

Given the accuracy of the titrations and burette measurements, the above result

cannot indicate the presence of a significant residual concentration C^b of oxygen in the bulk solution.

6.5 Effect of Cobalt Catalyst Concentration

As discussed in Section 2.3.2.1, the reaction order in cobalt catalyst is almost always observed to be one, although Bengtsson and Bjerle [211] found zero and one-half orders. This is important because only these authors and Astarita *et al.* [210] have reported the use of sulphite concentrations at low levels (*i.e.* < 0.1M) similar to those used by DeGraaf. Moreover, DeGraaf [40] used one catalyst concentration at the 2000 ℓ scale (5 mg/ℓ, p. 43) and another at the 20 ℓ scale (25 mg/ℓ, p. 44). Thus the effect of the catalyst must be known to confirm if its concentration has no or little bearing on the results of this work and those of DeGraaf.

A series of experiments was performed with cobalt catalyst concentrations (in mg/ℓ of Co) of 10.0, 5.0, 2.5 and 0.059, with two 'blank' runs using no added catalyst. The K_G^{20} data are plotted in log-log form on an expanded vertical scale against the catalyst concentration in Figure 6.2. The data for this series aligned remarkably well to a regression line of slope 0.038 and R^2 of 1.000. Then, using the logarithm of their K_G^{20} values, the two data 'blanks' were placed on the regression line to determine their abscissa coordinates, *i.e.* the equivalent or effective catalyst concentration in the tap water. Values of 16 and 34 μg/ℓ (ppb) were obtained in this way (2.7 and 5.8×10^{-7}M Co).

Two more series were performed. Using catalyst concentrations of 20.0, 10.0 and 5.0 mg/ℓ Co a regression line was obtained with slope 0.049 and R^2 of 0.994. The other series used 10.0, 5.0, 1.0 and 0.1 mg/ℓ Co with another 'blank' run, and obtained a line with slope 0.043 and R^2 of 0.989, with the tap water 'blank' giving a K_G^{20} equivalent to 71 μg/ℓ Co (1.2×10^{-6}M).

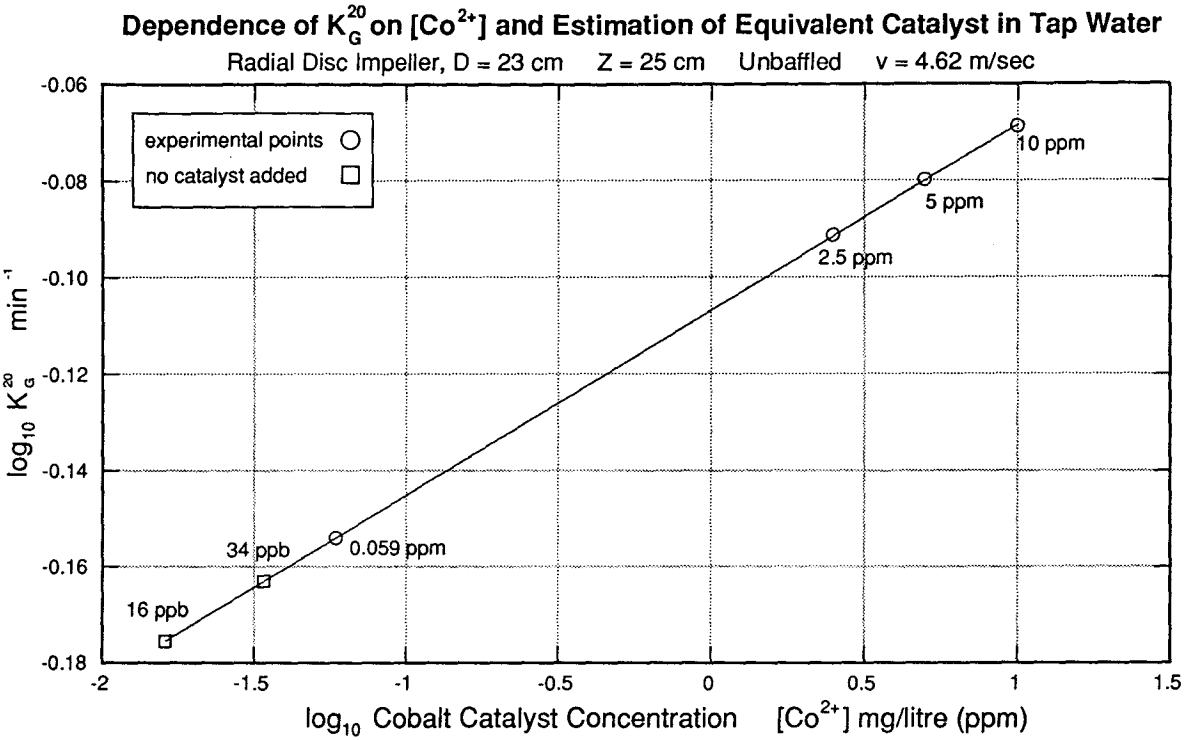

Figure 6.2: Effect of Cobalt Catalyst Concentration on K_G^{20}

The average of these three determinations is 0.043. While not apparently large, it does mean that experiments performed with 25 mg/ℓ Co as catalyst will yield a K_G^{20} about 7 per cent larger than those with only 5 mg/ℓ Co.

The variation in the estimate of the effective catalyst in the tap water generally has as much to do with the placement of the regression line as it does with chemical variation. However, these results do give an order-of-magnitude estimate of the catalytic power of stray cations in the tap water supply. Copper, iron and nickel ions should be present and it is expected their relative proportions would change as water temperature and cleanliness would change seasonally in Vancouver. Thus the safest conclusion is to suggest the equivalent catalyst strength of tap water is variable and ranges between about 10^{-6} and 10^{-7}M Co.

Chapter 7

Summary, Conclusions and Recommendations

7.1 Summary

- The theory that an impeller will not pump gas below its critical tip speed v_C, which is a function of depth of immersion *i.e.*

$$v_C = \sqrt{2gZ}$$

was confirmed experimentally for radial flow impellers in the unbaffled vessel. Departure from strict adherence to the theory appears to lie in the impeller blade geometry: the gap between the inner edges of the blades does not enable the impeller to pump gas when the nose of the vortex first reaches the impeller plane.

- The theory does not accurately predict critical tip speeds in a vessel with baffling, where experimentally determined values of the critical tip speed v_E smaller than v_C were observed where the impeller diameter was large and it was placed deep within the vessel. Gas pumping occurs by the capture of small bubbles by surface eddies and their subsequent draw-down and distribution by the impeller. The strong effect of the impeller diameter on v_E supports the postulation in the literature that recirculatory flow patterns, which carry gas bubbles to the impeller, likely are the dominant factor.

- Once the critical tip speed is attained, the rate of oxygen absorption is a linear

function of impeller tip speed, *i.e.*

$$K_G^{20} = c(v - v_E).$$

Over the range of D (or D/T) studied, the constant c was a strong function of impeller diameter D in the baffled vessel; in the unbaffled vessel D was significant only between its larger values.

- An upward pumping axial flow impeller requires a larger tip speed to begin to pump gas in an unbaffled vessel, and pumps less gas at a given tip speed. An exception occurs at very shallow immersions, where slopping of the vortex and splashing into the vessel freeboard may create a froth, which the axial impeller can pump and distribute effectively.

- The difference in v_E between axial and radial disc impellers in an unbaffled vessel likely is linked to the portion of energy which creates axial flow and that which is needed to create more radial flow to overcome whatever interference exists. The offset in v_E should characterize the degree of axial flow produced by an axial impeller and should be related to the blade pitch angle.

- It is possible to sustain a gas vortex in a baffled vessel at least over some tip speeds. This condition is favoured when the impeller is close to the surface and its diameter is not so large as to destroy the vortex by constriction or by splashing. The oxygen transfer rate is increased substantially, as much as four times greater than in a baffled vessel with no vortex, and eight times greater than in an unbaffled vessel.

- For the above condition, power consumption is about 60 per cent less than for typical flow with baffles, and about four times greater than without baffles. This indicates that when the gas vortex is present the vessel is providing a degree of baffling which is reduced from the 'fully baffled' condition.

- It should thus be possible to strike a balance between the two effects such that a gas vortex can be sustained in a baffled vessel, which would permit gas pumping by both vortex and surface aeration simultaneously.
- Large impellers ($D/T \simeq 0.46$) are able to pump gas at lower tip speeds when baffling is present. However, as tip speed increases the unbaffled vessel eventually becomes more energy efficient.
- In a dual impeller configuration in an unbaffled vessel, the lower impeller defines the shape of the gas vortex, and the critical tip speed v_E can be estimated using the lower impeller as the reference. Gas pumping performance, on the other hand, is very similar to the performance of a single radial disc impeller operating at the position of the lower radial disc impeller of the pair.
- The primary function of the lower impeller is to create the gas vortex. The upper impeller pumps from the existing gas vortex but it does contribute to over-all power consumption as well. As impeller tip speed increases or inter-impeller spacing decreases, the interaction of flow patterns between the two impellers must be considered.
- To increase the contribution to gas pumping by the upper impeller, axial flow impellers, an increased impeller diameter and a reduced immersion depth all might be used to advantage, especially if impeller spacing is sufficiently large to absorb the change in flow patterns. The increase in diameter enables better pumping from the gas vortex, while the decrease in immersion promotes more vigorous agitation at the surface, especially with upward axial flow impellers.
- To increase gas pumping by the lower impeller, the impeller immersion should be raised at least to mid-vessel height.

7.2 Conclusions

1. Mechanical agitators have a critical tip speed above which they pump gas from the freespace and disperse it into solution. A theory exists which predicts that under conditions of perfect energy transfer at the impeller tip, this critical tip speed is related to the immersion depth of the impeller *via*

$$v_C = \sqrt{2gZ}.$$

   In practice, radial disc impellers operating in a non-interacting tank—an unbaffled, right-cylindrical vessel with a dish-shaped bottom—have critical tip speeds which are close to those predicted by the equation above. Axial flow impellers with an upward pitch have critical tip speeds well in excess of those predicted.

2. The addition of baffling greatly alters the direction of discharge from the impeller and hence its gas-pumping action. This leads to critical tip speeds which are not predicted by the equation. In general, the larger the impeller diameter (and hence the smaller the distance between it and the baffles), and the deeper it is placed in the vessel, the poorer is the matching between experimental and predicted values for the critical tip speed.

3. Above the critical tip speed, the measured gas absorption rates (and, presumably, gas pumping rates) increase with increasing impeller tip speed. For radial disc impellers in an unbaffled vessel, this increase is linear with tip speed. When baffling is introduced, the rate of increase is also affected by the impeller diameter (and proximity to the baffles) and depth of immersion.

4. Gas pumping in an unbaffled vessel transfers oxygen at a slower rate than in a baffled vessel. However, it does so with an even greater decrease in power consumption. Thus it is the preferable means of gas pumping where minimizing the

energy (*i.e.* operating expenses) associated with mixing and oxygen transfer is more important than maximizing the throughput rates (*i.e.* minimizing capital expenses) associated with the process.

5. The rate and efficiency of oxygen absorption are greatest when a gas vortex can be sustained in a baffled vessel. This condition occurs with impellers of smaller diameter operating at shallow immersion depths.

6. In the unbaffled vessel, upward pumping axial impellers provide rates and efficiencies of oxygen transfer comparable to radial disc impellers only when placed at shallow immersion depths.

7. In an unbaffled cylindrical vessel, dual impellers are almost uniformly inferior at gas pumping to a single radial disc impeller mounted at the same position as the lower of the pair, or the position of the radial disc impeller if it is combined with an axial impeller.

8. In zinc pressure leaching autoclaves, multiple impellers are used where the lower impeller must maintain the solids in suspension. Oxygen utilization is increased when the upper impeller pumps gas from the freespace, thereby recirculating sparged oxygen which otherwise would have made only one pass through the slurry. For this reason a radial disc impeller at the upper position should be placed near the surface, to sustain a vortex in the presence of the baffling caused by the baffles and asymmetric shape of the autoclave compartments. An upward pumping axial impeller will consume less power, but its oxygen transfer rate is more sensitive to immersion depth than the radial disc impeller in the presence of baffling.

7.3 Recommendations

7.3.1 Physical Apparatus

Variable Speed Motor A variable speed motor would be desirable to eliminate the time-consuming manipulation of belts and pulleys. It would also permit custom-selection of tip speeds, which would greatly assist in generating data for the estimation of v_E.

Impeller Strain Gauges Shaft-mounted foil strain gauges such as those described in [93] would reduce the error associated with calculating the net power from the motor as the difference between the power drawn during the experiment and when running empty. This error was shown to become substantial when the net power was the small difference between these two measurements.

7.3.2 Further Areas of Investigation

Bubble Depletion A method for sampling and analysing bubbles should be developed to permit the evaluation of oxygen utilization efficiency.

Vessel Shape Until recently, laboratory mixing vessels usually have been flat bottomed while industrial reactors have featured dish bottoms. Work is needed in duplicate vessels with each bottom to evaluate bottom effects and determine the degree to which much of the extant literature can be applied to industrial problems.

Baffling:

Baffle Width This needs to be investigated in tandem with impeller diameter to begin to quantify the 'degree of baffling' spectrum which is available. Even for a baffled vessel where a vortex is not created, the effect of baffle-impeller interactions on flow

patterns will change the oxygen transfer and power consumption results for a given tip speed and immersion depth.

Baffle Height The use of half- or variable-height baffles and the proximity of the impeller plane to the baffle tops will also generate a series of flow patterns which cannot be predicted from 'present/absent' experiments. As well, the impeller diameter should play a role in determining the size and stability of the gas vortex.

'Baffling' by Other Methods Use of an eccentrically mounted impeller (offset fractionally from the cylindrical axis) may be another route to combining the two mechanisms of aeration. Non-standard vessel shape will also be important. This need not be limited to autoclave first-compartment shape but could also include a square vessel or the trough shape of the middle autoclave compartments.

Dual Impeller Systems Investigation should be continued in the cylindrical vessel with baffles. Impeller pairs with different diameters, and configurations with a very shallow upper (probably axial) impeller may improve gas pumping.

Impeller Design Radial disc impellers with larger or even full blades should be investigated to observe if pumping from a gas vortex can be made more efficient. A modified vaned disc impeller, with a full disc running through the middle of the blades, and a flat blade radial impeller (without disc) also should be incorporated into an investigation to determine if shear and radial flow can be manipulated to advantage by impeller disc design.

Bibliography

[1] Békétoff, M.N. 'Note sur l'Action de l'Hydrogène à Différentes Pressions sur Quelques Dissolutions Métalliques', *C.R.Aca.Sci. (Paris)*, 48 February 28, 1859, pp. 442-444.

[2] Bayer, K.J. 'Darstellung von Thonerdehydrat und Alkalialuminat', German Patent 65,604, 1892.

[3] Malzac, M. 'Procédé de Désulfuration par Voie Humide, des Minerais de Nickel, Cuivre, Zinc, etc., et d'Hydroxydation de leurs Métaux, en Vue de leur Extraction', French Patent 332,596, May 6, 1903.

[4] Forward, F.A. and Mackiw, V.N. 'Chemistry of the Ammonia Pressure Process for Leaching Ni, Cu, and Co from Sherritt Gordon Sulphide Concentrates', *AIME Trans.*, 203 (3) 1955, pp. 457-463.

[5] Caron, M.H. 'Fundamental and Practical Factors in Ammonia Leaching of Nickel and Cobalt Ores', *AIME Trans.*, 188 (1) 1950, pp. 67-90, 796.

[6] Forward, F.A., Samis, C.S. and Kudryk, V. 'A Method for Adapting the Ammonia-Leaching Process to the Recovery of Copper and Nickel from Sulphide Ore Concentrate', *Trans.CIM*, 51 1948, pp. 181-186.

[7] Habashi, F. 'Pressure Hydrometallurgy: Key to Better and Nonpolluting Processes, Part II', *Engng Min.J.*, 172 (5) 1971, pp. 88-94.

[8] Mancantelli, R.W. and Woodward, J.R. 'Use of Autoclaves and Flash Heat Exchangers at Beaverlodge', *AIME Trans.*, 203 (6) 1955, pp. 751-755.

[9] Mitchell, J.S. 'Pressure Leaching and Reduction at the Garfield Refinery', *Min. Engng*, 8 (11) 1956, pp. 1093-1095.

[10] Deliniois, S.L. 'Is Cuba Winning Battle to Develop Mining Industry?', *Engng Min.J.*, 171 (5) 1970, pp. 86-94.

[11] Vizsolyi, A., Veltman, H. and Forward, F.A. 'Aqueous Oxidation of Galena in Acid Media under Pressure', *AIME Trans.*, 227 (2) 1963, pp. 215-227.

[12] Forward, F.A. and Veltman, H. 'Direct Leaching Zinc-Sulfide Concentrates by Sherritt Gordon', *J.Metals*, 11 (12) 1959, pp. 836-840.

[13] Mackiw, V.N. and Veltman, H. 'Recovery of Zinc and Lead from Complex Low-Grade Sulphide Concentrates by Acid Pressure Leaching', *CIM Bull.*, 60 (657) January, 1967, pp. 80-85.

[14] Vizsolyi, A., Veltman, H., Warren, I.H. and Mackiw, V.N. 'Copper and Elemental Sulfur from Chalcopyrite by Pressure Leaching', *J.Metals*, 19 (11) 1967, pp. 52-59.

[15] Sarkar, K.M. 'Selection of Autoclaves in Hydrometallurgical Operations', *Trans. Instn Min.Metall. (Sect. C: Mineral Process.Extr.Metall.)*, 94 (4) December, 1985, pp. C184-C194.

[16] The Environment Act, C.C.S.M. c. E125, Regulation 165/88, March 31, 1988, *Man.Gaz.*, 117 (16) April 16, 1988, p. 1981 is an example.

[17] Forward, F.A. and Warren, I.H. 'Extraction of Metals from Sulphide Ores by Wet Methods', *Met.Revs*, 5 (18) 1960, pp. 137-164.

[18] Björling, G. 'Uber die Laugung von Sulfidmineralien unter Sauerstoffdruck', *Metallwiss.Tech.*, 8JG (19/20) October, 1954, pp. 781-784.

[19] Kawulka, P., Haffenden, W.J. and Mackiw, V.N. 'Recovery of Zinc from Zinc Sulphides by Direct Pressure Leaching', U.S. Patent 3,867,268, February 18, 1975.

[20] Owusu, G. 'Interfacial Studies in the Zinc Pressure Leach Technology', M.A.Sc. Thesis, University of British Columbia, 1989.

[21] Parker, E.G. and Romanchuk, S. 'Pilot Plant Demonstration of Zinc Sulphide Pressure Leaching', *Lead-Zinc-Tin '80*, World Symposium on Metallurgy and Environmental Control, TMS-AIME 109th Annual Meeting, Las Vegas, February 24-28, 1980; Cigan, J.M., Mackey, T.S. and O'Keefe, T.J., eds., pp. 407-425.

[22] CRC Handbook of Chemistry and Physics, 55th Ed., CRC Press, Cleveland, 1974-1975, p. F-55.

[23] Bruhn, G., Gerlach, J. and Pawlek, F. 'Untersuchungen Über die Löslichkeiten von Salzen und Gasen in Wasser und Wäßrigen Lösungen bei Temperaturen Oberhalb 100°C', *Z.Anorg.Allg.Chem.*, 337 (1/2) April, 1965, pp. 68-79.

[24] Whiteside, D. 'Simplified Zinc Process does not Generate SO_2', *Chem.Engng*, 86 (17) August 13, 1979, pp. 104-106.

[25] Private Communication with E. Peters, October, 1991.

[26] Anon. 'Pollution-Free Zinc Process to be Studied', *Engng Min.J.*, 171 (11) 1970, p. 332.

[27] Parker, E.G. 'Oxidative Pressure Leaching of Zinc Concentrates', *CIM Bull.*, 74 (829) May, 1981, pp. 145-150.

[28] Martin, M.T. and Jankola, W.A. 'Cominco's Trail Zinc Pressure Leach Operation', *CIM Bull.*, 78 (876) April, 1985, pp. 77-81.

[29] Johnston, B.H. and Doyle, B.N. 'Startup and Operation of the Kidd Creek Zinc Sulfide Pressure Leaching Plant', *Min.Met.Proc.*, 3 (1) February, 1986, pp. 1-7.

[30] Scott, T.R. and Dyson, N.F. 'The Catalyzed Oxidation of Zinc Sulfide under Acid Pressure Leaching Conditions', *AIME Trans.*, 242 (9) 1968, pp. 1815-1821.

[31] Pawlek, F.E. 'Research in Pressure Leaching', *J.S.Afr.Instn Min.Metall.*, 69 (12) July, 1969, pp. 632-654.

[32] Niederkorn, J.S. 'Kinetic Study on Catalytic Leaching of Sphalerite', *J.Metals*, 37 (7) 1985, pp. 53-56.

[33] Majima, H. and Peters, E. 'Oxidation Rates of Sulfide Minerals by Aqueous Oxidation at Elevated Temperatures', *AIME Trans.*, 236 (10) 1966, pp. 1409-1413.

[34] Downes, K.W. and Bruce, R.W. 'The Recovery of Elemental Sulphur from Pyrite and Pyrrhotite', *Trans.CIM*, 58 1955, pp. 77-82.

[35] Jan, R.J., Hepworth, M.T. and Fox, V.G. 'A Kinetic Study on the Pressure Leaching of Sphalerite', *Met.Trans.B*, 7B (11) 1976, pp. 353-361.

[36] Verbaan, B. and Crundwell, F.K. 'An Electrochemical Model for the Leaching of a Sphalerite Concentrate', *Hydrometall.*, 16 (3) August, 1986, pp. 345-359.

[37] Dreisinger, D.B. and Peters, E. 'The Mathematical Modelling of the Zinc Pressure Leach', 'The Mathematical Modelling of Metal Processing Operations', AIME, 1987; Szekely, J. ed., pp. 347-369.

[38] Chalkley, M.E., Masters, I.M. and Weir, D.R. 'Miniplant Pressure Leaching of Zinc', *Zinc '83*, 13th Annual Meeting, Hydrometallurgy Division, CIM Metallurgical Society, Edmonton-Trail, August 21- 26, 1983, pp. 12-1 - 12-27.

[39] Dreisinger, D.B. and Peters, E. 'The Oxidation of Ferrous Sulphate by Molecular Oxygen Under Zinc Pressure Leach Conditions', *Hydrometall.*, 22 (1,2) June, 1989, pp. 101-119.

[40] DeGraaf, K.B. 'An Investigation of Gas/Liquid Mass Transfer in Mechanically Agitated Pressure Leaching Systems', M.A.Sc. Thesis, University of British Columbia, 1984.

[41] Dawson-Amoah, J. 'Gas-Liquid Mass Transfer Rates by Gas-Pumping Agitators in Oxygen Pressure Leaching Systems', M.A.Sc. Thesis, University of British Columbia, to be completed in 1991.

[42] Astarita, G. 'Mass Transfer With Chemical Reaction', Elsevier, New York, 1967.

[43] Lewis, W.K. and Whitman, W.G. 'Principles of Gas Absorption', *Ind.Engng Chem.*, 16 (12) 1924, pp. 1215-1220.

[44] Treybal, R.E. 'Mass-Transfer Operations', 3rd Ed., McGraw-Hill, New York, 1980, p. 60.

[45] Higbie, R. 'The Rate of Absorption of a Pure Gas Into a Still Liquid During Short Periods of Exposure', *Trans.AIChE*, 31 (2) June 25, 1935, pp. 365-389.

[46] Danckwerts, P.V. 'Significance of Liquid-Film Coefficients in Gas Absorption', *Ind.Engng Chem.*, 43 (6) 1951, pp. 1460-1467.

[47] Danckwerts, P.V. and Kennedy, A.M. 'Kinetics of Liquid-Film Process in Gas Absorption. Part I: Models of the Absorption Process', *Trans.Instn Chem.Engrs*, 32 (Supp.) 1954, pp. S49-S52 is the first of many examples.

[48] Danckwerts, P.V. 'Gas-Liquid Reactions', McGraw-Hill, New York, 1970, pp. 99-103.

[49] White, A.McL., Brenner, E., Phillips, G.A. and Morrison, M.S. 'Studies in Agitation. IV. Power Measurements', *Trans.AIChE*, 30 1934, pp. 570-584.

[50] White, A.McL. and Brenner, E. 'Studies in Agitation. V. The Correlation of Power Data', *Trans.AIChE*, 30 1934, pp. 585-597.

[51] Thomson, J. 'Report Made to the President and Council of the Royal Society, of Experiments on the Friction of Discs Revolving in Water', *Proc.Roy.Soc.(London)*, 7 June 21, 1855, pp. 509-511.

[52] Hixson, A.W. and Luedeke, V.D. 'Wall Friction in Liquid Agitation Systems', *Ind.Engng Chem.*, 29 (8) 1937, pp. 927-933.

[53] Hixson, A.W. and Baum, S.J. 'Agitation: Power Requirements of Turbine Agitators', *Ind.Engng Chem.*, 34 (2) 1942, pp. 194-208.

[54] Stoops, C.E. and Lovell, C.L. 'Power Consumption of Propeller-Type Agitators', *Ind.Engng Chem.*, 35 (8) 1943, pp. 845-850.

[55] Middleton, J.C., Edwards, M.F. and Stewart, I. 'Recommended Standard Terminology and Nomenclature for Mixing', *Chem.Engr*, (359/360) August/September, 1980, pp. 557-562.

[56] Oldshue, J.Y. 'Fluid Mixing Technology and Practice', *Chem.Engng*, 90 (12) June 13, 1983, pp. 82-108.

[57] Miller, S.A. and Mann, C.A. 'Agitation of Two-Phase Systems of Immiscible Liquids', *Trans.AIChE*, 40 (6) December 25, 1944, pp. 709-745.

[58] Hixson, A.W. and Tenney, A.H. 'Quantitative Evaluation of Mixing as the Result of Agitation in Liquid-Solid Systems', *Trans.AIChE*, 31 (1) March 25, 1935, pp. 113-127.

[59] Hooker, T. 'Prediction of Power Consumption for Geometrically Dissimilar Agitators', *Chem.Engng Prog.*, 44 (11) 1948, pp. 833-838.

[60] Rushton, J.H., Costich, E.W. and Everett, H.J. 'Power Characteristics of Mixing Impellers. Part I.', *Chem.Engng Prog.*, 46 (8) 1950, pp. 395-404.

[61] Rushton, J.H., Costich, E.W. and Everett, H.J. 'Power Characteristics of Mixing Impellers. Part II.', *Chem.Engng Prog.*, 46 (9) 1950, pp. 467-476.

[62] O'Connell, F.P. and Mack, D.E. 'Simple Turbines in Fully Baffled Tanks—Power Characteristics', *Chem.Engng Prog.*, 46 (7) 1950, pp. 358-362.

[63] Nagata, S., Yokoyama, T. and Maeda, H. 'Studies on the Power Requirement of Mixing Impellers (III): Empirical Equations for Paddle Agitators in Cylindrical Vessels', *Mem.Fac.Engng Kyoto Univ.*, 18 (1) January, 1956, pp. 13-29.

[64] Nagata, S., Yamamoto, K., Yokoyama, T. and Shiga, S. 'Studies on the Power Requirement of Mixing Impellers (IV): Empirical Equations Applicable for a Wide Range', *Mem.Fac.Engng Kyoto Univ.*, 19 (3) July, 1957, pp. 274-290.

[65] Nagata, S., Yamamoto, K. and Ujihara, M. 'Flow Patterns of Liquid in a Cylindrical Mixing Vessel without Baffles', *Mem.Fac.Engng Kyoto Univ.*, 20 (4) October, 1958, pp. 336-349.

[66] Nagata, S., Yamamoto, K., Hashimoto, K. and Naruse, Y. 'Flow Patterns of Liquids in a Cylindrical Mixing Vessel with Baffles', *Mem.Fac.Engng Kyoto Univ.*, 21 (3) July, 1959, pp. 260-274.

[67] Rushton, J.H. and Oldshue, J.Y. 'Mixing—Present Theory and Practice. Part II.', *Chem.Engng Prog.*, 49 (5) 1953, pp. 267-275.

[68] Cooper, C.M., Fernstrom, G.A. and Miller, S.A. 'Performance of Agitated Gas-Liquid Contactors', *Ind.Engng Chem.*, 36 (6) 1944, pp. 504-509.

[69] Blakebrough, N. and Sambamurthy, K. 'Performance of Turbine Impellers in Sparger-Aerated Fermentation Vessels', *J.Appl.Chem.*, 14 (10) 1964, pp. 413-422.

[70] Ōyama, Y. and Endō, K. 'Power Characteristics of Gas-Liquid Contacting Mixers', *Chem.Engng (Japan)*, 19 (2) 1955, pp. 2-8.

[71] Michel, B.J. and Miller, S.A. 'Power Requirements of Gas-Liquid Agitated Systems', *AIChE J.*, 8 (2) May, 1962, pp. 262-266.

[72] Uhl, V.W., Winter, R.L. and Heimark, E.L. 'Mass Transfer in Large Secondary Treatment Aerators', 'Water—1976: Biological Wastewater Treatment', *AIChE*

Symp. Series No. 167, 73 1976, pp. 33-41.

[73] Brown, D.E. 'Impeller Power Input Measurements in a Production-Scale Fermenter', 'Fluid Mixing', *IChemE Symp. Series No. 64*, 1981, pp. N1-N28.

[74] Lee, J.C. and Meyrick, D.L. 'Gas-Liquid Interfacial Areas in Salt Solutions in an Agitated Tank', *Trans.Instn Chem.Engrs*, 48 (2) March, 1970, pp. T37-T45.

[75] Bruijn, W., van't Riet, K. and Smith, J.M. 'Power Consumption with Aerated Rushton Turbines', *Trans.Instn Chem.Engrs*, 52 (1) January, 1974, pp. 88-104.

[76] Hassan, I.T.M. and Robinson, C.W. 'Stirred-Tank Mechanical Power Requirement and Gas Hold-Up in Aerated Aqueous Phases', *AIChE J.*, 23 (1) January, 1977, pp. 48-56.

[77] Greaves, M. and Kobbacy, K.A.H. 'Power Consumption and Impeller Dispersion Efficiency in Gas-Liquid Mixing', 'Fluid Mixing', *IChemE Symp. Series No. 64*, 1981, pp. L1-L33.

[78] Greaves, M. and Loh, V.Y. 'Power Consumption Effect in Three Phase Mixing', 'Fluid Mixing II', *IChemE Symp. Series No. 89*, 1984, pp. 69-97.

[79] Westerterp, K.R., van Dierendonck, L.L. and de Kraa, J.A. 'Interfacial Areas in Agitated Gas-Liquid Contactors', *Chem.Engng Sci.*, 18 (3) 1963, pp. 157-176.

[80] Westerterp, K.R. 'Design of Agitators for Gas-Liquid Contacting', *Chem.Engng Sci.*, 18 (8) 1963, pp. 495-502.

[81] Calderbank, P.H. 'Physical Rate Processes in Industrial Fermentation. Part II: Mass Transfer Coefficients in Gas-Liquid Contacting With and Without Mechanical Agitation', *Trans.Instn Chem.Engrs*, 37 (3) 1959, pp. 173-185.

[82] Mehta, V.D. and Sharma, M.M. 'Mass Transfer in Mechanically Agitated Gas-Liquid Contactors', *Chem.Engng Sci.*, 26 (3) 1971, pp. 461-479.

[83] Rennie, J. and Valentin, F.H.H. 'Gas Dispersion in Agitated Tanks', *Chem.Engng Sci.*, 23 (6) August, 1968, pp. 663-664.

[84] Miller, D.N. 'Scale-Up of Agitated Vessels—Gas-Liquid Mass Transfer', *AIChE J.*, 20 (3) May, 1974, pp. 445-453.

[85] Nienow, A.W. and Wisdom, D.J. 'The Effect of Scale on Specific Absorption Rates in Aerated Vessels With a Constant Gas Residence Time', International Symposium on Mixing, Faculté Polytechnique Mons, France, February 21-24, 1978, pp. C12-1 - C12-12.

[86] Boerma, H. and Lankester, J.H. 'The Occurrence of Minimum Stirring Rates in Gas-Liquid Reactors', *Chem.Engng Sci.*, 23 (7) August, 1968, pp. 799-801.

[87] van't Riet, K. and Smith, J.M. 'The Behaviour of Gas-Liquid Mixtures Near Rushton Turbine Blades', *Chem.Engng Sci.*, 28 (4) 1973, pp. 1031-1037.

[88] Nienow, A.W. and Wisdom, D.J. 'Flow Over Disc Turbine Blades', *Chem.Engng Sci.*, 29 (9) 1974, pp. 1994-1996.

[89] Nienow, A.W., Wisdom, D.J. and Middleton, J.C. 'The Effect of Scale and Geometry on Flooding, Recirculation, and Power in Gassed Stirred Vessels', Second European Conference on Mixing, Cambridge, England, March 30-April 1, 1977, pp. F1-1 - F1-16.

[90] Warmoeskerken, M.M.C.G., Feijen, J. and Smith, J.M. 'Hydrodynamics and Power Consumption in Stirred Gas-Liquid Dispersions', 'Fluid Mixing', *IChemE Symp. Series No. 64*, 1981, pp. J1-J14.

[91] Warmoeskerken, M.M.C.G., Speur, J. and Smith, J.M. 'Gas-Liquid Dispersion with Pitched Blade Turbines', *Chem.Engng Commun.*, 25 (1-6) January, 1984, pp. 11-29.

[92] Warmoeskerken, M.M.C.G. and Smith, J.M. 'Flooding of Disc Turbines in Gas-Liquid Dispersions: A New Description of the Phenomenon', *Chem.Engng Sci.*, 40 (11) 1985, pp. 2063-2071.

[93] Kuboi, R., Nienow, A.W. and Allsford, K. 'A Multipurpose Stirred Tank Facility for Flow Visualisation and Dual Impeller Power Measurement', *Chem.Engng Commun.*, 22 (1-2) July, 1983, pp. 29-39.

[94] Nienow, A.W., Konno, M. and Bujalski, W. 'Studies on Three-Phase Mixing: A Review and Recent Results', Fifth European Conference on Mixing, Wurzburg, FRG, June 10-12, 1985, pp. 1-13.

[95] Nienow, A.W., Warmoeskerken, M.M.C.G., Smith, J.M. and Konno, M. 'On the Flooding/Loading Transition and the Complete Dispersal Condition in Aerated Vessels Agitated by a Rushton-Turbine', Fifth European Conference on Mixing, Wurzburg, FRG, June 10-12, 1985, pp. 143-154.

[96] Nagata, S., Yamamoto, K., Hashimoto, K. and Naruse, Y. 'Studies on the Flow Patterns of Liquids in a Cylindrical Mixing Vessel, Over a Wide Range of Reynolds Number', *Mem.Fac.Engng Kyoto Univ.*, 22 (1) January, 1960, pp. 68-85.

[97] Metzner, A.B. and Taylor, J.S. 'Flow Patterns in Agitated Vessels', *AIChE J.*, 6 (1) March, 1960, pp. 109-114.

[98] Holmes, D.B., Voncken, R.M. and Dekker, J.A. 'Fluid Flow in Turbine-Stirred, Baffled Tanks—I. Circulation Time', *Chem.Engng Sci.*, 19 (3) 1964, pp. 201-208.

[99] Wilhelm, R.H., Donohue, W.A., Valesano, D.J. and Brown, G.A. 'Gas Absorption in a Stirred Vessel: Locale of Transfer Action', *Biotechnol.Bioengng*, 8 (1) February, 1966, pp. 55-69.

[100] Chapman, C.M. 'Studies of Gas-Liquid-Particle Mixing in Stirred Vessels', Ph.D. Thesis, University of London, 1981.

[101] Chapman, C.M., Nienow, A.W., Cooke, M. and Middleton, J.C. 'Particle-Gas-Liquid Mixing in Stirred Vessels. Part II: Gas-Liquid Mixing', *Trans.Instn Chem.Engrs Chem.Engng Res.Des.*, 61 (2) March, 1983, pp. 82-95.

[102] Frijlink, J.J., Kolijn, M. and Smith, J.M. 'Suspension of Solids with Aerated Pitched Blade Turbines', 'Fluid Mixing II', *IChemE Symp. Series No. 89*, 1984, pp. 49-58.

[103] Warmoeskerken, M.M.C.G. and Smith, J.M. 'Description of the Power Curves of Turbine Stirred Gas-Liquid Dispersions', Fourth European Conference on Mixing, Noordwijkerhout, The Netherlands, April 27-29, 1982, pp. 237-246.

[104] Reed, X.B., Princz, M. and Hartland, S. 'Laser Doppler Measurements of Turbulence in a Standard Stirred Tank', Second European Conference on Mixing, Cambridge, England, March 30-April 1, 1977, pp. B1-1 - B1-26.

[105] Greaves, M. and Kobbacy, K.A.H. 'Surface Aeration in Agitated Vessels', 'Fluid Mixing', *IChemE Symp. Series No. 64*, 1981, pp. H1-H22.

[106] Heywood, N.I., Madhvi, P. and McDonagh, M. 'Design of Ungassed Baffled Mixing Vessels to Minimize Surface Aeration of Low Viscosity Liquids', Fifth European Conference on Mixing, Wurzburg, FRG, June 10-12, 1985, pp. 243-261.

[107] Nienow, A.W., Chapman, C.M. and Middleton, J.C. 'Gas Recirculation Rate through Impeller Cavities and Surface Aeration in Sparged Agitated Vessels', *Chem.Engng J.*, 17 (2) April, 1979, pp. 111-118.

[108] Chapman, C.M., Nienow, A.W. and Middleton, J.C. 'Surface Aeration in a Small, Agitated, and Sparged Vessel', *Biotechnol.Bioengng*, 22 (5) 1980, pp. 981-993.

[109] Reith, T. and Beek, W.J. 'Bubble Coalescence Rates in a Stirred Tank Contactor', *Trans.Instn Chem.Engrs*, 48 (2) March, 1970, pp. T63-T68.

[110] Fuchs, R., Ryu, D.D.Y. and Humphrey, A.E. 'Effect of Surface Aeration on Scale-Up Procedures for Fermentation Processes', *Ind.Engng Chem.Process Des.Develop.*, 10 (2) April, 1971, pp. 190-196.

[111] Clark, M.W. and Vermeulen, T. 'Incipient Vortex Formation in Baffled Vessels', *AIChE J.*, 10 (3), May, 1964, pp. 420-422.

[112] Tsao, G.T.N. 'Vortex Behavior in the Waldhof Fermentor', *Biotechnol.Bioengng*, 10 (2) March, 1968, pp. 177-188.

[113] Zlokarnik, M. 'Trombentiefe beim Rühren in unbewehrten Behältern', *Chemie-Ing.-Techn.*, 43 (18) September, 1971, pp. 1028-1030.

[114] van de Vusse, J.G. 'Mixing by Agitation of Miscible Liquids. Part I.', *Chem.Engng Sci.*, 4 (4) August, 1955, pp. 178-200.

[115] Nagata, S., Yoshioka, N. and Yokoyama, T. *Mem.Fac.Engng Kyoto Univ.*, 17 (3) July, 1955, p. 175.

[116] Nagata, S., Yamaguchi, I., Yabuta, S. and Harada, M. 'Mass Transfer in Agitated Liquid-Solid Systems', *Mem.Fac.Engng Kyoto Univ.*, 22 (1) January, 1960, pp. 86-122.

[117] Chain, E.B., Paladino, S., Callow, D.S., Ugolini, F. and van der Sluis, J. 'Studies on Aeration—I.', *Bull.World Hlth Org.*, 6 (1-2) 1952, pp. 73-97.

[118] Zwietering, T.N. 'Suspending of Solid Particles in Liquid by Agitators', *Chem. Engng Sci.*, 8 (3-4) 1958, pp. 244-253.

[119] Mack, D.E. and Kroll, A.E. 'Effect of Baffles on Agitator Power Consumption', *Chem.Engng Prog.*, 44 (3) 1948, pp. 189-194.

[120] Oldshue, J.Y. 'Fermentation Mixing Scale-Up Techniques', *Biotechnol.Bioengng*, 8 (1) February, 1966, pp. 3-24.

[121] Connolly, J.R. and Winter, R.L. 'Approaches to Mixing Operation Scale-Up', *Chem.Engng Prog.*, 65 (8) 1969, pp. 70-78.

[122] Brennan, D.J. and Lehrer, I.H. 'Impeller Mixing in Vessels: Experimental Studies on the Influence of Some Parameters and Formulation of a General Mixing Time Equation', *Trans.Instn Chem.Engrs*, 54 (3) July, 1976, pp. 139-152.

[123] Brennan, D.J. 'Vortex Geometry in Unbaffled Vessels with Impeller Agitation', *Trans.Instn Chem.Engrs*, 54 (4) October, 1976, pp. 209-217.

[124] Joosten, G.E.H., Schilder, J.G.M. and Broere, A.M. 'The Suspension of Floating Solids in Stirred Vessels', *Trans.Instn Chem.Engrs*, 55 (3) July, 1977, pp. 220-222.

[125] Bryant, J. and Sadeghzadeh, S. 'Circulation Rates in Stirred and Aerated Tanks', Third European Conference on Mixing, York, England, April 4-6, 1979, April 4-6, 1979, pp. 325-336.

[126] Wiedmann, J.A., Steiff, A. and Weinspach, P.-M. 'Experimental Investigations of Suspension, Dispersion, Power, Gas Hold Up and Flooding Characteristics in Stirred Gas-Solid-Liquid Systems (Slurry Reactors)', *Chem.Engng Commun.*, 6 (4-5) August, 1980, pp. 245-256.

[127] Cliff, M.J., Edwards, M.F. and Ohiaeri, I.N. 'The Suspension of Settling Solids in Agitated Vessels' 'Fluid Mixing', *IChemE Symp. Series No. 64*, 1981, pp. M1-M11.

[128] Novák, V., Ditl, P. and Rieger, F. 'Mixing in Unbaffled Vessels: The Influence of an Eccentric Impeller Position on Power Consumption and Surface Aeration', Fourth European Conference on Mixing, Noordwijkerhout, The Netherlands, April 27-29, 1982, pp. 57-70.

[129] Warmoeskerken, M.M.C.G., van Houwelingen, M.C., Frijlink, J.J. and Smith, J.M. 'Role of Cavity Formation in Stirred Gas-Liquid-Solid Reactors', *Trans.Instn Chem.Engrs Chem.Engng Res.Des.*, 62 (3) May, 1984, pp. 197-200.

[130] Buurman, C., Resoort, G. and Plaschkes, A. 'Scaling-Up Rules for Solids Suspension in Stirred Vessels', Fifth European Conference on Mixing, Wurzburg, FRG, June 10-12, 1985, pp. 15-26.

[131] Greaves, M. and Loh, V.Y. 'Effect of High Solids Concentrations on Mass Transfer and Gas Hold-Up in Three-Phase Mixing', Fifth European Conference on Mixing, Wurzburg, FRG, June 10-12, 1985, pp. 451-467.

[132] Roustan, M. 'Power Consumed by Rushton Turbines in Non-Standard Vessels Under Gassed Conditions', Fifth European Conference on Mixing, Wurzburg, FRG, June 10-12, 1985, pp. 127-141.

[133] Holland, F.A. and Chapman, F.S. 'Liquid Mixing and Processing in Stirred Tanks', Reinhold, New York, 1966, p. 12.

[134] Bates, R.L., Fondy, P.L. and Corpstein, R.R. 'An Examination of Some Geometric Parameters of Impeller Power', *Ind.Engng Chem.Process Des.Develop.*, 2 (4) October, 1963, pp. 310-314.

[135] Nienow, A.W. 'Suspension of Solid Particles in Turbine Agitated Baffled Vessels', *Chem.Engng Sci.*, 23 (12) December, 1968, pp. 1453-1459.

[136] Queneau, P.B., Jan, R.J., Rickard, R.S. and Lowe, D.F. 'Turbine Mixer Fundamentals and Scale-Up Method at the Port Nickel Refinery', *Met.Trans.B*, 6B (3) 1975, pp. 149-157.

[137] Nienow, A.W. and Miles, D. 'The Effect of Impeller/Tank Configurations on Fluid-Particle Mass Transfer', *Chem.Engng J.*, 15 (1) February, 1978, pp. 13-24.

[138] Chapman, C.M., Nienow, A.W., Cooke, M. and Middleton, J.C. 'Particle-Gas-Liquid Mixing in Stirred Vessels. Part III: Three Phase Mixing', *Trans.Instn Chem.Engrs Chem.Engng Res.Des.*, 61 (3) May, 1983, pp. 167-181.

[139] Nienow, A.W. and Miles, D. 'Impeller Power Numbers in Closed Vessels', *Ind.Engng Chem.Process Des.Develop.*, 10 (1) January, 1971, pp. 41-43.

[140] Rushton, J.H. and Bimbinet, J.-J. 'Holdup and Flooding in Air Liquid Mixing', *Can.J.Chem.Engng*, 46 (1) February, 1968, pp. 16-21.

[141] Solomon, J., Elson, T.P., Nienow, A.W. and Pace, G.W. 'Cavern Sizes in Agitated Fluids with a Yield Stress', *Chem.Engng Commun.*, 11 (1-3) July, 1981, pp. 143-164.

[142] Smith, J.M., van't Riet, K. and Middleton, J.C. 'Scale-Up of Agitated Gas-Liquid Reactors for Mass Transfer', Second European Conference on Mixing, Cambridge, England, March 30-April 1, 1977, pp. F4-51-F4-66.

[143] Blakebrough, N., Hamer, G. and Walker, M.W. 'Agitation and Aeration in Fermentation Vessels. Part I.', *Chem.Engr*, (157) October, 1961, pp. A71-A81.

[144] Hamer, G. and Blakebrough, N. 'Turbine Impellers as Gas-Liquid Contacting Devices', *J.Appl.Chem.*, 13 (11) 1963, pp. 517-524.

[145] Medek, J. 'Power Characteristics of Agitators with Flat Inclined Blades', *Intl Chem.Engng*, 20 (4) October, 1980, pp. 664-672.

[146] Bowen, R.L. 'Agitation Intensity: Key to Scaling up Flow-Sensitive Liquid Systems', *Chem.Engng*, 92 (6) March 18, 1985, pp. 159-168.

[147] Rieger, F., Ditl, P. and Novák, V. 'Vortex Depth in Mixed Unbaffled Vessels', *Chem.Engng Sci.*, 34 (3) 1979, pp. 397-403.

[148] Chapman, C.M., Nienow, A.W., Cooke, M. and Middleton, J.C. 'Particle-Gas-Liquid Mixing in Stirred Vessels. Part I: Particle-Liquid Mixing', *Trans.Instn Chem.Engrs Chem.Engng Res.Des.*, 61 (2) March, 1983, pp. 71-81.

[149] Chapman, C.M., Nienow, A.W., Cooke, M. and Middleton, J.C. 'Particle-Gas-Liquid Mixing in Stirred Vessels. Part IV: Mass Transfer and Final Conclusions', *Trans.Instn Chem.Engrs Chem.Engng Res.Des.*, 61 (3) May, 1983, pp. 182-185.

[150] Joshi, J.B. and Sharma, M.M. 'Mass Transfer and Hydrodynamic Characteristics of Gas Inducing Type of Agitated Contactors', *Can.J.Chem.Engng*, 55 (6) December, 1977, pp. 683-695.

[151] Bruxelmane, M. 'Conditions de Loading et de Flooding', International Symposium on Mixing, Faculté Polytechnique Mons, France, February 21-24, 1978, pp. XC-1 - XC-6.

[152] Calderbank, P.H. and Moo-Young, M.B. 'The Power Characteristics of Agitators for the Mixing of Newtonian and Non-Newtonian Fluids', *Trans.Instn Chem.Engrs*, 39 (5) October, 1961, pp. 337-347.

[153] Johnson, D.L., Saito, H., Polejes, J.D. and Hougen, O.A. 'Effects of Bubbling and Stirring on Mass Transfer Coefficients in Liquids', *AIChE J.*, 3 (3) September, 1957, pp. 411-417.

[154] van't Riet, K., Boom, J.M. and Smith, J.M. 'Power Consumption, Impeller Coalescence and Recirculation in Aerated Vessels', *Trans.Instn Chem.Engrs*, 54 (2) April, 1976, pp. 124-131.

[155] Yoshida, F., Ikeda, A., Imakawa, S. and Miura, Y. 'Oxygen Absorption Rates in Stirred Gas-Liquid Contactors', *Ind.Engng Chem.*, 52 (5) 1960, pp. 435-438.

[156] Rushton, J.H., Gallagher, J.B. and Oldshue, J.Y. 'Gas-Liquid Contacting with Multiple Mixing Turbines', *Chem.Engng Prog.*, 52 (8) 1956, pp. 319-323.

[157] Bowen, R.L. 'Unraveling the Mysteries of Shear-Sensitive Mixing Systems', *Chem. Engng*, 93 (11) June 9, 1986, pp. 55-63.

[158] Bujalski, W., Nienow, A.W., Chatwin, S. and Cooke, M. 'The Dependency on Scale of Power Numbers of Rushton Disc Turbines', *Chem.Engng Sci.*, 42 (2) 1987, pp. 317-326.

[159] Finn, R.K. 'Agitation-Aeration in the Laboratory and in Industry', *Bacteriol.Revs*, 18 (4) December, 1954, pp. 254-274.

[160] Kuboi, R. and Nienow, A.W. 'The Power Drawn by Dual Impeller Systems Under Gassed and Ungassed Conditions', Fourth European Conference on Mixing, Noordwijkerhout, The Netherlands, April 27-29, 1982, pp. 247-261.

[161] Nienow, A.W. and Lilly, M.D. 'Power Drawn by Multiple Impellers in Sparged Agitated Vessels', *Biotechnol.Bioengng*, 21 (12) 1979, pp. 2341-2345.

[162] Hicks, R.W. and Gates, L.E. 'How to Select Turbine Agitators for Dispersing Gas into Liquids', *Chem.Engng*, 83 (15) July 19, 1976, pp. 141-148.

[163] Hixson, A.W. and Wilkens, G.A. 'Performance of Agitators in Liquid-Solid Chemical Systems', *Ind.Engng Chem.*, 25 (11) 1933, pp. 1196-1203.

[164] Vermeulen, T., Williams, G.M. and Langlois, G.E. 'Interfacial Area in Liquid-Liquid and Gas-Liquid Agitation', *Chem.Engng Prog.*, 51 (2) 1955 pp. 85-F - 94-F.

[165] Benedek, A. and Heideger, W.J. 'Effect of Additives on Mass Transfer in Turbine Aeration', *Biotechnol.Bioengng*, 13 (5) September, 1971, pp. 663-684.

[166] Marrucci, G. and Nicodemo, L. 'Coalescence of Gas Bubbles in Aqueous Solutions of Inorganic Electrolytes', *Chem.Engng Sci.*, 22 (9) 1967, pp. 1257-1265.

[167] Calderbank, P.H. 'Physical Rate Processes in Industrial Fermentation. Part I: The Interfacial Area in Gas-Liquid Contacting With Mechanical Agitation', *Trans.Instn Chem.Engrs*, 36 1958, pp. 443-463.

[168] Preen, B.V. 'Gas-Liquid Mass Transfer in a Mechanically Agitated Vessel', Ph.D. Thesis, University of Natal, 1961.

[169] Sideman, S., Hortaçsu, Ö. and Fulton, J.W. 'Mass Transfer in Gas-Liquid Contacting Systems', *Ind.Engng Chem.*, 58 (7) 1966, pp. 32-47.

[170] Matheron, E.R. and Sandall, O.C. 'Effective Interfacial Area Determination by Gas Absorption Accompanied by Second-Order Irreversible Chemical Reaction', *AIChE J.*, 25 (2) March, 1979, pp. 332-338.

[171] Carpani, R.E. and Roxburgh, J.M. 'Studies on Fermentation Aeration. I. The Oxygen Transfer Coefficient', *Can.J.Chem.Engng*, 36 (2) April, 1958, pp. 73-77.

[172] Kataoka, H. and Miyauchi, T. 'Gas Absorption into the Free Liquid Surface of Agitated Vessels in Turbulent Region', *Kagaku Kōgaku (English Ed.)*, 4 (2) Autumn, 1966, pp. 335-338.

[173] Koetsier, W.T. and Thoenes, D. 'Mass Transfer in a Closed Stirred Gas/Liquid Contactor. Part II: The Liquid Phase Mass Transfer Coefficient k_L', *Chem.Engng J.*, 5 (1) February, 1973, pp. 71-75.

[174] Prasher, B.D. and Wills, G.B. 'Mass Transfer in an Agitated Vessel', *Ind.Engng Chem.Process Des.Develop.*, 12 (3) July, 1973, pp. 351-354.

[175] Topiwala, H.H. and Hamer, G. 'Mass Transfer and Dispersion Properties in a Fermenter with a Gas-Inducing Impeller', *Trans.Instn Chem.Engrs*, 52 (2) April, 1974, pp. 113-120.

[176] Alper, E., Deckwer, W.-D. and Danckwerts, P.V. 'Comparison of Effective Interfacial Areas with the Actual Contact Area for Gas Absorption in a Stirred Cell', *Chem.Engng Sci.*, 35 (6) 1980, pp. 1263-1268.

[177] Gollakota, S.V. and Guin, J.A. 'Comparative Study of Gas-Liquid Mass Transfer Coefficients in Stirred Autoclaves, Tubing Bomb Microreactors, and Bubble Columns', *Ind.Engng Chem.Process Des.Develop.*, 23 (1) January, 1984, pp. 52-59.

[178] Robinson, C.W. and Wilke, C.R. 'Oxygen Absorption in Stirred Tanks: A Correlation for Ionic Strength Effects', *Biotechnol.Bioengng*, 15 (4) July, 1973, pp. 755-782.

[179] Hassan, I.T.M. and Robinson, C.W. 'Mass Transfer Coefficients in Mechanically Agitated Gas-Aqueous Electrolyte Dispersions', *Can.J.Chem.Engng*, 58 (2) April, 1980, pp. 198-205.

[180] Calderbank, P.H. and Moo-Young, M.B. 'The Continuous Phase Heat and Mass-Transfer Properties of Dispersions', *Chem.Engng Sci.*, 16 (1-2) December, 1961, pp. 39-54.

[181] Lamont, J.C. 'Gas Absorption in Cocurrent Turbulent Bubble Flow', Ph.D. Thesis, University of British Columbia, August, 1966, pp. 154-157.

[182] Mann, R., Middleton, J.C. and Parker, I.B. 'Deteriorating Mixing Quality and Yield Losses on Scaling-Up Gas-Liquid Reactors', Second European Conference on Mixing, Cambridge, England, March 30-April 1, 1977, pp. F3-35 - F3-50.

[183] Hudcova, V., Nienow, A.W., Haozhung, W. and Huoxing, L. 'On the Effect of Liquid Height on the Flooding/Loading Transition', *Chem.Engng Sci.*, 42 (2) 1987, pp. 375-377.

[184] Smith, J.M. and Warmoeskerken, M.M.C.G. 'The Dispersion of Gases in Liquids

with Turbines', Fifth European Conference on Mixing, Wurzburg, FRG, June 10-12, 1985, pp. 115-126.

[185] van't Riet, K. 'Review of Measuring Methods and Results in Nonviscous Gas-Liquid Mass Transfer in Stirred Vessels', *Ind.Engng Chem.Process Des.Develop.*, 18 (3) July, 1979, pp. 357-364.

[186] Cutter, L.A. 'Flow and Turbulence in a Stirred Tank', *AIChE J.*, 12 (1) January, 1966, pp. 35-45.

[187] Levins, D.M. and Glastonbury, J.R. 'Particle-Liquid Hydrodynamics and Mass Transfer in a Stirred Vessel. Part II—Mass Transfer', *Trans.Instn Chem.Engrs*, 50 (2) April, 1972, pp. 132-146.

[188] Richards, J.W. 'Studies in Aeration and Agitation', *Prog.Ind.Microbiol.*, 3 1961, pp. 141-172.

[189] Procházka, J. and Landau, J. 'Studies on Mixing. XVI. Exact Determination of Power Consumption of Rotational Mixers', *J.Coll.Czechoslov.Chem.Commun.*, 28 (5) 1963, pp. 1102-1109.

[190] Nienow, A.W. and Miles, D. 'A Dynamometer for the Accurate Measurement of Mixing Torque', *J.Sci.Instr.*, 3 (Ser. 2) (2) 1969, pp. 994-995.

[191] Valentin, F.H.H. and Preen, B.V. 'Stoffübertragung Gas/Flüssigkeit in einem Rührgefäß', *Chemie-Ing.-Techn.*, 34 (3) 1962, pp. 194-199.

[192] Porter, K.E., Davies, B.T. and Wong, P.F.Y. 'Mass Transfer and Bubble Sizes in Cellular Foams and Froths', *Trans.Instn Chem.Engrs*, 45 (7) September, 1967, pp. T265-T273.

[193] Titoff, A. 'Beiträge zur Kenntnis der Negativen Katalyse im Homogenen System', *Z.Physik.Chem.*, 45 (6) December 15, 1903, pp. 641-683.

[194] Bäckström, H.L.J. 'The Chain-Reaction Theory of Negative Catalysis', *J.Amer. Chem.Soc.*, 49 (6) June 7, 1927, pp. 1460-1472.

[195] Bäckström, H.L.J. 'Der Kettenmechanismus bei der Autoxydation von Natriumsulfitlösungen', *Z.Physik.Chem., Abt.B.*, 25 (1-2) March, 1934, pp. 122-138.

[196] Barron, C.H. and O'Hern, H.A. 'Reaction Kinetics of Sodium Sulfite Oxidation by the Rapid-Mixing Method', *Chem.Engng Sci.*, 21 (5) May, 1966, pp. 397-404.

[197] Chen, T.-I. and Barron, C.H. 'Some Aspects of the Homogeneous Kinetics of Sulfite Oxidation', *Ind.Engng Chem.Fundam.*, 11 (4) November, 1972, pp. 466-470.

[198] Sawicki, J.E. and Barron, C.H. 'On the Kinetics of Sulfite Oxidation in Heterogeneous Systems', *Chem.Engng J.*, 5 1973, pp. 153-159.

[199] Linek, V. and Vacek, V. 'Chemical Engineering Use of Catalyzed Sulfite Oxidation Kinetics for the Determination of Mass Transfer Characteristics of Gas-Liquid Contactors', *Chem.Engng Sci.*, 36 (11) 1981, pp. 1747-1768.

[200] Cotton, F.A. and Wilkinson, G. 'Advanced Inorganic Chemistry', Wiley Interscience, New York, 1962, p. 721.

[201] DeVuyst, E.A., Mosoiu, A. and Krause, E. 'Oxidizing Properties and Applications of the SO_2–O_2 System', *Hydrometallurgy—Research, Development and Plant Practice*, Third International Symposium on Hydrometallurgy, 112th TMS-AIME Annual Meeting, Atlanta, March 6-10, 1983; Osseo-Asare, K. and Miller, J.D., eds., pp. 391- 403.

[202] Hayon, E., Treinin, A. and Wilf, J. 'Electronic Spectra, Photochemistry, and Autoxidation Mechanism of the Sulfite–Bisulfite–Pyrosulfite Systems. The SO_2^-, SO_3^-, SO_4^-, and SO_5^- Radicals', *J.Amer.Chem.Soc.*, 94 (1) January 12, 1972, pp. 47-57.

[203] Milbauer, J. and Pazourek, J. 'Sur L'Oxydation des Sulfites en Solutions Concentrées', *Bull.Soc.Chim.*, 30 1921, p. 557.

[204] Milbauer, J. and Pazourek, J. 'L'Oxydation des Sulfites en Solutions Concentrées', *Bull.Soc.Chim.*, 31 1922, pp. 676-678.

[205] Reinders, W. and Vles, S.I. 'Reaction Velocity of Oxygen with Solutions of Some Inorganic Salts. III. The Catalytic Oxidation of Sulphites', *Rec.Trav.Chim.*, 44 1925, pp. 249-268.

[206] Fuller, E.C. and Crist, R.H. 'The Rate of Oxidation of Sulfite Ions by Oxygen', *J.Amer.Chem.Soc.*, 63 (6) 1941, pp. 1644-1650.

[207] Altwicker, E.R. 'The Role of Inhibitors in the Kinetics of Sulphite Oxidation', *Trans.Instn Chem.Engrs*, 55 (4) October, 1977, pp. 281-282.

[208] Benedek, A., Bennett, G.F. and Ho, K.W.A. 'Aeration and the Sulfite Oxidation Test', 'Water—1974: Municipal Waste Treatment', *AIChE Symp. Series No. 145*, 71 1974, pp. 190-201.

[209] Kountz, R.R. 'Evaluating Proprietary Aeration Devices', 'Biological Treatment of Sewage and Industrial Wastes', Vol. 1, Reinhold, New York, 1956; McCabe, J. and Eckenfelder, W.W. Jr., eds., pp. 212-214.

[210] Astarita, G., Marrucci, G. and Coleti, L. *Chim.e L'Ind. (Milano)*, 46 (9) 1964, p. 1021.

[211] Bengtsson, S. and Bjerle, I. 'Catalytic Oxidation of Sulphite in Diluted Aqueous Solutions', *Chem.Engng Sci.*, 30 (11) 1975, pp. 1429-1435.

[212] Linek, V. and Beneš, P. 'Enhancement of Oxygen Absorption into Sodium Sulfite Solutions', *Biotechnol.Bioengng*, 20 (5) 1978, pp. 697-707.

[213] Schultz, J.S. and Gaden, E.L. 'Sulfite Oxidation as a Measure of Aeration Effectiveness', *Ind.Engng Chem.*, 48 (12) 1956, pp. 2209-2212.

[214] Onda, K., Takeuchi, H. and Maeda, Y. 'The Absorption of Oxygen into Sodium Sulphite Solutions in a Packed Column', *Chem.Engng Sci.*, 27 (2) 1972, pp. 449-451.

[215] Sutton, F. and Grant, J. 'A Systematic Handbook of Volumetric Analysis', 13th Ed., Butterworths, London, 1955, p. 187.

[216] Westerterp, K.R. 'The Specific Surface in Stirred Gas-Liquid Reactors', Ph.D. Thesis, Technical University, Delft, 1962, cited in [105].

[217] 'Standard Methods for the Examination of Water and Wastewater', 14th Ed., American Public Health Association, Baltimore, 1975, pp. 446-447.

[218] Conway, R.A. and Kumke, G.W. 'Field Techniques for Evaluating Aerators', *J.San.Engng Div., Proc.Amer.Soc.Civil Engrs*, 92 (SA2) April, 1966, pp. 21-42.

[219] MacArthur, C.G. 'Solubility of Oxygen in Salt Solutions and the Hydrates of these Salts', *J.Phys.Chem*, 20 (7) October, 1916, pp. 495-502.

[220] Linek, V. and Mayrhoferová, J. 'The Kinetics of Oxidation of Aqueous Sodium Sulphite Solution', *Chem.Engng Sci.*, 25 (5) 1970, pp. 787-800.

[221] Yasunishi, A. 'Solubilities of Sparingly Soluble Gases in Aqueous Sodium Sulfate and Sulfite Solutions', *J.Chem.Engng Japan*, 10 (2) April, 1977, pp. 89-94.

[222] Gestrich, W. and Pontow, B. 'Die Sauerstoff-Löslichkeit in Wäßrigen Sulfit-Lösungen mit einer Konzentration bis zu 1,2 mol/ℓ', *Chemie-Ing.-Techn.*, 49 (7) 1977, pp. 564-565.

[223] Othmer, D.F. and Thakar, M.S. 'Correlating Diffusion Coefficients in Liquids', *Ind.Engng Chem.*, 45 (3) 1953, pp. 589-593.

[224] Wilke, C.R. and Chang, P. 'Correlation of Diffusion Coefficients in Dilute Solutions' *AIChE J.*, 1 (2) June, 1955, pp. 264-270.

[225] Ratcliff, G.A. and Holdcroft, J.G. 'Diffusivities of Gases in Aqueous Electrolyte Solutions', *Trans.Instn Chem.Engrs*, 41 1963, pp. 315-319.

Appendix A

Estimation of Oxygen Solubilities

The rate of sulphite ion depletion during an experiment is proportional to the rate of oxygen transfer; thus from Equation 4.1,

$$R = k_L^o \cdot a \cdot (C^I - C^b) \tag{A.1}$$

it is a measure of the k_L^o and a provided by the particular (D or D/T, Z, v, impeller type). The oxygen concentration C^b in the bulk of the sodium sulphite solution is taken to be always zero. But since the oxygen concentration C^I at the interface is essentially equal to that of a liquid saturated with oxygen at concentration $\mathcal{P}^g$, the term C^I depends on the oxygen solubility at the temperature and sulphite ion concentration at which the experiment was performed.

The oxygen transfer rate R can be made independent of these two effects by dividing by the C^I for the particular experiment. In this way the result is applicable to other systems where C^I is known for the particular temperature and sulphite ion concentration. Of course the result cannot be applied to systems where changes in viscosity and ionic strength, for example, are so significant they induce changes in k_L^o and/or a.

There are several possible methods of estimation for C^I. First, since the concentration of Na_2SO_3 used in this work is relatively small it could be considered negligible, and values for the solubility of oxygen in water published, for example, in 'Standard Methods for the Examination of Water and Wastewater' could be used [217, Table 422:1, pp. 446-447].

Conway and Kumke stated the equation

$$(k_L a)_{20°C} = (k_L a)_T \cdot (1.024^{20-T}) \tag{A.2}$$

could be used to correct $k_L a$ for the effects of temperature on diffusivity and viscosity, although their table of values of 1.024^{20-T} [218, Table 1, p. 24] is based only on oxygen solubility in distilled water and thus does not cover diffusivity or ionic strength effects on k_L^o and a. Consequently the equation offers no improvement upon the published values mentioned above [217].

Several authors have published solubility data for Na_2SO_4 solutions at a series of temperatures [219,220,221,222]; it is assumed the solubilities in Na_2SO_3 and Na_2SO_4 are identical. Linek and Vacek [199] produced the following correlation from the published data:

$$\alpha = 5.909 \times 10^{-6} \exp\left(\frac{1602.1}{T} - \frac{0.940\,7\,C_{Na_2SO_4}}{1 + 0.193\,3\,C_{Na_2SO_4}}\right) \text{mol}/\ell \cdot \text{atm}. \tag{A.3}$$

A comparison of its predictions for $[Na_2SO_3] = 0$ with the data published for water in reference [217], along with its predictions for the 0.02M Na_2SO_3 solution used in this work, are given in Figure A.1. The prediction for water is in good agreement with the published values to about 10°C, above which it tends to overestimate, the degree of overestimation increasing as temperature increases, to a maximum of about 0.2 mg/ℓ. This computes to a maximum deviation of about 2 per cent for the highest temperatures which have the lowest solubilities.

The figure shows it is inadvisable to select an arbitrary temperature and use its solubility value as a 'blanket value' to cover every experiment regardless of their actual solution temperatures. Relative to 15°C, the solubilities at 20°C and 10°C are 8 per cent lower and 11 per cent higher respectively, which would cause K_G to be underestimated by 9 per cent at 20°C and overestimated by 12 per cent at 10°C.

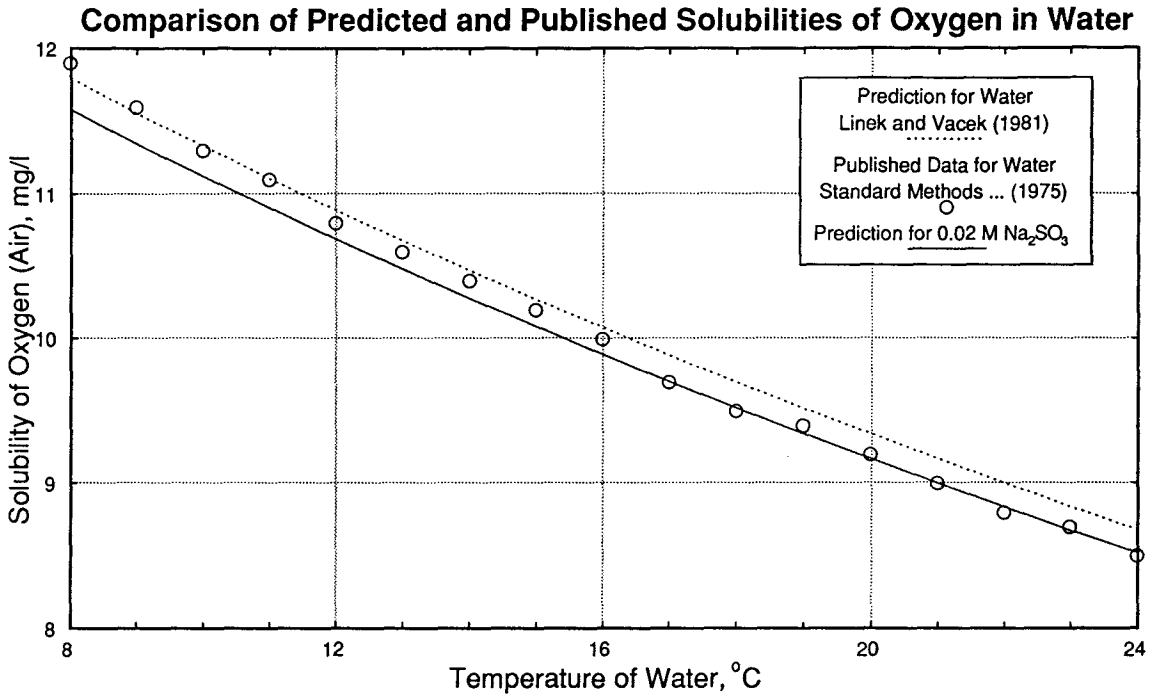

Figure A.1: Comparison of Predicted and Published Oxygen Solubility Data

The predictions for the 0.02M Na_2SO_3 solution are included to indicate the magnitude of the decrease in solubility with respect to the water reference.

Appendix B

Normalization Factors for Oxygen Diffusivity

Oxygen diffusivity is related to the mass transfer coefficient by

$$k_L^o \propto \mathcal{D}_{O_2}^n \tag{B.1}$$

where n is predicted to be equal to 1 by the film theory and equal to 0.5 by the penetration and surface renewal theories. Laboratory investigation has placed the value of n between 0 and 0.8 or 0.9, depending upon the experimental circumstances [44, p. 60].

B.1 Estimation Methods

Data for the diffusivity of oxygen in water usually are reported only for a few temperatures, which requires interpolation for the intermediate temperatures or perhaps resort to the Stokes-Einstein relation,

$$\frac{\mathcal{D}_A \cdot \mu}{T} = \text{constant.} \tag{B.2}$$

Othmer and Thakar [223] developed the relation

$$\mathcal{D}_w \times 10^5 = \frac{14.0}{\mu^{1.1} \mathcal{V}_m^{0.6}} \tag{B.3}$$

for the diffusion coefficient $\mathcal{D}_w$ of a substance in water in cm^2/sec, where μ is the viscosity of water in cp and $\mathcal{V}_m$ is the molal volume of the diffusing substances in mℓ/gm·mole. The exponents to μ and V_m were derived from the best-fit plots *vs.* $\mathcal{D}_w$ for 31 gases, liquids and solids with widely varying molecular weights and molal volumes.

Wilke and Chang [224] expanded upon the Othmer-Thakar equation and reasoned that the Stokes-Einstein group $\mathcal{D}\mu/T$ was more appropriate at representing the temperature dependence than $\mathcal{D}\mu^{1.1}$. They proposed

$$\mathcal{D} = 7.4 \times 10^{-8} \left(\frac{(xM)^{0.5} T}{\mu \mathcal{V}^{0.6}} \right) \tag{B.4}$$

in cm^2/sec. The term x is an association parameter which defines the effective molecular weight of the solvent; they assigned a value of 2.6 for water. M is the molecular weight of the solvent, and $\mathcal{V}$ the molal volume of the solute, 25.6 for O_2.

Because of the link between $\mathcal{D}_{O_2}^{20}$ and k_L^o, diffusivity cannot be factored from the equation for R in the same way as the solubility (Appendix A). But K_G^{20} can be normalized to a reference value by dividing R by the ratio of $\mathcal{D}_{O_2}$ at the temperature of the experiment and $\mathcal{D}_{O_2}$ at the reference temperature. In this way the absolute values of $\mathcal{D}_{O_2}$ need not be known. Equation B.4 thus reduces to a Stokes-Einstein group .

Data for the ratios, relative to a 20°C standard, for both the Othmer-Thakar and Wilke-Chang equations are presented in Figure B.1. There is only a minute difference on either side of the equivalence point near 19°C. The Wilke-Chang equation usually is recommended for the prediction of diffusivities. The normalization factors for both the film and the penetration/surface renewal theories are plotted in Figure B.2.

The raw R data after division by the oxygen solubility estimate were normalized by the diffusivity factors for both theories. The film theory factors are not quite as linear with temperature as are those for the penetration/surface renewal theory. For both theories, the normalization factor for a given experiment was calculated by taking the *average* temperature (the mean of the temperatures at the beginning and end of the run) and interpolating linearly from the normalization factors for the immediate integer temperatures. For the sake of reference both sets of data appear in Figures 4.1 (as triangles) and 4.5 (as pyramids). Only the K_G^{20} values for the $n = 0.5$ factors are

presented in the remainder of the figures and analysis.

The exponent $n = 0.5$ was chosen because:

1. The values of R for the experiments which evaluated the water temperature effect are harmonized much better by the factors for $n = 0.5$ (Figure 6.1, Section 6.1);
2. Experimental values of n vary but 0.5 often is considered to be the best estimate [42, p. 4];
3. It produces a more conservative estimate of K_G^{20} .

The temperature of 20°C was selected since it is much more meaningful than 0°C, and because the viscosity of water at 20°C is very nearly 1.000 cp ($\mu = 1.002$ cp [22, p. F-49]). This causes 20°C to be used as a reference for matters concerning viscosity (e.g. Othmer and Thakar [223]).

From Figure B.2 it is seen for the P/SR theory that the diffusivity factor decreases about 7 per cent in moving only 5 C° from 20°C. (For the film theory this difference is approximately doubled.) This would cause K_G to be underestimated by about 8 per cent at 15°C and overestimated by about 7 per cent at 25°C.

B.2 Viscosity Effects

This treatment method assumes the viscosity of 0.02M Na_2SO_3 solution and the diffusivity of oxygen into it are identical to pure water. No data were found in the literature for $\mathcal{D}_{O_2}$ for Na_2SO_4 solutions, but Ratcliff and Holdcroft [225] absorbed CO_2 into various electrolytes[1] including Na_2SO_4. The smallest concentration of Na_2SO_4 used was 0.318M but the data were only mildly non-linear (curved) with $[Na_2SO_4]$ ($R^2 = 0.991$) such that

[1] While CO_2 is more soluble in water and aqueous electrolytes than oxygen, it is still sparingly soluble when compared for example with the very soluble HCl.

interpolation to 0.02M does not induce error. By this method the viscosity in 0.02M Na_2SO_4 would be only 0.89 per cent greater than in pure water.

Ratcliff and Holdcroft proceeded to plot their data on a log-log plot and derived the equation

$$\log_{10}\left(\frac{\mathcal{D}_o}{\mathcal{D}}\right) = 0.637 \log_{10}\left(\frac{\mu}{\mu_{H_2O}}\right) \tag{B.5}$$

from linear regression for data from the six electrolytes studied, where $\mathcal{D}_o$ is the diffusivity of CO_2 in pure water. Extracting only their data for Na_2SO_4 the coefficient is reduced to 0.609 ($R^2 = 0.966$ with intercept 0). Substituting for 0.02M Na_2SO_4, the increase in $\mathcal{D}$ is only 0.54 per cent. Thus the differences in viscosity and diffusivity between water and 0.02M Na_2SO_3 solution are not considered to be significant.

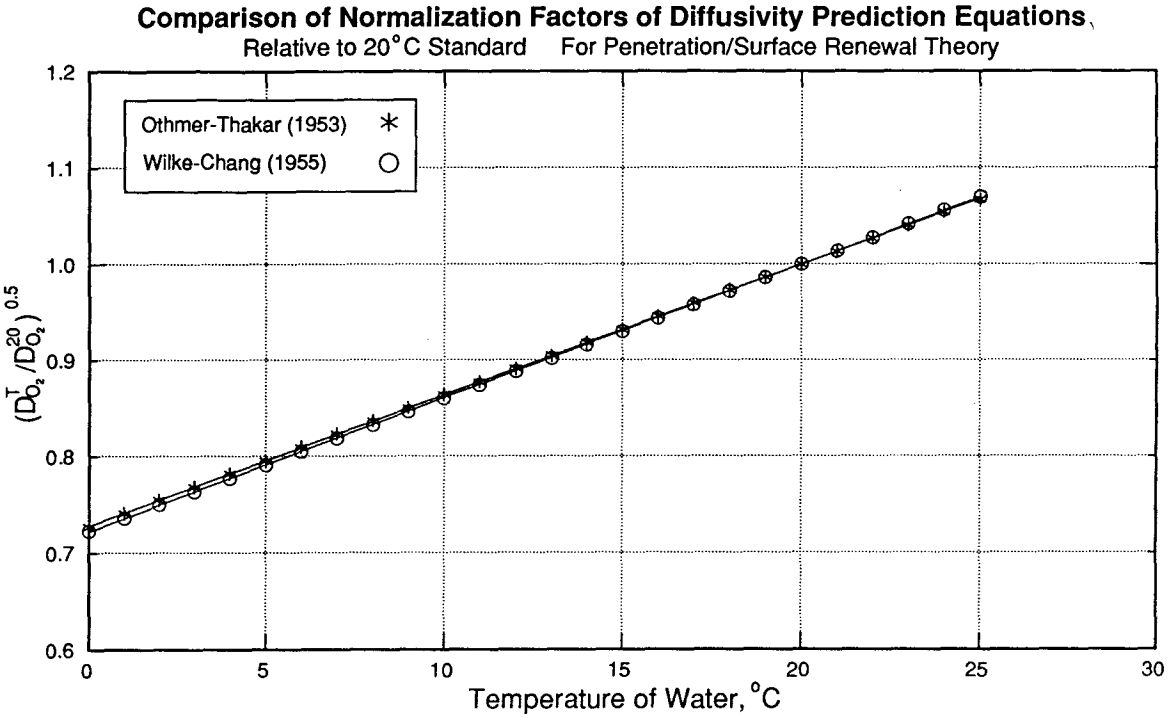

Figure B.1: Comparison of the Normalization Factors for the Two Equations

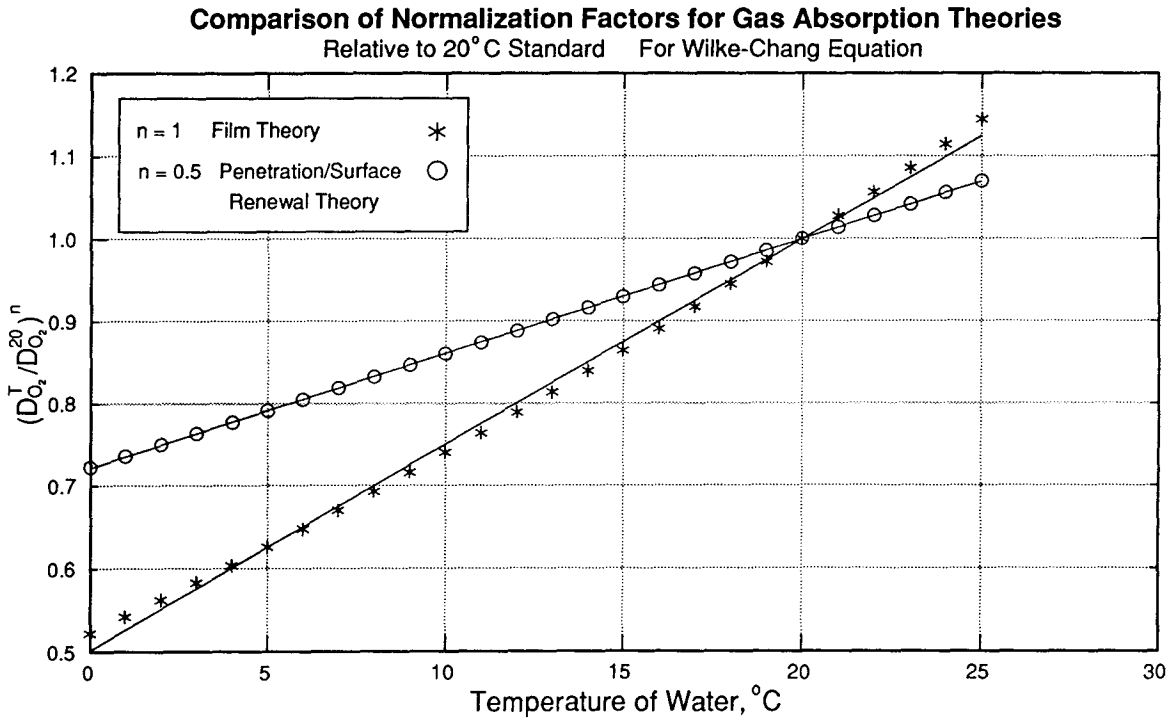

Figure B.2: Comparison of the Normalization Factors for the Two Theories